

Review

# A Review of Recent Passive Heat Transfer Enhancement Methods

Seyed Soheil Mousavi Ajarostaghi <sup>1</sup>, Mohammad Zaboli <sup>2</sup>, Hossein Javadi <sup>3</sup>, Borja Badenes <sup>3</sup> and Javier F. Urchueguia <sup>3,\*</sup>

<sup>1</sup> Department of Energy Conversion, Faculty of Mechanical Engineering, Babol Noshirvani University of Technology, Babol 47148-71167, Iran; s.s.mousavi@stu.nit.ac.ir

<sup>2</sup> Department of Thermal, Fluids, and Energy Conversion, Faculty of Mechanical Engineering, Semnan University, Semnan 35131-19111, Iran; zaboli@semnan.ac.ir

<sup>3</sup> Information and Communication Technologies versus Climate Change (ICTvsCC), Institute of Information and Communication Technologies (ITACA), Universitat Politècnica de València (UPV), Camino de Vera S/N, 46022 Valencia, Spain; hjavadi@upv.es (H.J.); borbaba@upv.es (B.B.)

\* Correspondence: jfurchueguia@fis.upv.es; Tel.: +34-963-877-000 (ext. 85246)

**Abstract:** Improvements in miniaturization and boosting the thermal performance of energy conservation systems call for innovative techniques to enhance heat transfer. Heat transfer enhancement methods have attracted a great deal of attention in the industrial sector due to their ability to provide energy savings, encourage the proper use of energy sources, and increase the economic efficiency of thermal systems. These methods are categorized into active, passive, and compound techniques. This article reviews recent passive heat transfer enhancement techniques, since they are reliable, cost-effective, and they do not require any extra power to promote the energy conversion systems' thermal efficiency when compared to the active methods. In the passive approaches, various components are applied to the heat transfer/working fluid flow path to improve the heat transfer rate. The passive heat transfer enhancement methods studied in this article include inserts (twisted tapes, conical strips, baffles, winglets), extended surfaces (fins), porous materials, coil/helical/spiral tubes, rough surfaces (corrugated/ribbed surfaces), and nanofluids (mono and hybrid nanofluids).

**Keywords:** heat transfer enhancement; passive techniques; heat exchanger; nanofluid; swirl flow; twisted tape; porous; coil tube; rough surface

**Citation:** Mousavi Ajarostaghi, S.S.; Zaboli, M.; Javadi, H.; Badenes, B.; Urchueguia, J.F. A Review of Recent Passive Heat Transfer Enhancement Methods. *Energies* **2022**, *15*, 986. <https://doi.org/10.3390/en15030986>

Academic Editor: Chi-Ming Lai

Received: 30 November 2021

Accepted: 19 January 2022

Published: 28 January 2022

**Publisher's Note:** MDPI stays neutral with regard to jurisdictional claims in published maps and institutional affiliations.



**Copyright:** © 2022 by the authors. Licensee MDPI, Basel, Switzerland. This article is an open access article distributed under the terms and conditions of the Creative Commons Attribution (CC BY) license (<https://creativecommons.org/licenses/by/4.0/>).

## 1. Introduction

During the past decades, in consequence of the global energy crisis, researchers have conducted numerous studies hoping to improve the thermal efficiency of energy systems leading to the reduction of both their size and their energy consumption rates. Heat transfer enhancement/intensification/augmentation implies the increase of thermal performance of every heat transfer procedure, heat exchange device, piece of equipment, medium, or component, provided that the overall conception of the systems is not being considerably influenced. For instance, the specific heat capacity, thermal conductivity, or latent heat of a thermal energy storage (TES) system can be enhanced; the critical heat flux of boiling heat transfer for a pool can be increased; the heat transfer rate of a surface can be improved; the peak temperature for a chip hot spot can be decreased, and so on [1]. In addition, heat transfer enhancement plays a vital role in electronic components [2], the energy and power industry [3–5], engines [6,7], thermal management [8,9], aerospace technologies [10,11], electronics packaging [12,13], new building technology [14,15], etc. Based on the literature [16–19], the methods for enhancing heat transfer have been broadly classified into three categories: active, passive, and compound techniques.

### 1.1. Active

In the active techniques, an external energy source, such as an injection, an electric or magnetic field, fluid vibration, mechanical aids, jet impingement, surface vibration, suction, etc. [20], is required to enhance the heat transfer.

### 1.2. Passive

On the other hand, the passive techniques deal with the modifications made in the configuration of thermal systems to improve the systems' thermal performance, while external energy sources are no longer needed [21]. Various techniques have been employed to initiate the effect, including the use of porous materials [22,23], inserts (e.g., turbulators, wire coils, swirl flow tools, and twisted strips) [24–27], rough surfaces (e.g., corrugated surfaces) [28–30], extended surfaces (e.g., fins), dimples and protrusions, nanofluids [1,31], displaced enhancement devices, coil/helical/spiral tube, etc.

### 1.3. Compound

In the compound enhancement technique, two or more passive and active methods are used simultaneously to improve the system's thermal performance, which will produce a superior heat transfer rate compared to that provided by any of the techniques operating individually [32,33].

In the present review paper, the scope is on the investigations conducted using different passive techniques for heat transfer enhancement, as they have some advantages over other methods, such as simplicity of production, ease of installation, and cost-effectiveness. Besides, active methods used in scientific fields are finite, as generating external power in most applications is complicated [1,20,34]. However, there have been few articles reviewing every single method of the passive approach in just one review paper. For example, in 2018, Maradiya et al. [35] studied the influence of different passive enhancement methods, but the role of the porous media, conical strips, baffles, and novel types of nanofluids (e.g., hybrid nanofluids) has not been addressed in detail.

Therefore, the novelty of this paper is to summarize all the passive heat transfer enhancement techniques, including inserts (twisted tape (TT), conical strips, baffles, winglets), extended surfaces, porous materials/surfaces, coil/helical/spiral tubes, rough surfaces, and nanofluids (mono and hybrid nanofluids) comprehensively. In addition, to promote better understanding and to make the current manuscript more readable, the authors have included several tables showing the geometries for each section.

## 2. Passive Techniques of the Heat Transfer Enhancement

This article evaluates various passive heat transfer improvement methods, focusing on the most recent published papers, as presented below.

### 2.1. Inserts

In past years, inserts such as twisted tapes, winglets, swirl generators, baffle, etc., have been considered one of the most effective passive heat transfer techniques for different systems.

#### 2.1.1. Twisted Tape

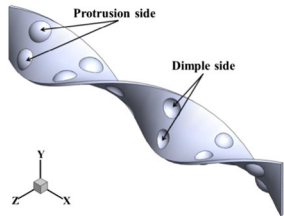
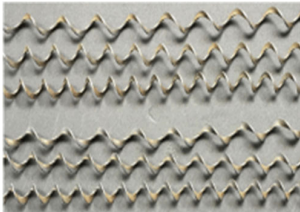
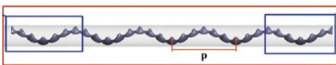
Twisted Tapes are flat pieces of metal or twisted strips used to obtain a regular pattern offering a moderate enhancement of heat transfer at a relatively low-pressure increase across laminar, transitional, and turbulent flow regimes. The twisted tape heat transfer enhancement mechanism generally induces the flows to collide to improve flow mixing. Another insert mentioned in the twisted tape section is conical strips. Twisted tapes and conical strips are widely used in the geometries for industrial applications in chemical engineering processes, power plants, chemical reactors, refrigeration, and nuclear reactors to create swirl fluid flow and increase the heat exchange in order to decrease size, weight,

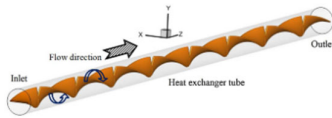

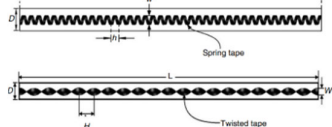
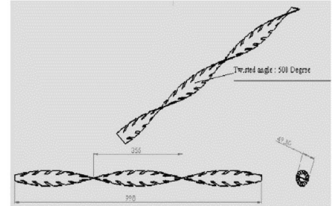
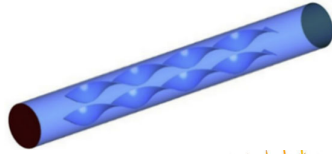
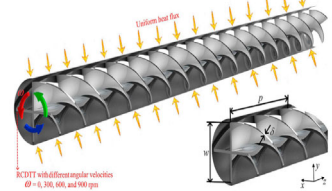
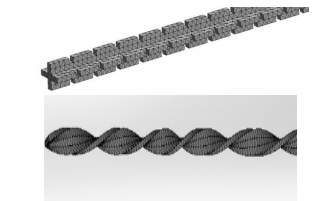
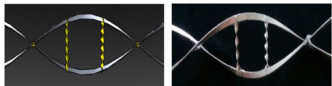
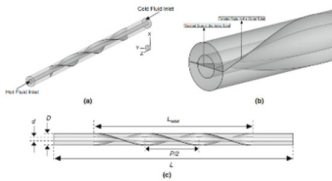
and cost. The secondary flow produced by these inserts affects the fluid flowing via the pipe and increases the turbulence and heat transfer coefficient. This swirl flow causes turbulence near the pipe wall and increases the period of fluid retention in the pipe.

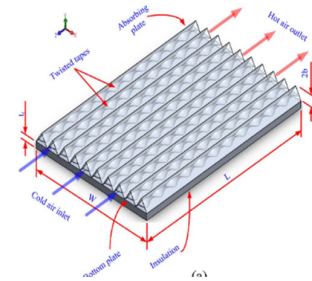
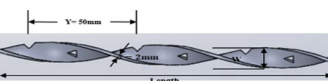
Murugesan et al. [36] investigated the square-cut twisted tapes. The ratio of the heat transfer of this model to that of a pipe without tape is 1.15. Springy wire functioning as the twisted tapes was investigated by Shaji [37]. The outcomes demonstrated that the use of twisted tapes leads to more heat exchange. By checking the four different attack corners and four different axial distances for twisted tape, Zhi Min Lin [38] found out that using inserts such as twisted tape can improve heat exchange. Eiamsa-ard et al. [39] investigated a simple tube with a short, twisted tape. The twisted tape was presented as a swirling flow to create a bouncing and swirling flow in the pipe. Suri et al. [40] investigated a heat exchanger using twisted tape. Their outcome showed that the heat transfer rate was 6.9 times higher than that of the plain pipe. Salam et al. [41] evaluated a circular pipe fitted with a twisted tape with a rectangular cut. Heat exchange enhancement performance was found to be 2.3. Eiamsa-ard et al. [42] created a 3D numerical model of a twisted tube coupled with a triple-channel twisted tape to study the heat transfer enhancement. According to the outcomes, the case using the three-start spirally twisted tube and triple-channel twisted tape at a tape width ratio of 0.34 and a belly-to-neck arrangement resulted in the highest thermal efficiency. In an experimental investigation conducted by Suri et al. [43], the influence of using square perforated twisted tape on the heat transfer enhancement in a heat exchanger is examined. It was proven that the heat transfer rate could increase markedly with the application of square perforated twisted tape with a twist ratio and perforation width ratio of 2.5 and 0.25, respectively. In another experimental study done by Man et al. [44], the application of a new type of twisted tape, called alternation of clockwise and counterclockwise twisted tape, is evaluated in a double pipe heat exchanger with the presence of single-phase forced convective flow. Based on the results, the maximum heat transfer rate will be obtained at the total length of the novel twisted tape of 2.4 m, compared to the common types of twisted tape inserts.

Some of the recent articles on the utilization of twisted tape to improve thermal performance are listed in Table 1. The list of several articles related to the use and aftereffects of using conical strips is given in Table 2.

**Table 1.** Various examples of twisted tapes for heat transfer enhancement.

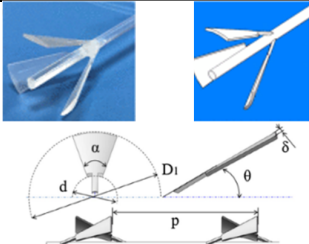
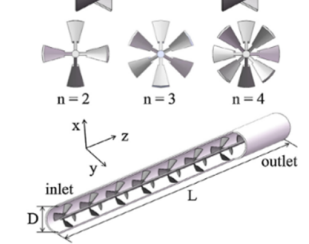
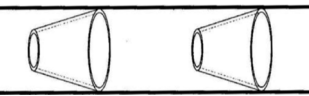
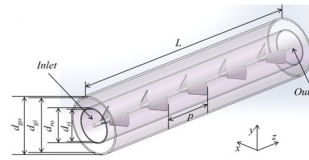

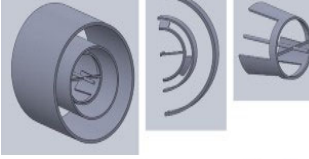
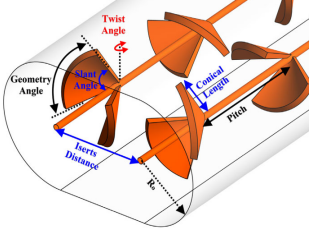
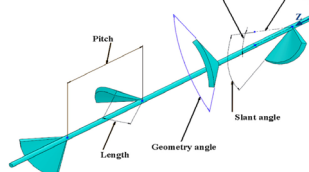
Author	Year	Type of Study	Application	Working Fluid	Type of Twisted Tape	Geometry	Remarks
Zheng et al. [45]	2017	Numerical	Circular tubes	Al <sub>2</sub> O <sub>3</sub> /Water	Dimpled twisted		- Dimpled twisted tape gave a 25.53% higher convective heat transfer coefficient.
Hong et al. [46]	2018	Experimental	Plain tube	Air	Short-length helical tapes		- The heat transfer is increased by 2.64 times.
Li et al. [47]	2018	Numerical	Heat exchanger	Al <sub>2</sub> O <sub>3</sub> /Water	Helical twisted tape		- The heat transfer is enhanced up to 14.7%.

Nakhchi et al. [48]	2019	Numerical	Heat exchanger tube	Water	Twisted tape (double cut)		- The heat transfer is improved by 117% using twisted tape with a V-cut.
Murugan et al. [49]	2019	Experimental	Trapezoidal-trough thermosyphon solar collector	Water	Wing-cut twisted tape		- The thermal performance is enhanced up to 137%.
Bhattacharyya [50]	2020	Experimental	Solar air heater tube	Air	Short-length and total-length twisted tape		- By using swirl generators, heat transfer increases by 27%.
Gnanavel et al. [51]	2020	Numerical	Double pipe heat exchanger	TiO <sub>2</sub> /water, BeO/water, ZnO/water, CuO/water	Rectangular cut on twisted tape		- Twisted tape enhanced the thermal performance factor by 1.55.
He et al. [52]	2020	Numerical	Heat exchanger tube	CuO/water	Twisted tape		- The maximum efficiency coefficient in the tube with one twisted tape is 2.18.
Bahiraee et al. [53]	2020	Numerical	Heat exchanger tube	Graphene nanoplatelets nanofluid	Coaxial cross double-twisted tape		- Twisted tape enhanced the thermal performance factor by 1.46.
Murali et al. [54]	2020	Numerical	Simple tube	Fe <sub>3</sub> O <sub>4</sub> /Water	Trapezoidal-cut twisted tape	-	- The proposed geometry could enhance the heat transfer rate by almost 36%.
Panelya et al. [55]	2020	Experimental	Heat exchanger tube	Water	X-shaped tape		- The X-shaped tape showed an enhancement of 1.27 times in heat transfer rate compared to twisted tape.
Samruaisin et al. [56]	2020	Experimental	Circular channel	Air	Transverse twisted tape		- The highest heat transfer coefficient is 1.32.
Noorbakhsh et al. [57]	2020	Numerical	Double-pipe heat exchanger	Water	Twisted tape		- Increasing the number of twisted tapes leads to improving the coefficient of performance by 63.9%.

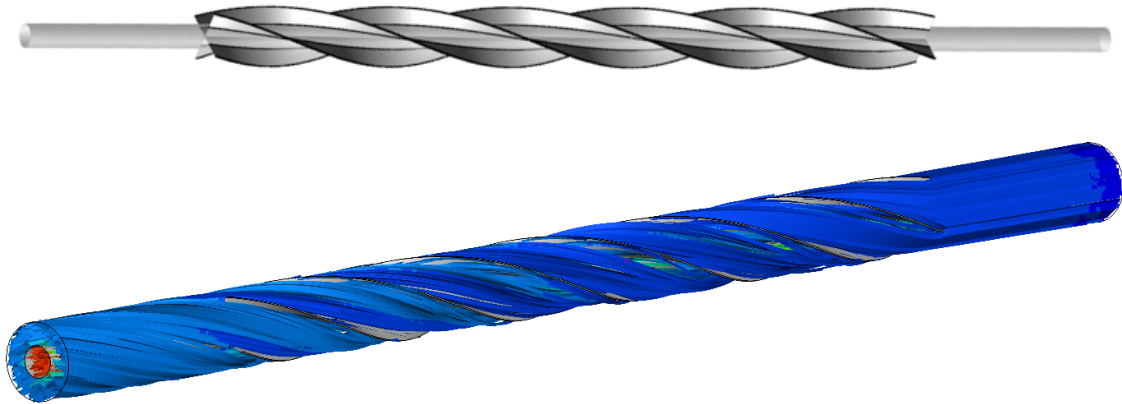
Farhan et al. [58] 2021	Numerical	Solar air heater	Air	Single twisted tape		- Thermal efficiencies are 17.5 higher than without twisted tape.
Kumar et al. [59] 2021	Numerical	Double pipe heat exchanger	Water	Perforated twisted tape		- The thermal performance factor for twisted tape with a V-cut insert is 1.49 times greater than that of a plain twist tape insert.

In addition to the items listed in the table above, other related work has been done in this area. For instance, Wijayanta et al. [60] evaluated the heat transfer increment numerically in a tube equipped with a short-length tape, type TT, as a swirl generator. Various length ratios of the proposed TT (0.25–1.0) were considered and examined. The other geometrical parameters of the proposed TT were kept constant. The numerical results showed an increase in both the heat transfer rate and the pressure drop when evaluating the proposed TT. Moreover, the maximum Nusselt (Nu) number and pressure drop figures were 0.51 and 2.84 times superior, respectively, to the tube without TT. Yaningsih et al. [61] proposed a new type of TT, V-cut TT, and investigated the heat transfer process using this tape in a tube. The evaluated geometrical parameter was the width ratio ( $w/W$ ) of the proposed V-cut TT, of which three values were considered for this parameter. Obtained numerical results revealed that the increase in the heat transfer rate and the pressure drop was about 97% and 3.48 times the results for the tube without any TT, respectively. In other work, Wijayanta et al. [62] numerically evaluated (in a tube) the impact of utilizing a new type of TT, square-cut TT (CTT), on the enhancement of thermal performance. Parameters under consideration were the twist ratios ( $y/W$ ) of the square-cut TT (three values) and the Reynolds (Re) number (between 8000–18,000). The numerical results showed that CTT enhanced the Nu number and pressure drop by about 40.3–74.4% and 1.7–3.0 times, respectively, more than the plain tube. Yaningsih et al. [63] examined the impact of utilizing TT with various wings in a tube by performing the experimental tests. The parameters under consideration were wing shape (three various shapes) and Re number (5800–18,500). The obtained practical results depicted that the highest calculated thermal performance was 1.44. In other work, Yaningsih et al. [64] investigated the heat transfer process of the perforated TT considering different axial pitch ratios in a heat exchanger. The highest achieved increase in the Nu number was by about 32%. In addition to the above-listed references related to utilizing TT as a swirl generator, there are additional works that numerically evaluate the impact of the different types of TT shapes, including curved type (Outokesh et al. [65]) and dual-modified TT (Afsharpanah et al. [66]), on the thermal performance of a heat exchanger.

**Table 2.** Various examples of conical strips used for heat transfer enhancement.

Author	Year	Type of Study	Application	Working Fluid	Geometry	Remarks
Liu et al. [67]	2018	Experimental	Heat exchanger tube	Water		- The heat transfer is enhanced by approximately 2.54–7.63 times.
Liu et al. [68]	2018	Numerical	Heat exchanger	Water		- The heat transfer is significantly enhanced (by 9.85 times) compared to the smooth tube results.
Ibrahim et al. [69]	2019	Numerical	Circular tube	Air		- The maximum Nusselt number increased by 765% compared to the Nusselt number using the plain geometry.
Liu et al. [70]	2019	Numerical	Parabolic trough receiver	Air		- The thermal efficiency is increased by 5.04% compared to the base cases.
Bahraei and Gharagozloo [71]	2020	Experimental	Plain tube	Water		- The most significant improvement of the Nusselt number is 133.8%.
Amani et al. [72]	2020	Numerical	Parabolic trough solar collector	Water		- The overall thermal-hydraulic performance is obtained in the range of 0.679–1.107.
Mashayekhi et al. [73]	2020	Numerical	Oval channel	Al <sub>2</sub> O <sub>3</sub> /Water		- The highest enhancement of the heat transfer coefficient is 17%.
Bahraei et al. [74]	2021	Numerical	Heat exchanger tube	Graphene nanoparticles/Water		- The Nusselt number increases by about 40.4%.

With twisted tapes, the fluid rotation between the tube and the twisted tape increases, causing more contact of the fluid flow with the pipe wall and the twisted tapes, providing an increased heat exchange rate. As a result, utilizing twisted tape has a significant effect on the creation of swirl flow (see Figure 1).

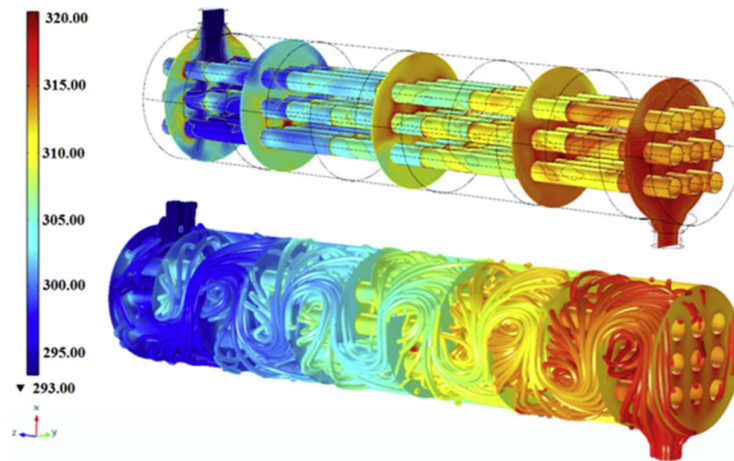


**Figure 1.** The streamline through the twisted tape [57]. (Reprinted from Noorbakhsh, M.; Zaboli, M.; Ajarostaghi, S.S.M. Numerical evaluation of the effect of using twisted tapes as turbulator with various geometries in both sides of a double-pipe heat exchanger. *J. Therm. Anal. Calorim.* 2020, 140, 1341–1353. Copyright (2020), with permission from Springer).

In addition to the references related to using conical strips with various shapes as swirl generators for heat transfer augmentation listed in Table 2, other work proposes a new strip type, the louvered strip insert. For instance, Wijayanta et al. [75] proposed a backward louvered strip as a new insert type for increasing the heat transfer rate. The factors under consideration were the insert pitch and the Re number (10,000–17,500). The numerical analysis results showed that the maximum Nu number (1.81 times more than simple tube) and the friction factor (7.59 times more than simple tube) were obtained with a pitch equal to 40 mm. In other work, Yaningsih et al. [76] proposed louvered strip inserts in a pipe in the presence of turbulent fluid flow. The factors under consideration were the slant angle of the louvered strip inserts and the Re number. According to the obtained results, the range of the thermal performance for the proposed system was 1.00–1.12.

### 2.1.2. Baffles

Baffles are flow-directing panels used to direct the flow of gas or liquid. Using helical baffles reduces pressure drop due to the removal of dead areas. As an outcome, despite reducing these areas, heat transfer improves. It can also be noted that the pumping power increases due to the reduction of pressure drop, which increases the system's overall efficiency. To better understand the influence of the baffles on the flow structure and heat transfer enhancement mechanism of the systems, streamlines of the flow through a heat exchanger are illustrated in Figure 2. As can be seen, the diverged flows run into each other near the baffle. Longitudinal swirl flows and secondary flows are created due to the upwards movement of the flow.



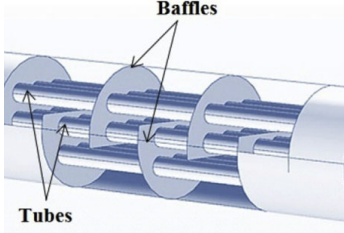

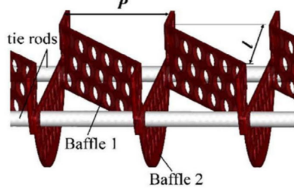
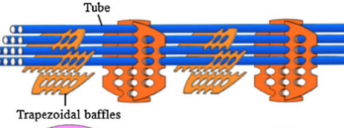
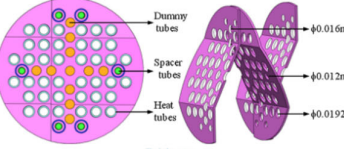
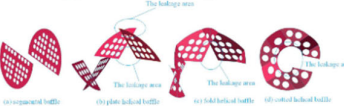
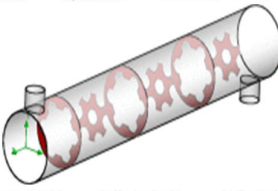
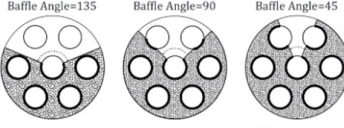
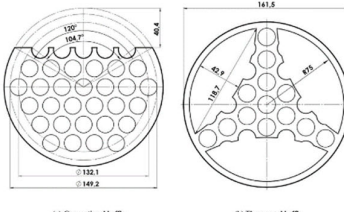
**Figure 2.** The streamline with baffle [77]. (Reprinted from Mellal, M.; Benzeguir, R.; Sahel, D.; Ameer, H. Hydro-thermal shell-side performance evaluation of a shell and tube heat exchanger under different baffle arrangement and orientation. *Int. J. Therm. Sci.* 2017, 121, 138–149. Copyright (2017), with permission from Elsevier).

Zhou et al. [78] examined the effects of trefoil-hole baffles on improving the heat transfer coefficient in a shell-and-tube heat exchanger. With the baffle, fluid velocity gradually increases, as does the flow in the region near baffles. The secondary flow is also produced. Jedsadaratanachai et al. [79] developed a finite volume method (FVM) for investigating a periodic flow in a circular tube equipped with 45-degree V-baffles. It can be concluded that by increasing the Reynolds number, the enhancement factor improved. Sriromreun et al. [80] have numerically and experimentally investigated the effect of baffle turbulators on increasing the heat transfer in a rectangular channel. Their results showed that increase of the coefficient of thermal performance for 45° baffles is significantly higher than for other models. Wang et al. [81] have numerically investigated the effect of folding baffles on increasing the heat exchange in a shell-and-tube heat exchanger. Their results showed that folding baffles significantly improved thermal performance. In another study, the increase and performance of heat transfer in a two-pipe heat exchanger were investigated by El Maakoul et al. [82]. They found that the use of helical ring baffles increased heat transfer performance. In 2016, Kumar et al. [83] examined the thermal behavior of several 60-angle V-shaped baffles in a solar air duct and found that higher overall thermal performance occurred at a relative width of 5.0. Moreover, broken V-type baffles are superior thermo-hydraulic baffles compared to other solar air ducts. Kumar et al. [84] investigated the effect of using a V-perforated baffle in a rectangular duct on heat transfer enhancement. It was concluded that using the V-down perforated baffle at a baffle width of 5.0 could achieve the highest efficiency compared to the other models. The impact of applying baffles with different cross-sections in a shell-and-coil heat exchanger on heat transfer enhancement was conducted experimentally by Andrzejczyk et al. [85]. It was indicated that the proposed model is very effective for increasing thermal performance on the shell side, but had a less substantial impact on the Reynolds numbers (less than 150). In a numerical study carried out by Sahel et al. [86], the influence of using a perforated baffle with four holes at various locations in a rectangular channel on the thermal performance was examined. It was concluded that the heat transfer rate could increase up to 65% when using the studied baffle as opposed to a typical baffle.

Some of the recent articles on the utilization of baffles to improve thermal performance in shell-and-tube heat exchangers are listed in Table 3. A list of several articles related to the use of baffles in other geometries, along with their aftereffects, is shown in Table 4.



**Table 3.** Various examples of baffles used in shell-and-tube heat exchangers for heat transfer enhancement.

Author	Year	Type of Study	Working Fluid	Type of Baffle	Geometry	Remarks
Mellal et al. [77]	2017	Numerical	Water	Baffle cut		- The thermal efficiency factor is 3.55 times more than for a case without the baffle.
Zhang et al. [87]	2017	Numerical	Water	Screw cinquefoil orifice baffles		- The heat transfer coefficient goes up by 9.2%.
Chen et al. [88]	2018	Experimental	Water	Helical baffles		- Overall heat transfer performance is increased by 161.3%.
Gu et al. [89]	2018	Experimental-Numerical	Water	Trapezoidal baffles		- The heat transfer coefficient of the heat exchanger is improved by 10.2%.
Xiao et al. [90]	2019	Experimental	Coal water slurry	Ladder-type fold baffles		- The heat transfer coefficient is increased by 290.2%.
Liu et al. [91]	2019	Numerical	Water	Fold helical baffles		- The heat transfer coefficient is improved by 8.05%.
Arani et al. [92]	2019	Numerical	Water	Segmental baffle		- The heat transfer performance is increased by 39%.
Abbasi et al. [93]	2020	Numerical	Water	Segmental baffles		- The heat transfer performance is enhanced by 11.15%.
Biçer et al. [94]	2020	Numerical	Water	Novel three-zonal baffle		- The difference in shell temperature is increased by up to 7%.

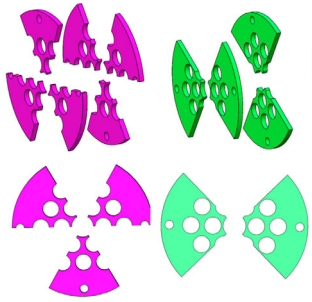
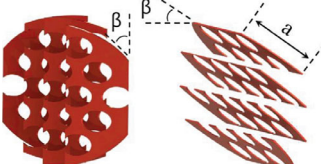
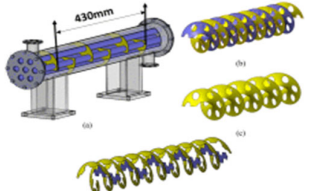

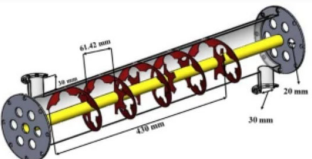
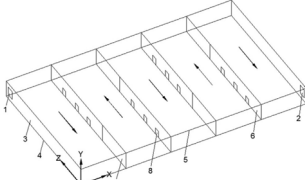
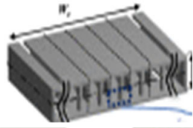
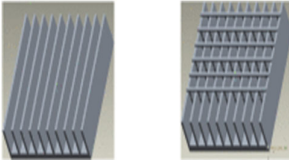
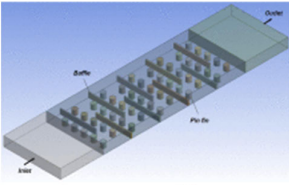
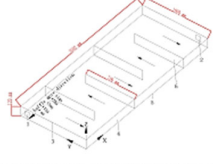
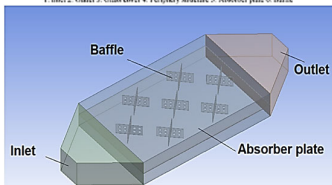
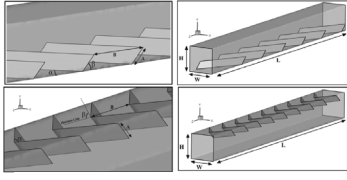
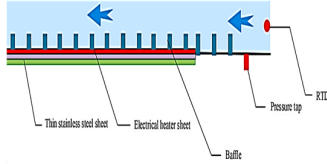
Chen et al. [95]	2020	Experimental	Water	Flower Baffles		- The heat transfer performance is improved by 11.15%.
Bahiraee et al. [96]	2021	Numerical	Nanofluid	Trapezoidal oblique baffles		- The difference in shell temperature is increased by up to 4.04%.
Abbasian and Uosofvad. [97]	2021	Numerical	Water	Combined baffle		- The heat transfer performance is increased by 22.4%.
El-Said et al. [98]	2021	Numerical	Water	Convex core baffles		- The heat transfer performance is enhanced by 51.31%.
Uosofvand and Abbasian [99]	2021	Numerical	Water	Hybrid segmental-helical baffles		- The heat transfer performance is improved by 41%.

Table 4. Various examples of baffles used for heat transfer enhancement.

Author	Year	Type of Study	Application	Working Fluid	Geometry	Remarks
Hu et al. [100]	2018	Experimental	Solar collector	Air		- The optimum collector efficiency reached 86.83% despite the baffle.
Ansari et al. [101]	2018	Numerical	Micro-combustor	-		- The average temperature meliorates by 6% and the uniformity by 87%.
Saravananakumar and Kumar [102]	2019	Experimental	Heat sink	Air		- There is an increase in the heat transfer rate of about 12.9% when applying the baffles instead of using the plain heat sink.

Karami et al. [103]	2019	Numerical	Micro-pin-fin heat sink	Air		- The heat transfer performance is increased by 47.3%.
Hu et al. [104]	2019	Experimental	Solar collector	Air		- The heat transfer performance is improved by 16.1%.
Khanlari et al. [105]	2020	Experimental	Solar air collector	Air		- The highest efficiency of 84.30% is obtained when using the baffle in a single air channel.
Olfian et al. [106]	2020	Numerical	Solar air heater	Air		- The pressure drop and Nusselt number rise by about 316.67% and 148.15%, respectively, at $Re = 2000$ .
Promvong et al. [107]	2021	Experimental	Channel	Water		- The heat transfer efficiency is enhanced by 5.8%.

### 2.1.3. Winglets

The “wing” describes the condition when the wing’s backing edge is conjoined to the extended surface. The foundation of the wing remains attached to the fin, and the apex faces the incoming stream of flow. The angle between the apex and fin surface is called the “angle of attack” or the “inclination angle”. If the wing’s chord is conjoined to the end, it is called a “winglet”. As mentioned in the beginning, all of these inserts contain elements of swirling flow. Therefore, in the presence of winglets, the resulting rotational flow leads to an adequate temperature distribution in both the radial and longitudinal directions. The presence in the models of barriers in the flow direction and the resulting turbulence produce a better temperature distribution than in the standard geometry. A noteworthy point in the use of winglets is the fluid used, which in most of the reviewed articles is air fluid.

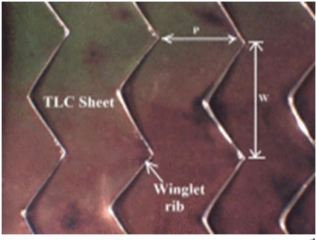
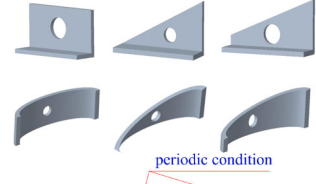
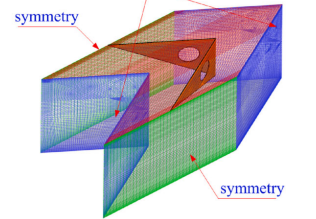
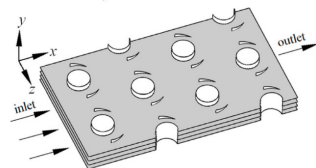
Two applications, a plate-fin heat exchanger and a solar air heater, make the most use of winglets. Solar air heating is a thermal technology in which sunlight or energy is absorbed by an element and used to heat the air. This is a renewable energy heating technology used for air conditioning or heating for thermal applications or buildings. A plate heat exchanger is a design that uses finned chambers to transfer heat between fluids. The reason for using this type of converter is its high surface-to-volume ratio. Therefore, this type of converter is usually used for small places. It is used for its ability to facilitate heat transfer with minor temperature differences [108]. Salviano et al. [109] numerically designed a delta-winglet vortex generator using the genetic algorithm method. They found that the geometric parameters of the vortex generator must be asymmetric to achieve maximum thermal-hydraulic performance. Huisseune et al. [110] studied the effect of arm and delta geometry on a round tube heat exchanger. According to their results, a small fin and a large open angle cause a strong flow deflection, resulting in a large share of windows.

A numerical investigation on the influence of using rectangular winglet pairs on the thermal performance of a rectangular channel is done by Khanjian et al. [111]. Based on the results, it is indicated that the heat transfer improved by increasing the roll angle of vortex generators. Oneissi et al. [112] numerically studied the impact of two different types of winglets with protrusions on the heat transfer rate of a parallel plate-fin heat exchanger. According to the outcomes, the maximum thermal efficiency of up to almost 7% can be achieved by using an inclined projected winglet pair with protrusions compared to the delta winglet type. A 2D numerical model of a fin-and-tube compact heat exchanger combined with different winglet configurations is built and evaluated by Modi and Rathod [113]. It was shown that the curved down geometry of the rectangular winglet vortex generator obtained the most desirable enhancement in heat transfer among the other cases.

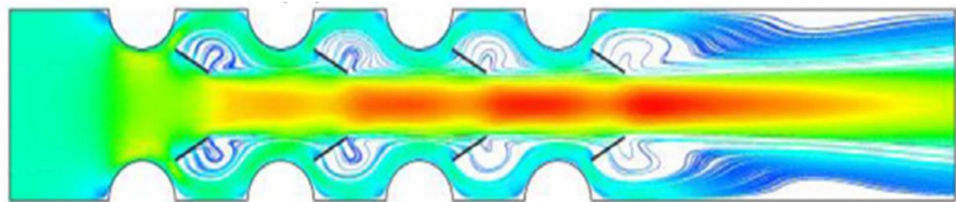
Some of the recent articles related to the utilization of winglets to improve thermal performance are listed in Table 5.

**Table 5.** Various examples of winglets used for heat transfer enhancement.

Author	Year	Type of Study	Application	Geometry	Remarks
Chamoli et al. [114]	2018	Numerical	Solar air heater		- Winglet vortex generator inserts show an excellent thermal enhancement factor with a maximum value of 2.20.
Samadifar et al. [115]	2018	Numerical	Plate-fin heat exchanger		- The vortex generator increases the heat transfer of the heat exchanger by 7%.
Luo et al. [116]	2019	Experimental	Plate-fin heat exchanger		- The thermal performance factor is increased by up to 26.4%.
Zhai et al. [117]	2019	Experimental	Circular tube		- The maximum increase in the Nusselt number is observed, with the delta winglet pairs producing numbers 73% higher than those with the smooth tube.
Sun et al. [118]	2020	Experimental	Circular heat exchanger tubes		- The heat transfer is improved by 11.63 times.

Kumar et al. [119]	2020	Experimental	Solar air heater		- The Nusselt number is increased by up to 5%.
Modi et al. [120]	2020	Experimental	Plate-fin heat exchanger		- The heat transfer is increased by up to 57.37%.
Promvongse et al. [121]	2021	Numerical	Solar air heater		- The punched delta winglet provides a more significant Nusselt number by 78.21 times.
Shi et al. [122]	2021	Numerical	Plate-fin heat exchanger		- The heat transfer is enhanced by 43.9%.

To better understand the influence of the winglet on the flow structure and heat transfer enhancement mechanism of the systems, streamlines of the flow are illustrated in Figure 3. Winglets generate a counter-spinning vortex appearing along the duct, whereas the flat plate indicates no vortex. This phenomenon creates a remarkable increase in heat exchange.



**Figure 3.** The streamline with the contour of velocity [120]. (Reprinted from Modi, A.J.; Kalel, N.A.; Rathod, M.K. Thermal performance augmentation of fin-and-tube heat exchanger using rectangular winglet vortex generators having circular punched holes. *Int. J. Heat Mass Transf.* 2020, 158, 119724. Copyright (2020), with permission from Elsevier).

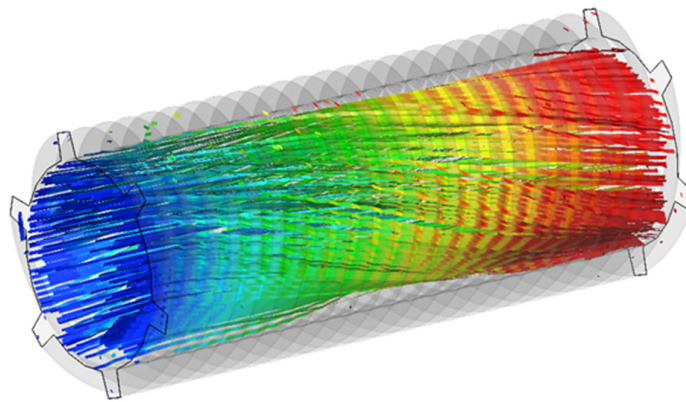
Khan et al. [123] used an artificial neural network (ANN) to calculate the thermal performance efficiency of a heat exchanger equipped with delta-wing tape as a turbulator. The factors under consideration were the wing-width ratios (three values) and the Re number. The found mean square error was less than 0.7, which showed the effectiveness of the proposed ANN method. Wijayanta et al. [124–126] evaluated heat transfer enhancement in the internal flow. Double-sided delta-wing tape was employed as a swirl generator. The impact of the wing-pitch ratio was analyzed. The results revealed that the proposed swirl generator shows a greater average Nu number and friction factor than the case without any swirl generator. In other work, Yaningsih et al. [127] employed double-

sided delta-winglet tape in a tube to experimentally study the increment in the heat transfer process and pressure drop. The parameters under consideration were the blockage ratio (the ratio of winglet height to inner tube diameter—three values) and the flow rate (between  $3.35 \times 10^{-5}$ – $8.33 \times 10^{-5}$  m<sup>3</sup>/s). The results obtained from the experimental tests depicted that by employing the proposed insert, the Nu number increased by about 364.3%. Heat transfer improvement in a tube with punched delta winglet vortex generators was studied by Wijayanta et al. [128]. The influence of the attack angle of the proposed turbulator on the enhancement of thermal performance was evaluated. The proposed swirl generator presented a greater heat transfer rate and friction factor than the plain tube.

## 2.2. Extended Surfaces

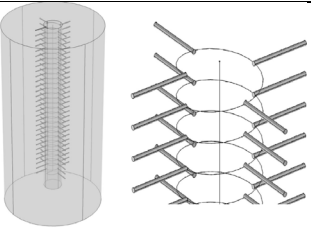
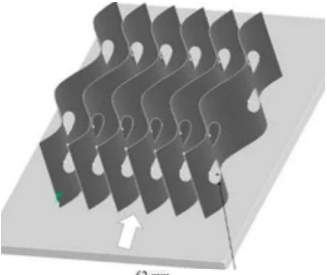
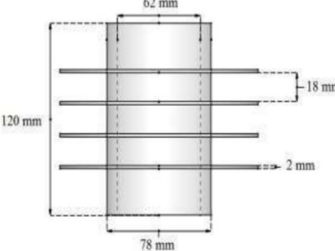
Another method of passive heat transfer enhancement is the utilization of fins. In the study of heat transfer, fins are surfaces that extend from an object to increase the heat transfer rate to or from the environment by increasing convection. Thus, adding a fin to an object increases the surface area and can sometimes be an economical solution to heat transfer problems. The fins can be divided into a constant area straight fin, a variable area straight fin, a pin fin, and an annular fin.

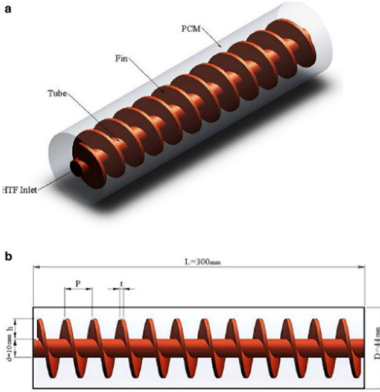
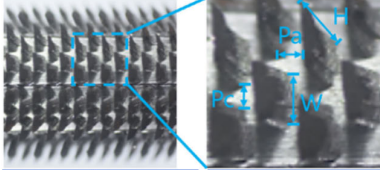
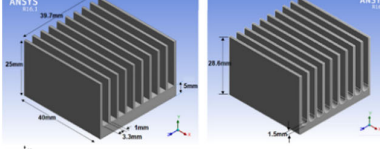
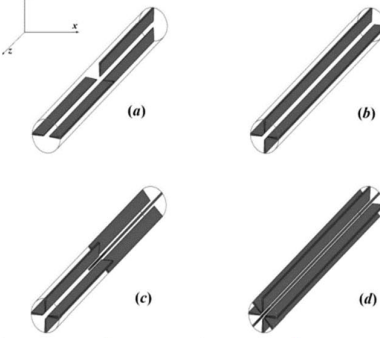
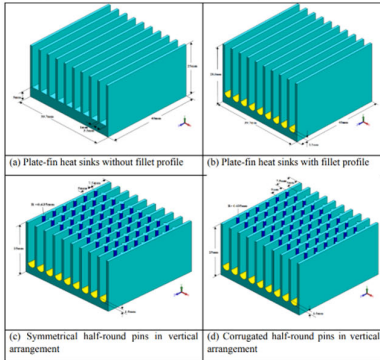
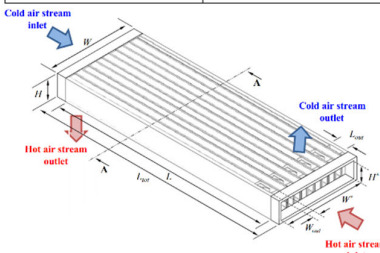
Dastmalchi et al. [129] investigated heat transfer and pressure drop changes inside a heat sink under constant wall temperature. It was found that heat transfer improves by increasing angles up to 45 degrees. The CFD simulation of wavy-fin and elliptical-tube HEX with various vortex generators was completed by Lotfi et al. [130]. They discovered that heat transfer rate is improved with an increase in wavy fin height and a decrease in the tube elasticity ratio. The CFD simulation of wavy-fin and elliptical-tube HEX has been accomplished by Kim et al. [131]. They found that the optimized cross-cut flow control could increase the efficiency of the wavy fin. Singh and Anil [132] performed an experimental simulation to evaluate the heat transfer and fluid flow inside a fin heat sink under natural convection. It was found that an angle of 45° and an impression pitch of 12 mm bring out the highest growth. Awasarmol et al. [133] experimentally studied heat transfer and fluid flow with various inclination angles and various perforation diameters. It was indicated that a 32% growth in the heat transfer coefficient was observed when the fins were perforated. Lotfi et al. [134] performed an experimental simulation to evaluate the heat transfer and fluid flow inside smooth wavy fin-and-elliptical tube heat exchangers. It was found that fins with  $w/l = 0.5$  produced the best heat transfer efficiency. Some recent articles related to the utilization of fins to improve thermal performance are listed in Table 6. To better understand the influence of the fins on the flow structure and heat transfer enhancement mechanism of the systems, streamlines of the flow through a heat exchanger are illustrated in Figure 4. As can be seen, the geometry of fins leads to the creation of swirl flows inside the tube. Consequently, longitudinal swirl and secondary flows are created [135,136].



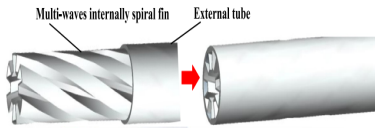
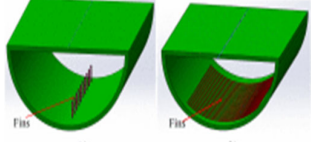
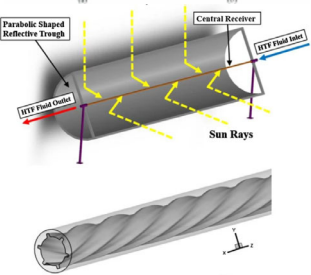
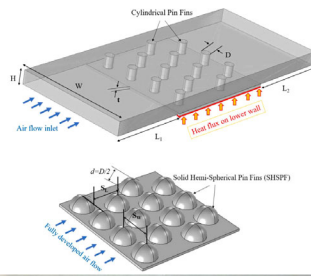
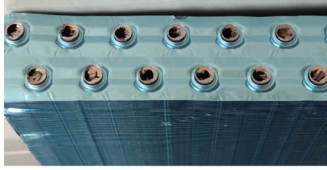
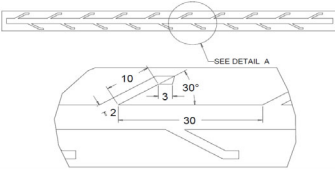
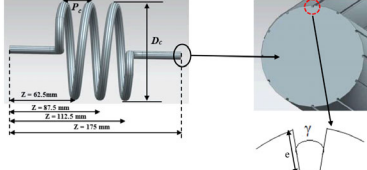
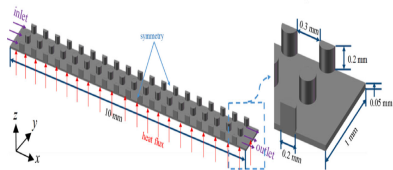
**Figure 4.** The streamline with fins [136]. (Reprinted from Zaboli, M.; Ajarostaghi, S.S.M.; Saedodin, S.; Pour, M.S. Thermal Performance Enhancement Using Absorber Tube with Inner Helical Axial Fins in a Parabolic Trough Solar Collector. *Appl. Sci.* 2021, 11, 7423. Copyright (2021), with permission from Multidisciplinary Digital Publishing Institute (MDPI)).

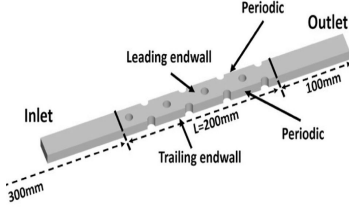
**Table 6.** Various examples of fins used for heat transfer enhancement.

Author	Year	Type of Study	Application	Working Fluid	Geometry	Remarks
Saeidi et al. [137]	2018	Numerical	Geothermal heat pump	Air		- The heat transfer of the system improves by 31%.
Zhang et al. [138]	2018	Numerical	Plate-fin heat exchanger	Air		- The Nusselt number ratio increases by 1.5 times.
Vyas et al. [139]	2018	Numerical	Internal combustion engine	Engine fuel		- Using fins improved the engine cooling by 22%.

Borhani et al. [140]	2019	Numerical	Spiral-fin heat exchanger	Water		- The spiral-fin improves the heat transfer rate by about 56%.
Zhang et al. [141]	2019	Experimental	Heat exchanger	Air		- The finned tube's performance criterion is revealed to be 2.9 times higher than without fins.
Hussain et al. [142]	2019	Numerical	Heat sink	Air		- The heat transfer performance is improved by approximately 3.78% with fins compared to without fins.
Hajmohammadi et al. [143]	2020	Numerical	Circular channel	Air		- The heat transfer is increased by 46%.
Freegah et al. [144]	2020	Numerical	Heat sink	Air		- The Nusselt number is enhanced by approximately 31.6%.
Kim et al. [145]	2020	Numerical	Gas turbine	Air		- The maximum heat transfer rate reaches 811 W.



Liu et al. [146]	2021	Numerical-Experimental	Heat exchanger	Air		- The heat transfer coefficient is improved by 8.67 times.
Gong et al. [147]	2021	Numerical	Solar concentrator	Water		- Long and thin fins showed the most remarkable efficiency improvement of 1.6%.
Saedodin et al. [148]	2021	Numerical	Parabolic trough solar collector	Nano-tubes/Iron Oxide		- The heat transfer is increased by 37.2%.
Sahel et al. [149]	2021	Numerical	Heat sink	Air		- The highest hydrothermal performance factor is 1.87.
Zhang et al. [150]	2021	Numerical-Experimental	Fin-and-tube heat exchanger	Air		- The heat transfer is enhanced by 8%.
Sandhya et al. [151]	2021	Numerical	Radiator	Graphene + Crystal/Water + Ethylene glycol		- The highest enhancement in the heat transfer rate (60%) is achieved using a louvered fin.
Kumar et al. [152]	2021	Numerical	Helically coiled tubes	Water		- The Nusselt number is improved by 39%.
Yan et al. [153]	2021	Numerical	Heat sink	Air		- The maximum heat transfer efficiency of the heat sink is 1.4.

Liang et al. [154]	2021	Numerical	Channel	Air		- The heat transfer is improved by 16.9%.
--------------------	------	-----------	---------	-----	--	---

### 2.3. Porous Materials

Metal foams (MFs), porous metal structures with an extraordinarily high thermal conductivity and a large surface area in a relatively small volume, have attracted researchers' attention to increase the heat transfer rate in thermal systems. Incorporating porous media into any thermal system enhances the thermal performance in terms of heat transfer. Because of the high heat transfer area and the high thermal diffusion capacity, incorporating MFs produces excellent conductive heat transfer that augments the heat transfer rate considerably. On the contrary, it should be emphasized that using foam structures in thermal systems remarkably limits the fluid motion and thus the natural convection streams. Consequently, the temperature distribution could be relatively superior using MFs [155–157]. The MF can save a significant amount of energy when used in sensible thermal form. The geometric factors of MFs have a significant impact on thermal performance. In redesigning a thermal system equipped with MF, the pore density and porosity are vital factors that could significantly influence effective thermal conductivity. The porous materials used include various kinds of material, which the most common and efficient of them being copper foam, aluminum foam, nickel foam, and carbon-based foams such as graphite, employed mainly for high-temperature uses [158,159].

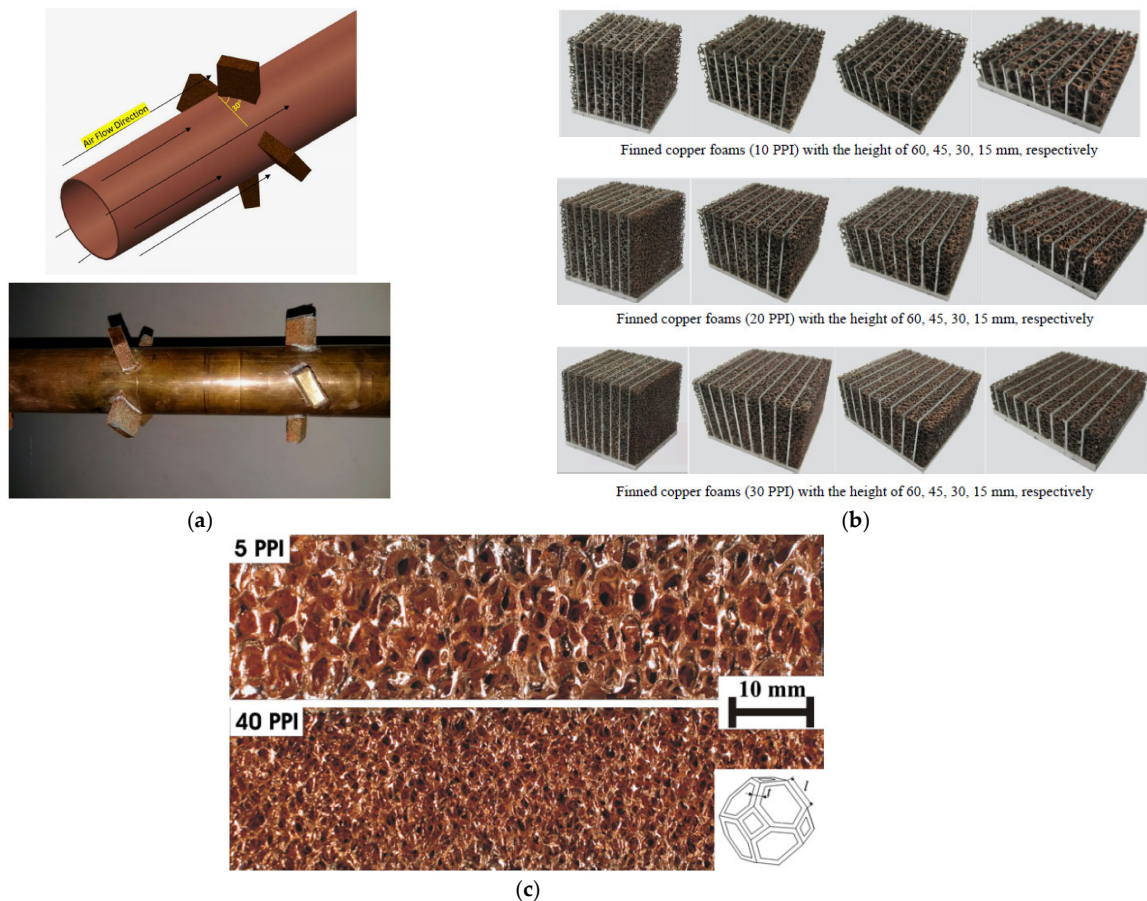
#### 2.3.1. Metal Foam Type

##### Copper Foam

As a material with very high thermal conductivity, copper is extensively employed to augment the heat transfer rate in a thermal system. Because of its high thermal conductivity of about 400 W/(mK), copper foam is commonly used in foam structures. Scientists investigated copper foam performance by performing experimental tests and numerical simulations to obtain improved thermo-physical properties, namely thermal conductivity. Consequently, different studies have been conducted on the augmentation of heat transfer rates and thermal performance of thermal systems equipped with copper foams, along with studies on related characteristics like geometric structure.

Hamzah and Nima [160] experimentally investigated the heat transfer rate in a double-pipe heat exchanger with copper foam fins as porous media (Figure 5a). The metal foam fins of 40 PPI (pores per inch) were made from copper and placed at a 30° angle with the pipe inlet. They were located inside the annular section around the inner copper pipe to steer the fluid flow to disrupt its structure through the annular gap. The range of studied Reynolds numbers is 616–2343. Both parallel and counter flows were considered and analyzed. The obtained experimental results have been compared with the case without porous fins. Results showed that an increase in the inlet Reynolds number causes augmentation of the heat transfer rate. The best-obtained case is suggested using copper foam fins and counter fluid flow in the suggested heat exchanger. The critical point is that no significant pressure drop was obtained with the improvement of the heat transfer rate. Wang et al. [161] experimentally analyzed the impact of utilizing finned copper foams by jet impingement on the cooling process of a heat sink. Three new finned copper foams were proposed and tested (Figure 5b). Impacts of copper foam porosity, height, and impinging gas flow rate were evaluated. Results indicated that finned copper foam is superior to finned heat sinks in thermal performance. Also, finned copper foam can replace finned heat sinks in narrow spaces. Mancin et al. [162] appraised the heat transfer process of airflow through five copper foams by performing experimental tests. Several pores per

inch and porosities have been considered for the porous media. The obtained experimental results depicted that the Cu-10-9.5 copper foam sample can be considered a viable method for designing innovative thermal management solutions for electronic cooling applications. Nilpueng et al. [163] experimentally investigated the heat transfer process in a small plate heat exchanger filled with copper foam for small-scale electronic cooling. The impact of copper foam pore density (see Figure 5c) and water velocity on the optimum thermal performance was assessed. The results presented that the heat transfer coefficient and pressure drop increased when the water velocity and pore density were augmented. The heat transfer coefficient was improved by 20.23, 29.37, and 40.28%, respectively, with the pore densities of 30, 40, and 50 PPI over the use of a plate heat exchanger without porous media.



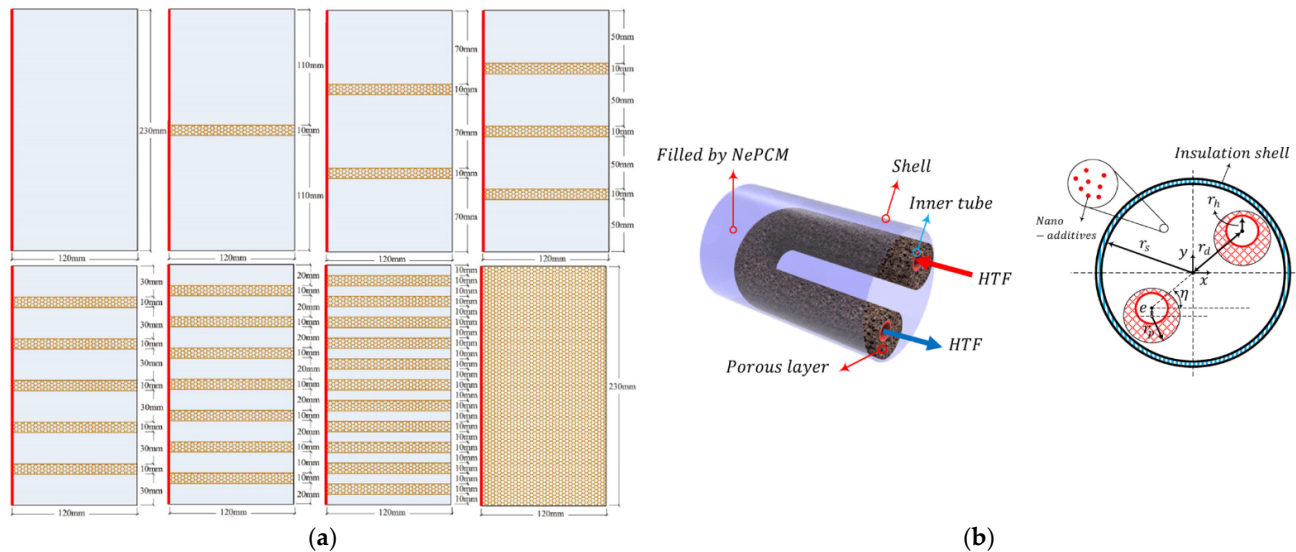
**Figure 5.** Various utilization of copper foams for heat transfer enhancement: (a) a double-pipe heat exchanger equipped with porous fins [160]; (b) different heat sinks as test specimens [161]; (c) a picture of pore density on the foam structure [162]. (Reprinted from Hamzah, J.A.; Nima, M.A. Experimental study of heat transfer enhancement in double-pipe heat exchanger integrated with metal foam fins. *Arab. J. Sci. Eng.* 2020, 45, 5153–5167. Copyright (2020), with permission from Springer.); (Reprinted from Wang, J.; Kong, H.; Xu, Y.; Wu, J. Experimental investigation of heat transfer and flow characteristics in finned copper foam heat sinks subjected to jet impingement cooling. *Appl. Energy* 2019, 241, 433–443. Copyright (2019), with permission from Elsevier.); (Reprinted from Mancin, S.; Zilio, C.; Diani, A.; Rossetto, L. Experimental air heat transfer and pressure drop through copper foams. *Exp. Therm. Fluid Sci.* 2012, 36, 224–232. Copyright (2012), with permission from Elsevier).

One of the porous material's main and practical applications is its use in TES systems, particularly latent heat TES (LHTES) [164,165]. Cui [166] performed some experimental tests on the charging mode (melting process) of PS 58 as a phase change material (PCM)

in the case with a top porosity copper foam (96% porosity and 20 PPI). The PCM was bounded in a cylindrical shell made of stainless steel, and the temperature changes were evaluated. Besides the uniform temperature gained in the composite, the charge rate was more than that of the case without porous material. Consequently, utilizing porous material led to a reduction in the charge time by about 36%. Mancin et al. [167] examined the phase change behavior of the PCM (paraffin) fixed in the copper foam of various pore densities by applying different heat fluxes. The PCM storage equipped with copper foam displayed an enhanced charge rate compared to the plain PCM storage. Moreover, the influence of pore density was minor. Wang et al. [168] experimentally studied the helpfulness of copper foam in augmenting the thermal conductivity of the PCM (paraffin). The obtained results depicted about a 40% decline in the complete melting of PCM as a charging process. Li et al. [169] performed experiments showing that inserting copper foam with a porosity of 92.4% in sodium acetate trihydrate led to a 40% decrease in charge time.

Jin et al. [170] evaluated the impact of copper foam pore density on the charge time of paraffin wax as a PCM by performing experimental tests. The pore densities under consideration included 15, 30, and 50 PPI in various superheat values of 20 and 30 °C. The porosity of the copper foam was kept constant at 95% in all experiments. The obtained results showed that cases with 30 and 50 PPI displayed the same charge process for a 20°C superheat value. Conversely, at 30°C superheat value, the case with 30 PPI illustrated better thermal performance than the case with 50 PPI. Zheng et al. [171] examined the phase change process of PCM inside a rectangular storage equipped with copper foam as the porous material under the condition of uniform heat flux by performing experiments and numerical simulations. According to the achieved results, the case using copper foam showed a lower melting time by about 20.5% compared to the case using plain PCM storage. Yang et al. [172] experimentally investigated the impact of utilizing open-cell copper foam as a porous material in a PCM (paraffin wax) storage on the phase change behavior (melting rate). The considered PCM storage was a shell-and-tube type. Results depicted that utilizing the proposed porous material causes a decline of about 60.6% in the charge rate. The impact of employing copper foam as a porous material on the melting rate of PCM in a TES system was evaluated by Yang et al. [173]. According to the obtained results, using porous material led to a reduction in the total melting time of the PCM by about 88.548%. Hu et al. [174] studied the impact of contact conditions on the PCM (paraffin) phase change process when fixed in copper foam by doing numerical simulations. The outcomes illustrated that the contact conditions have significant effects on the phase change behavior of the proposed system. Duan [175] evaluated the usefulness of utilizing metal foam in a PCM storage for cooling a photovoltaic concentrator system considering various porosity. According to the obtained outcomes, the case using a foam porosity of 0.85 showed optimum cooling performance. Li et al. [176] investigated the impact of employing metal foam on the charging behavior of a nano-enhanced PCM (NEPCM) composite. A considerable decrease in wall temperature (up to 47°C) was observed.

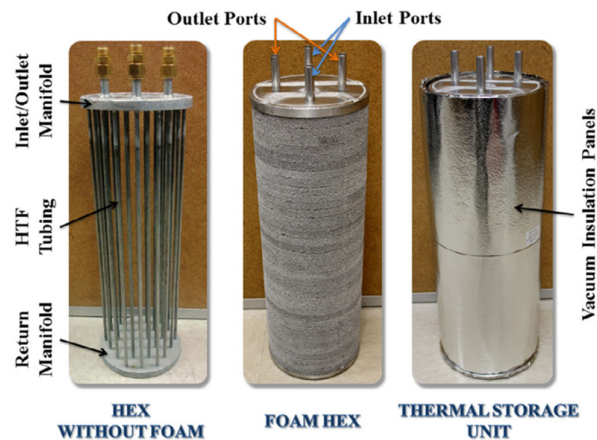
Meng et al. [177] numerically investigated the charge and discharge processes (PCM melting and solidification) inside a rectangular cavity partially filled with copper foam as a porous material (see Figure 6a). The factors under consideration were the filling ratio and the location of the copper foam. The numerical outcomes showed higher thermal performance belonged to the cases with copper foam fractions of 5 and 50%. Zadeh et al. [178] numerically evaluated the impact of employing copper foam (partial filling condition) and nanoparticles for augmenting the PCM phase change process in a heat pipe (see Figure 6b). Results showed that employing both methods, including the partial filling with a porous materials and nanoparticles, led to the best charge process compared to each method individually.



**Figure 6.** Partial use of metal foams (copper foams) for heat transfer enhancement: (a) rectangular enclosures partially filled with metal foam in different locations [177]; (b) LHTES system partially filled with metal foam [178]. (Reprinted from Meng, X.; Yan, L.; He, F. Filling copper foam partly on thermal behavior of phase-change material in a rectangular enclosure. *J. Energy Storage* 2020, 32, 101867. Copyright (2020), with permission from Elsevier.); (Reprinted from Zadeh, S.M.H.; Mehryan, S.A.M.; Ghalambaz, M.; Ghodrati, M.; Young, J.; Chamkha, A. Hybrid thermal performance enhancement of a circular latent heat storage system by utilizing partially filled copper foam and Cu/GO nano-additives. *Energy* 2020, 213, 118761. Copyright (2020), with permission from Elsevier).

### Aluminum Foam

As material other than copper that also exhibits high thermal conductivity, aluminum is extensively employed to augment the heat transfer rate. The impact of utilizing aluminum foam as a porous material to improve the heat transfer characteristics in thermal systems has been investigated in several works. Chen et al. [179] studied the usefulness of employing a PCM/aluminum foam composite in a flat-plate solar collector. The results obtained showed considerable improvement in the heat transfer rate of the proposed thermal system. Moreover, both thermal and non-thermal equilibrium models were tested to model the fluid flow and heat transfer in the porous medial, and accordingly, it can be found that the non-thermal equilibrium model is more precise than the thermal. Atal et al. [180] presented a numerical study on the melting and solidification behaviors of the PCM/aluminum foam composite in a shell-and-tube PCM (paraffin wax) storage using empiric and numerical methods. Results showed that in the PCM's melting and solidification processes, employing a porous matrix in the storage considerably increased the heat transfer rate. Moreover, the impact of the porosity and pore size of the porous matrix on the charge/discharge modes was evaluated. Fleming et al. [181] experimentally examined the PCM's charge and discharge behavior in a shell-and-tube PCM storage equipped with aluminum foam (Figure 7). The experimental results reported the improvement in both the charge and discharge processes. Accordingly, by employing open-cell aluminum foam, the melting rate of the PCM augmented by about 100%; however, a lower augmentation rate (20%) was observed for the solidification rate.



**Figure 7.** A thermal storage unit with metal foam [181]. (Reprinted from Fleming, E.; Wen, S.; Shi, L.; da Silva, A.K. Experimental and theoretical analysis of an aluminum foam enhanced phase change thermal storage unit. *Int. J. Heat Mass Transf.* 2015, 82, 273–281. Copyright (2015), with permission from Elsevier).

Wang and Qin [182] presented a numerical study on the melting behavior of PCM in storage equipped with aluminum foam. The results revealed that utilizing metal foam had a considerable influence on accelerating the phase change process. Consequently, the numerical outcomes displayed that the copper and aluminum matrix materials decrease the melting time by about 9.7 and 4%, respectively, compared to the iron foam. Sundarram and Li [183] evaluated the impact of porosity and pore size on the phase change process in a PCM storage filled with aluminum foam by performing numerical simulations. According to the obtained outcomes, the optimum case in terms of the highest heat transfer augmentation belonged to the aluminum porosity of 84% at 25  $\mu\text{m}$  pore size. Sardari et al. [184] studied the phase change process of the PCM in a radiator equipped with PCM/metal foam storage as the TES. The results showed that the PCM/ metal foam composite reduced the total melting time by about 95%. Zhu et al. [185] presented a work related to the influences of three porosities, including 67, 75, and 84%, by performing experiments and numerical simulations. Consequently, the results displayed that the heat transfer is conduction-dominant in the case with low porosity.

#### Nickel Foam

Nickel foam, a material with a high melting point (1455  $^{\circ}\text{C}$ ), is appropriate for high-temperature uses, although its thermal conductivity is somewhat less than that of copper and aluminum (89  $\text{W}/(\text{mK})$ ). Numerous works have examined the capability of nickel foam to increase the thermal properties of PCM. Oya et al. [186] experimentally investigated the thermophysical characteristics of the PCM/ nickel foam composite in which the erythritol was employed as the PCM. The results displayed an up to 16 times improvement in the effective thermal conductivity compared to the plain PCM. The optimum enhancement was obtained with 15 vol% of nickel foam and 85 vol% of erythritol. Xiao et al. [187] presented a steady-state test rig to evaluate the impact of thermal properties of paraffin/nickel foam and paraffin/copper foam composites. The outcomes depicted that by decreasing the porosity, the effective thermal conductivity of the PCM/nickel composite augments. Liang et al. [188] evaluated the thermophysical characteristics of the graphene-coated nickel foam/PCM composite. The results displayed that the amount of heat storage by the proposed composite was reduced by up to 32%. Huang et al. [189] considered the influence of employing nickel foam on the thermal performance of a PCM storage. The outcomes depicted that by employing the proposed composite, the latent heat reduced up to 29%, which showed that the foam occupies a considerable volume, leading to a decline in the PCM filling space.

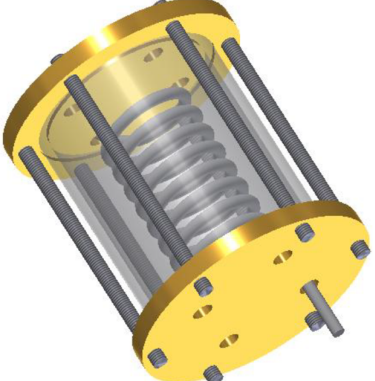
### Graphite

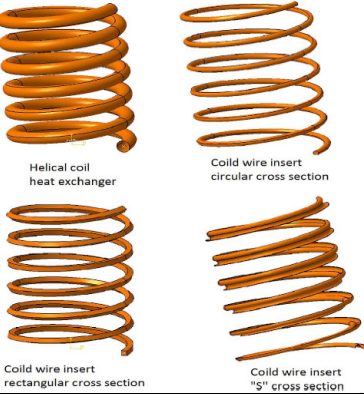
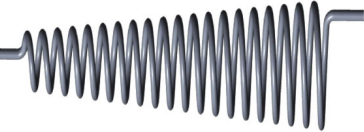
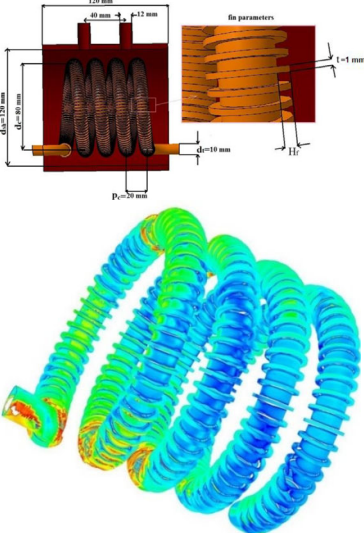
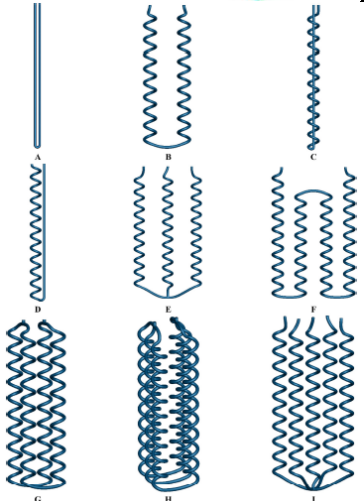
Because of the durability and suitability of using graphite in high temperatures, graphite is one of the materials widely used to enhance the PCM storage’s effective thermal conductivity, especially for high-temperature applications. Graphite has a superior thermal conductivity (about 300 W/(mK)) and a high porosity (about 90%). Expanded graphite (EG), which has a very high thermal conductivity and chemical stability, can be employed to enhance the thermal performance of high-temperature PCMs. Zhong et al. [190] evaluated the impact of utilizing a compressed, expanded natural graphite matrix on phase change behavior of paraffin wax in a PCM storage. They found that the thermal conduction property of the proposed composite was about 28–180 times greater than with pure paraffin. Pokhrel et al. [191] experimentally and numerically studied the thermal properties of a PCM/graphite composite. The obtained results depicted that employing graphite with a 16.5% mass fraction did not reduce the latent heat. Wang et al. [192] used experiments to evaluate the improvement influence of EG on the thermal conductivity of a composite based on eutectic salt. The obtained experimental results displayed an augmentation of the effective thermal conductivity of up to 183%. Jin et al. [193] presented an experimental study related to employing EG for improving the thermophysical characteristics of a salt PCM. The outcomes showed that 9% wt EG has the best thermal performance. Another study on employing a PCM/graphite foam composite was done by Opolot et al. [194] by considering concentrated solar power plants. The outcomes revealed that using the proposed composite led to a decline in the total melting and solidification times by about 5 and 4%, respectively.

### 2.4. Coil/Helical/SPIRAL Tube

This section focuses on utilizing coil/helical/spiral tubes (instead of straight ones) for improvement of thermal performance in thermal systems. The researchers tried to change the geometries of the tube so that more heat would transfer from the heat transfer fluid (HTF) channel to the system, or the reverse. The utilization of spiral tubes in various heat exchangers for different applications, such as geothermal uses [195,196], cold storage systems [197], thermal systems [198], etc., has been studied. The review of the previous related works is listed in detail in Table 7.

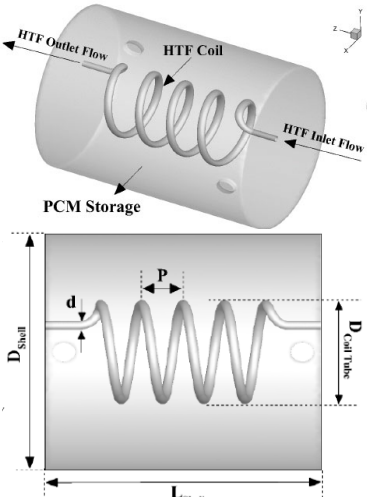
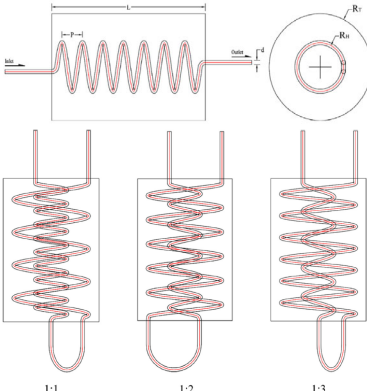
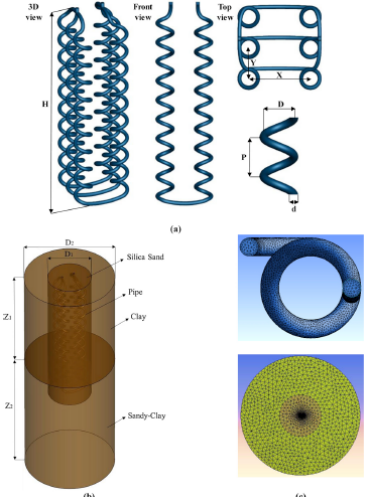
**Table 7.** Various examples of works related to utilizing coil/helical/spiral tubes for heat transfer enhancement.

Author	Year	Type of Study	Application	Working Fluid	Geometry	Remarks
Andrzejczyk and Muszynski [199]	2017	Experimental	Heat Exchanger	Water		<ul style="list-style-type: none"> <li>- The influence of water mass flow and heat flux on the HTC is presented.</li> <li>- The experimental correlation for the investigated configurations is developed.</li> </ul>

Gholamalizadeh et al. [200]	2019	Numerical	Heat Exchanger	Water	 <p>Helical coil heat exchanger</p> <p>Cold wire insert circular cross section</p> <p>Cold wire insert rectangular cross section</p> <p>Cold wire insert "S" cross section</p>	<ul style="list-style-type: none"> <li>- The effect of inserts on heat transfer and pressure drop is investigated.</li> <li>- A correlation is proposed to predict the Nusselt number.</li> <li>- The maximum value of COP for the inlet mass flow rate of 0.1 is 2519.</li> </ul>
Palanisamy and Kumar [201]	2019	Experimental	Heat Exchanger	Carbon nanotubes/ Water nanofluids		<ul style="list-style-type: none"> <li>- The maximum overall heat transfer coefficient of nanofluids is 52% higher than the water at 0.5% nanofluid with the Dean number 4200.</li> </ul>
Alimoradi et al. [202]	2017	Numerical	Heat Exchanger	Water	 <p>fin parameters</p> <p><math>d_o = 120 \text{ mm}</math></p> <p><math>d_i = 40 \text{ mm}</math></p> <p><math>d = 12 \text{ mm}</math></p> <p><math>d_o = 10 \text{ mm}</math></p> <p><math>t = 1 \text{ mm}</math></p> <p><math>d_i = 10 \text{ mm}</math></p> <p><math>P_c = 10 \text{ mm}</math></p>	<ul style="list-style-type: none"> <li>- The annular fins were used on the outer surface of the helically coiled tube.</li> <li>- The maximum increase in the heat transfer rate was about 44.11%.</li> </ul>
Javadi et al. [203]	2019	Numerical	Borehole Heat Exchanger	Water	 <p>a</p> <p>b</p> <p>c</p> <p>d</p> <p>e</p> <p>f</p> <p>g</p> <p>h</p>	<ul style="list-style-type: none"> <li>- Eight new types of helical ground heat exchangers were proposed in terms of the heat exchange rate.</li> <li>- The triple helix ground heat exchanger achieved the best thermal performance considerably.</li> </ul>



Afsharpanah et al. [204]	2019	Numerical	Ice Storage	Water/Ethylene Glycol		<ul style="list-style-type: none"> <li>- A double-helical coil heat exchanger was evaluated in the charging process of an ice storage system with a volume of 15 L.</li> <li>- The results indicated that with higher values for pitch length and inner and outer coil distance, compared to the smallest values for these parameters, the distribution of ice formed in the storage improves, and the rate of ice formation increases by 22.81% and 13.99%, respectively.</li> </ul>
Pakzad et al. [205]	2019	Numerical	Ice Storage	Water/Ethylene Glycol		<ul style="list-style-type: none"> <li>- An ice storage system was equipped with a serpentine tube heat exchanger.</li> <li>- The ice formation rate for the highest distance between serpentine tube rows compared to the lowest distance between serpentine tube rows is higher by 24.68%.</li> <li>- The smallest tube diameter shows an almost 5.9% greater ice formation rate than the case with the largest tube diameter.</li> </ul>
Saydam et al. [206]	2019	Experimental	TES	Water		<ul style="list-style-type: none"> <li>- A prototype PCM heat exchanger with a helical coil tube was designed, fabricated, and experimentally analyzed for its thermal storage performance under different operational conditions.</li> <li>- Increasing the HTF inlet temperature from 70 to 75 °C shortens the charging time by 35%, while the charging time is reduced up to 21% by increasing the flow rate from 0.5 to 4 L/min.</li> </ul>

Mousavi Ajarostaghi et al. [207]	2019	Numerical	Ice Storage	Water/Ethylene Glycol		<ul style="list-style-type: none"> <li>- Increasing the coil pitch by 200% decreases the melting rate by 4.7%.</li> <li>- By increasing the coil diameter by 37.5%, the melting rate decreases by 31.0% after 266.7 min.</li> <li>- The coil height has an opposite effect on the melting rate so that by increasing it by 75%, at <math>t = 160</math> min, the melting rate is increased only by 1.32%.</li> </ul>
Zheng et al. [208]	2018	Numerical	TES	Water		<ul style="list-style-type: none"> <li>- The optimal structures of the LHTEs system with single and double coil tubes were determined using the quasi-steady state method.</li> <li>- The heat storage performance of the LHTEs system with a double coil tube is better than that of a single coil tube.</li> </ul>
Javadi et al. [209]	2019	Numerical	Borehole Heat Exchanger	Water		<ul style="list-style-type: none"> <li>- A new type of helical ground heat exchanger (triple helix) was introduced.</li> <li>- The effects of various geometric parameters on heat exchanger performance were studied.</li> <li>- Helical coil length is the most influential parameter in heat exchanger performance.</li> <li>- Proposed equations are capable of predicting the thermal properties of the heat exchanger.</li> </ul>

### 2.5. Rough Surfaces

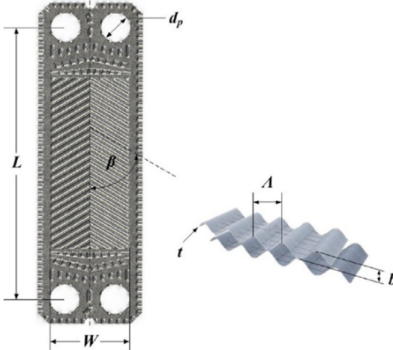

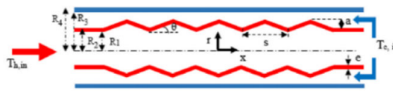
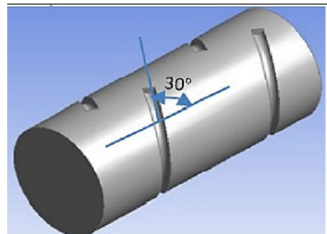
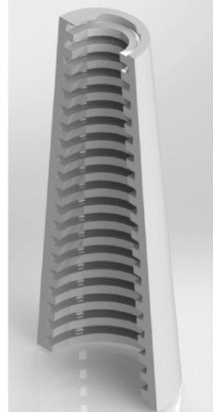
In recent decades, rough/corrugated/ribbed surfaces have been considered as one of the most effective passive heat transfer enhancement techniques for different systems [209–214]. Table 8 shows various examples of rough surfaces for heat transfer enhancement. The heat transfer enhancement mechanism of rough surfaces generally induces the flows to collide to improve flow mixing. Moreover, because of the long path of rough surfaces, the thermal performance of the systems improves significantly compared to that of a smooth surface. More importantly, intermittently interrupting and redeveloping the

boundary layers caused by the corrugated channels enhances the heat transfer markedly. The height, pitch, arrangement, and shape of rough surfaces are the most common geometrical parameters affecting thermal performance. Different types of channel corrugation that directly impact heat transfer and pressure drop rates of the thermal systems are the rectangular corrugated channel, trapezoidal-shaped corrugated channel, sharp corrugated channel, triangular-shaped corrugated channel, arc-shaped corrugated channel, and sinusoidal corrugated channel.

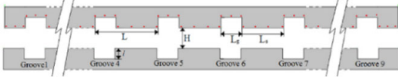
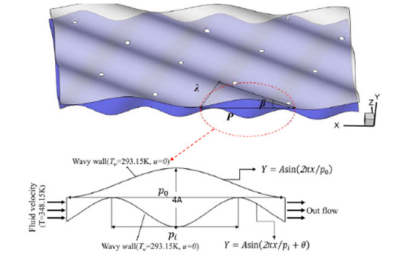
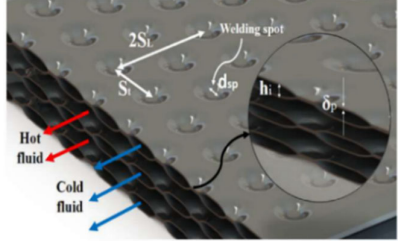
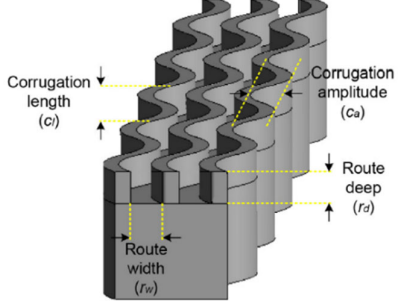
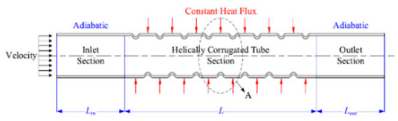
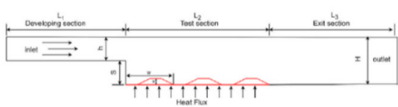


Elshafei et al. [215] investigated heat transfer and pressure drop changes inside a sharp corrugated channel under constant wall temperature. It was found that the maximum thermal performance is achieved at a phase shift of  $180^\circ$  and with lower space variation of the corrugated channels. The impact of wavy plate phase shift on heat transfer and airflow inside a sinusoidal corrugated channel under constant wall temperature was studied numerically by Yin et al. [216]. Based on the results, the most suitable phase angle is  $0^\circ$  for airflow using low Reynolds numbers. Moreover, the thermal performance can be improved when the Reynolds number is at lower values. Sui et al. [217] numerically examined the airflow and heat transfer in a sinusoidal corrugated channel with rectangular cross-section under constant wall temperature. According to the outcomes, in the studied configuration, the thermal performance factor is more than unity, which means that the heat transfer increased significantly, justifying the pressure drop increment.

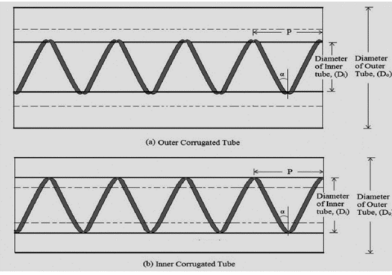
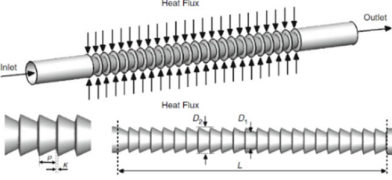
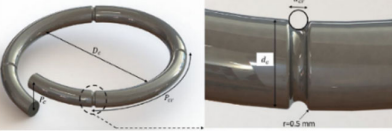
In another study, the influence of buoyancy force on the convection heat transfer of a turbulent flow through a sinusoidal corrugated channel under constant wall heat flux was evaluated numerically by Forooghi and Hooman [218]. It was concluded that to increase the heat transfer rate and the aspect ratio of the channels, it is necessary to create superior levels of buoyancy. Sui et al. [219] numerically studied heat transfer and laminar fluid flow inside a wavy microchannel (sinusoidal corrugated channel) under fixed wall heat flux and fixed wall temperature. It was indicated that the thermal performance is enhanced by increasing the relative waviness. Sarkar et al. [220] performed a numerical simulation to evaluate the heat transfer and fluid flow inside a furrowed wavy channel (sinusoidal corrugated channel) considering various wave amplitudes and wavelengths under a constant wall temperature. As the ratio of amplitude and hydraulic diameter and the ratio of wavelength and hydraulic diameter increase, the thermal performance also improves. The influence of pulsating fluid flow on the heat transfer characteristic inside a sinusoidal corrugated channel is investigated numerically [221]. The thermal performance could be improved considerably by providing oscillating amplitude. The variation of heat transfer and fluid flow inside a rectangular corrugated channel under constant wall temperature was examined experimentally and numerically by Tokgoz et al. [222]. It was concluded that the phase shift of  $0^\circ$  is the most desirable phase shift for enhancing thermal performance. The pressure drop and heat transfer inside an arc-shaped corrugated channel were studied experimentally and numerically by Paisarn [223]. It was proved that heat transfer could be enhanced in the corrugated channel because of its recirculation regions compared to the plain channel. Three different corrugated channel configurations, including sinusoidal, trapezoidal, and triangular, were compared numerically under constant wall heat flux in terms of heat transfer, entropy generation, and pressure drop by Akbarzadeh et al. [224]. Based on the results, a sinusoidal-shaped corrugated channel was chosen as the best one to provide the minimum entropy generation and the maximum thermal performance. Huang and Pan [225] numerically studied the heat transfer enhancement of microchannels with various configurations, including a microchannel with ribs and a microchannel with cavities, compared to a smooth microchannel. According to the entransy method, i.e., assessing the thermal performance based on irreversibility, the secondary heat transfer enhancement design, which interrupts the growth of thermal and hydrodynamic boundary layers, creates superior convective heat transfer performance and lower entransy dissipation in the microchannel heat sinks.

**Table 8.** Various examples of rough surfaces used for heat transfer enhancement.

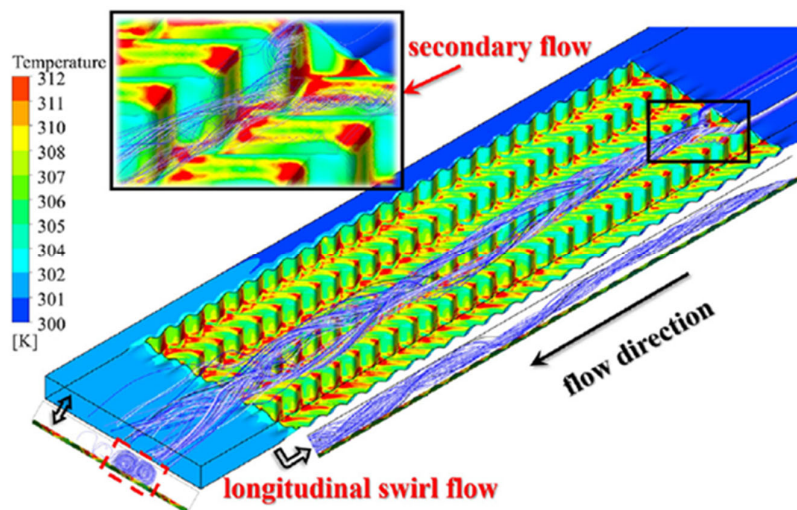
Author	Year	Type of Study	Application	Working Fluid	Geometry	Remarks
Soon-tarapiromsook et al. [226]	2020	Experimental	Plate heat exchanger	R-134a		- Thermal performance could improve between 46.12–102.20% by increasing the surface roughness compared to the smooth surface.
Akbarzadeh and Valipour [227]	2020	Experimental	Parabolic trough collector	Water		- The maximum thermal performance enhancement is 107.2% using the corrugated tube compared to the smooth tube.
Begag et al. [228]	2021	Numerical	Concentric mini-tube heat exchanger	Water		- Thermal performance improves up to 60% by applying the corrugated surface compared to the smooth surface.
Al-Obaidi and Alhamid [229]	2021	Numerical	Pipe heat exchanger	Water		- The pipe with a corrugated arc ring angle achieves a better thermal performance—about 1.3 times better than the smooth pipe.
Ashouri et al. [230]	2021	Experimental	Pool boiling heat transfer	Water		- The thermal performance is enhanced by 1302% and 19.8%, respectively, in the rotating and stationary modes, compared to the plain surface.

Mazhar et al. [231]	2021	Numerical	Pipe in a PCM	Water		<p>- The thermal performance is enhanced by 2.4 and 3.1 times in the solidification and melting modes, respectively, compared to the smooth tube.</p>
Dong et al. [232]	2021	Numerical	Solar air heater	Air		<p>- The thermal performance improves by 94% using inclined grooves compared to the plain surface.</p>
Cruz et al. [233]	2021	Experimental- Numerical	Helical tube	Water		<p>- The maximum thermal performance (up to 5 times) can be obtained using a tube with the lowest pitch when compared to the smooth tube.</p>
Khoshvaghht-Aliabadi and Feizabadi [234]	2020	Numerical	Helical channel with a square cross-section	Water		<p>- The maximum thermal performance of up to 1.46 times greater than the smooth tube can be achieved by applying a tube with a larger corrugation amplitude.</p>

Zontul et al. [235]	2021	Experimental-Numerical	Channel	Water		- Thermal performance increases by 2.5 times compared to a plain channel.
Qingchan et al. [236]	2021	Numerical	Plate heat exchanger	-		- Thermal performance could increase considerably (about 280 times) by applying a wavy wall compared to the plain wall.
Shirzad et al. [237]	2019	Numerical	Pillow plate heat exchanger	Water		- Thermal performance could increase (about four times) by increasing the height of the pillow plate channel compared to a plain channel.
Khoshvaght-Aliabadi et al. [238]	2021	Numerical	Miniature heat sink	Water		- Thermal performance can be enhanced by 34% using the corrugated surface where the cross-section diverges.
Hu et al. [239]	2021	Numerical	Intermediate heat exchanger	Water		- A helically corrugated tube increases the thermal performance up to 1.69 times compared to the smooth tube.
Talib and Hilo [240]	2021	Experimental-Numerical	Backward-facing step channel	Water		- Thermal performance improves by almost 40% compared to a plain channel.
Al-Obaidi and Jassim Alhamid [241]	2021	Numerical	Pipe	Water		- A corrugated configuration increases the thermal performance up to 1.65 times compared to the smooth tube.
Yang et al. [242]	2021	Numerical	Coaxial heat exchanger	-		- A hybrid smooth and spirally corrugated tube could increase the thermal performance (about 1.7 times) compared to the smooth tube.

Chaurasiya et al. [243]	2021	Numerical	Double pipe heat exchanger	Water		<p>- An externally corrugated inner tube could achieve a better rate of thermal performance (about 1.17 times) compared to the internally corrugated inner tube.</p>
Hamedani et al. [244]	2020	Numerical	Double pipe heat exchanger	Water		<p>- A higher large diameter of the cone, lower small diameter of the cone, and lower pitch and high roughness of the convergent-divergent tube could enhance the thermal performance compared to the smooth tube.</p>
Chen et al. [245]	2021	Numerical	Helical tube	Water		<p>- A corrugated configuration increases the thermal performance up to 1.01 times compared to the smooth tube.</p>

To better understand the influence of the rough surfaces on the flow structure and heat transfer enhancement mechanism of the systems, streamlines of the air flowing through a pair of inclined grooves are illustrated in Figure 8. As can be seen, the inclined grooves induce part of the air near the rippling surface, resulting in deviating the airflow from the main direction. In this configuration, due to the symmetrical arrangement of the rippling surfaces in the duct, the diverged airflows run into each other close to the heated wall. Consequently, longitudinal swirl flows and secondary flows have been created after the upwards movement of the airflow and the generation of a bulk flow.



**Figure 8.** Streamlines of the air flowing through the inclined grooves [232]. (Reprinted from Dong, Z.; Liu, P.; Xiao, H.; Liu, Z.; Liu, W. A study on heat transfer enhancement for solar air heaters with ripple surface. *Renew. Energy* 2021, 172, 477–487. Copyright (2021), with permission from Elsevier).

## 2.6. Nanofluids

Another enhancement of the passive heat transfer techniques can be achieved by altering the thermophysical properties of the heat transfer/working fluid [246,247].

### 2.6.1. Mono Nanofluid

Mono nanofluids are made of stable suspensions of high-thermal-conductive carbon, metallic, and non-metallic-based single nanoparticles suspended in ordinary heat transfer/working fluids, called base fluids, such as ethylene, water, acetone, glycol, oil, etc. For example, carbon-based nanoparticles are carbon nanofiber, graphene, carbon nanotube, graphite, and graphene oxide, while metallic-based nanoparticles include copper, gold, silver, titanium dioxide, copper oxide, aluminum oxide, silica, and zinc oxide. Mono nanofluids are well known because of their superior thermophysical properties, including their convective heat transfer coefficient, thermal diffusivity, and thermal conductivity when compared to conventional base fluids. Hence, mono nanofluids have displayed outstanding performance in heat transfer enhancement applications. Table 9 indicates various examples of mono nanofluids used for heat transfer enhancement. Prominent specifications of mono nanofluids are presented in Figure 9. However, despite the better thermal conductivity of mono nanofluids compared to the base fluids, it has been shown that the specific heat capacity of mono nanofluids decreases and the viscosity and density increase under certain conditions, which are not desirable for the systems' thermal performance. The thermal performance of a system is highly dependent on the thermophysical properties of the mono nanofluids, which can be obtained as follows [237,244]:

The density of mono nanofluids:

$$\rho_{NF} = \phi\rho_{NP} + (1-\phi)\rho_{BF} \quad (1)$$

The specific heat capacity of mono nanofluids:

$$(C_p)_{NF} = \frac{\phi(\rho C_p)_{NP} + (1-\phi)(\rho C_p)_{BF}}{\rho_{NF}} \quad (2)$$

The viscosity of mono nanofluids:

$$\mu_{NF} = \frac{\mu_{BF}}{(1-\phi)^{2.5}} \quad (3)$$

The thermal conductivity of mono nanofluids:

$$k_{NF} = k_{BF} \left[ \frac{k_{BF} + k_{NP} + nk_{BF} + \phi(k_{NP} - k_{BF}) - n\phi(k_{BF} - k_{NP})}{k_{BF} + k_{NP} + nk_{BF} + \phi(k_{BF} - k_{NP})} \right] \quad (4)$$

where  $n$  indicates the shape factor of the nanoparticles (Sphere:  $n = 3$ , Brick:  $n = 3.7$ , Cylinder:  $n = 4.9$ , Platelet:  $n = 5.7$ , Blade:  $n = 8.6$ ), and  $\phi$  is the volume fraction of the nanoparticles. The NF, BF, and NP subscripts represent the nanofluid, base fluid, and nanoparticle, respectively.



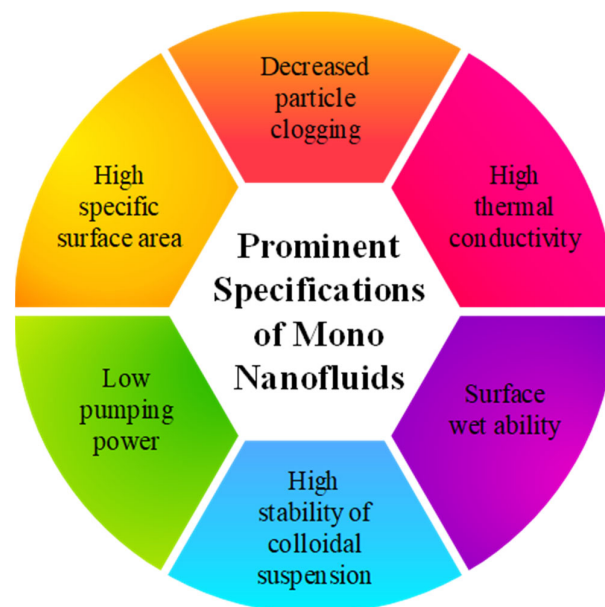
**Table 9.** Various examples of mono nanofluids for use in heat transfer enhancement.

Author	Year	Type of Study	Base Fluid	Nanoparticle	Concentration	Application	Remarks
Muruganandam et al. [248]	2020	Experimental	Water	Multi-wall carbon nanotube	0.1, 0.3, 0.5 vol%	Internal combustion engine	- Thermal performance increases by 18% compared to the base fluid.
Rasheed et al. [249]	2021	Experimental-Numerical	Water	Al <sub>2</sub> O <sub>3</sub> ; ZnO	1, 1.5, 2 vol%	Shell and helical microtube heat exchanger	- Al <sub>2</sub> O <sub>3</sub> /water could achieve a higher rate of thermal performance than ZnO/water.
Tong et al. [250]	2019	Experimental	Water	Al <sub>2</sub> O <sub>3</sub> ; CuO	0.1–1.5 vol%	Solar collector	- Al <sub>2</sub> O <sub>3</sub> /water and CuO/water nanofluids could improve the thermal performance by 21.9% and 16.2%, respectively, compared to the base fluid.
Ahmed et al. [251]	2021	Numerical	Water	Al <sub>2</sub> O <sub>3</sub>	1, 4 vol%	Mini channel	- Thermal performance increases by 32% compared to the base fluid.
Lari et al. [252]	2017	Numerical	Water	Ag	0.5 vol%	Photovoltaic/Thermal system	- Thermal performance increases by 18% compared to the base fluid. - Energy cost decreases by 82% compared to the regular price.
Nithyanantham et al. [253]	2020	Experimental	Eutectic salt	Al <sub>2</sub> O <sub>3</sub>	1 wt%	TES	- Thermal performance increases by 20% compared to the base fluid. Specific heat capacity improves by 6% compared to the base fluid.
Chaudhari et al. [254]	2019	Experimental	Water	Al <sub>2</sub> O <sub>3</sub> ; CuO	1 vol%	Machining	- Al <sub>2</sub> O <sub>3</sub> /water and CuO/water nanofluids could improve the thermal performance by 19.74% and 36.21%, respectively, compared to the base fluid.

Teruel et al. [255]	2019	Experimental	Diphenyl + Diphenyl oxide	MoSe <sub>2</sub>	-	Concentrating solar power	- Diffusivity and specific heat capacity improves by 4% and 7%, respectively. - Thermal performance increases by 11% compared to the base fluid.
Esmaeili-Faraj et al. [256]	2019	Experimental	Water	Synthesized silica; Exfoliated graphene oxide	0.02, 0.1 wt%	Bioscrubber	- Synthesized silica is better than exfoliated graphene oxide in improving the thermal performance of the bioscrubber.
Nazari et al. [257]	2019	Experimental-Analytical	Water	Cu <sub>2</sub> O	0.08 vol%	Solar still	- Exergy, productivity and energy increases by 92.6%, 82.4%, and 81.5%, respectively, compared to the base fluid.
Soltani et al. [258]	2017	Experimental	Water	SiO <sub>2</sub> ; Fe <sub>3</sub> O <sub>4</sub>	-	Hybrid photovoltaic/Thermoelectric system	- SiO <sub>2</sub> /water nanofluid cooling improves the power production and thermal performance by 54.29% and 3.35%, respectively, compared to other cooling methods.
Ahammed et al. [259]	2016	Experimental	Water	Al <sub>2</sub> O <sub>3</sub>	0.1, 0.2 vol%	Multiport minichannel heat exchanger	- Thermal performance increases by 40% compared to the base fluid.
Mohammadian et al. [260]	2014	Numerical	Water	Al <sub>2</sub> O <sub>3</sub>	-	Micro-pin-fin heat exchanger	- Thermal performance and entropy generation could increase and decrease, respectively, compared to the base fluid.
Ahammed et al. [261]	2016	Experimental	Water	Graphene	0.1 vol%	Multiport minichannel heat exchanger	- Thermal performance and cooling capacity increases by 72% compared to the base fluid. - The convective heat transfer coefficient improves by 88.62% compared to the base fluid.
Karana et al. [262]	2018	Theoretical	Water + Ethylene glycol	MgO; ZnO	1 vol%	Automotive waste heat recovery system	- MgO/water + ethylene glycol nanofluid increases the thermal performance and power output by 10.95% and 11.38%, respectively, compared to the base fluid.

Duan et al. [263]	2017	Experimental	Water	Carbon nanotube; Al <sub>2</sub> O <sub>3</sub>	-	Personal cooling system	- Both nanofluids could improve the heat density (up to 55%) compared to the base fluid.
Javadi et al. [264]	2020	Numerical	Paraffin	Cu; CuO; Al <sub>2</sub> O <sub>3</sub> ; TiO <sub>2</sub> ; SiO <sub>2</sub> ; Multi-wall carbon nanotube; Graphene	5, 10, 15, 20 vol%	Borehole heat exchanger	- Cu/Paraffin and SiO <sub>2</sub> /Paraffin are the best and worst NEPCMs, respectively, when used as backfill/grout for improving thermal performance compared to the base fluid.
Shirzad et al. [265]	2019	Numerical	Water	Al <sub>2</sub> O <sub>3</sub> ; CuO; TiO <sub>2</sub>	2–5 vol%	Pillow plate heat exchanger	- Al <sub>2</sub> O <sub>3</sub> /water at 2% of concentration is found to be better than the other nanofluids in improving thermal performance.
Hamedani et al. [244]	2019	Numerical	Water	Al <sub>2</sub> O <sub>3</sub> ; CuO	2–5 vol%	Convergent–divergent tube	- Al <sub>2</sub> O <sub>3</sub> /water at 4% concentration improves the thermal performance by 9.29% compared to the base fluid.
Zaboli et al. [266]	2019	Numerical	Water	Al <sub>2</sub> O <sub>3</sub> ; CuO; SiO <sub>2</sub>	2–5 vol%	Shell and coil tube heat exchanger	- CuO/water could achieve the highest thermal performance compared to the other nanofluids.
Mousavi Ajarostaghi et al. [267]	2020	Numerical	Water	Al <sub>2</sub> O <sub>3</sub> ; Cu; CuO; TiO <sub>2</sub>	2–5 vol%	Round tubular heat exchanger	- Cu/water and CuO/water are found to be the best and worst nanofluids, respectively, in improving the thermal performance compared to the other nanofluids.
Noorbakhsh et al. [268]	2021	Numerical	Water	Al <sub>2</sub> O <sub>3</sub> ; CuO; SiO <sub>2</sub>	2–5 vol%	Double-pipe heat exchanger	- CuO/water by 7% and SiO <sub>2</sub> /water by 2.5% could obtain the maximum and minimum thermal performance improvements compared to the base fluid.
Zaboli et al. [269]	2021	Numerical	Water	Al <sub>2</sub> O <sub>3</sub> ; CuO; SiO <sub>2</sub>	1.5, 3, 4, 5 vol%	Shell and corrugated coil tube heat exchanger	- CuO/water proves to be the best nanofluid in enhancing thermal performance compared to the other nanofluids.

Shahi et al. [270]	2020	Numerical	Water	Cu	-	Cold plate	- Applying Cu/water nanofluid as a liquid-cooling method for electronic equipment is much better than air-cooling methods by significantly improving the heat transfer rate thanks to its higher specific heat capacity and thermal conductivity.
Yang et al. [271]	2021	Experimental- Numerical	Water	TiO <sub>2</sub> ; Al <sub>2</sub> O <sub>3</sub> ; SiO <sub>2</sub>	0.1, 0.2, 0.3 vol%	Backward-step structure microchannel	- With the base fluid of water, the Nusselt numbers of Al <sub>2</sub> O <sub>3</sub> , SiO <sub>2</sub> , and TiO <sub>2</sub> are approximately 1.48, 1.25, and 1.28 times greater, respectively, than those using pure water.
Niazmand et al. [272]	2019	Numerical	Water	Cu	0, 1, 5 vol%	Cylindrical lid-driven cavity	-The influence of the volume fraction of Cu/water nanofluid on the thermal domain and flow is negligible. Nevertheless, the heat transfer rate and the Nusselt number can be notably enhanced when using the nanofluid, but with higher values of the Reynolds number.
Niazmand et al. [273]	2020	Numerical	Oil	Al <sub>2</sub> O <sub>3</sub>	0–5 vol%	Heat sink	- The usage of Al <sub>2</sub> O <sub>3</sub> /Oil nanofluid as the liquid immersion cooling process presents much more efficient heat transferring than with air cooling.



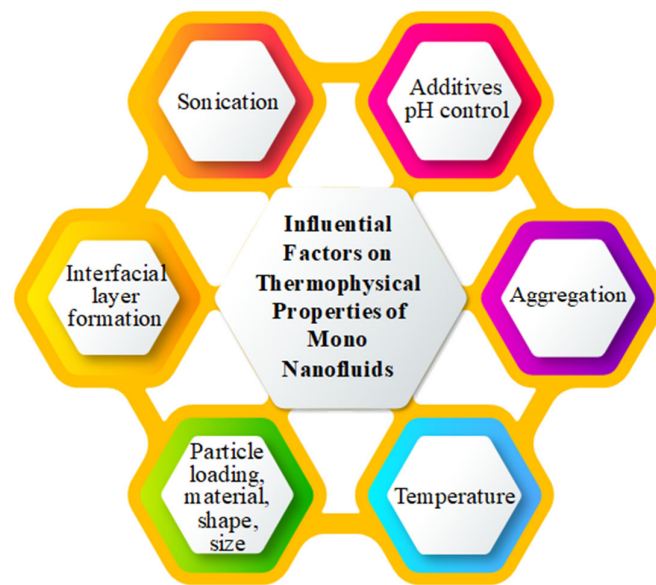
**Figure 9.** Prominent specifications of mono nanofluids.

Kristiawan et al. [274] numerically studied the influence of employing two passive heat transfer improvement methods, including a microfin structure and nanofluids, on thermal performance.  $\text{TiO}_2/\text{water}$  was considered as the nanofluid. The results indicated that the heat transfer rate could be augmented by the utilization of nanofluid with a volume fraction of 0.01%. In other work, Kristiawan et al. [275] numerically analyzed the heat transfer process of a titania-based nanofluid flow inside a circular tube under the boundary condition of a horizontal uniformly heated wall for both laminar and turbulent flows. The impact of the nanoparticle volume concentration and the Re number (4000–14,000) on the hydrothermal behavior were investigated. The results showed that nanoparticles significantly improved the heat transfer rate at the laminar and turbulent flows. Rifa'i et al. [276] studied the heat transfer process of water/ $\text{TiO}_2$  flow in a counter-flow double-tube heat exchanger. The results displayed that the heat transfer rate of the nanofluid is higher than the base fluid for the same mass flow rate and inlet temperature. The Nu number rises by increasing the Re number and the nanofluid volume concentration. Kristiawan et al. [277] studied numerically the  $\text{TiO}_2/\text{water}$  nanofluids flow and heat transfer process in a double-tube heat exchanger equipped with a helical microfin. The obtained numerical outcomes depicted that the Nu number augments as the turbulence Re number increases. Moreover, the thermal performance in the case using nanofluids was better than the case using pure water. Although some passive methods, such as using inserts [278,279], can cause more chaotic flows and swirl flows and, consequently, a greater heat transfer rate, the results showed that combining these methods with nanofluid could significantly enhance the heat transfer rate.

The greater the thermophysical properties of the heat transfer/working fluid, the more portable and compact the industrial equipment, the more cost-effective the operation, the better the thermal performance, and the more environmentally friendly the system could be. Figure 10 shows the factors influencing the thermophysical properties of mono nanofluids. A mono nanofluid comprises a core made of nanoparticles, an interfacial layer with intermediate characteristics, and the base fluid that merges these two parts. The mixture produced acts like a multiphase system where the phase superposition is the most crucial matter influencing the thermophysical properties of the mono nanofluids, particularly thermal conductivity. On the other hand, there are some challenges with using mono nanofluids, as presented in Figure 11. For instance, one of the principal prob-

lems in creating good nanoparticle suspensions in all nanopowder technologies is the agglomerating of nanoparticles. Accordingly, the synthesis and suspension of uniformly dispersed or non-agglomerated nanofluids have a considerable impact on the heat transfer enhancement of mono nanofluids. Another critical factor affecting the heat transfer specifications of mono nanofluids is stability, i.e., a feature showing that the nanoparticles do not aggregate at a high rate. The nanofluids' thermophysical properties and periodic stability depend greatly on agglomerating and clogging, which occur during the formation process of mono nanofluids. The addition of surfactants or dispersants is one of the simplest and most economical ways to improve the stability of mono nanofluids by decreasing the surface tension of the base fluid and consequently increasing the nanoparticles' solubility.

Furthermore, the volume concentration and pH level have been considered as two factors that considerably affect the thermal conductivity of mono nanofluids. For example, at a certain pH level, the potential for agglomerating increases as the repulsive force among the nanoparticles reduces to zero. Thus, thermal conductivity and the mobility of the nanoparticles can be improved by increasing the difference in the pH level, which generates hydration forces. In addition to the factors mentioned above, another feature, called Brownian motion, i.e., a random thermal motion that prevents the sedimentation of particles in a mono nanofluid, increases the effective dispersion of the nanoparticles.



**Figure 10.** Factors influencing the thermophysical properties of mono nanofluids.

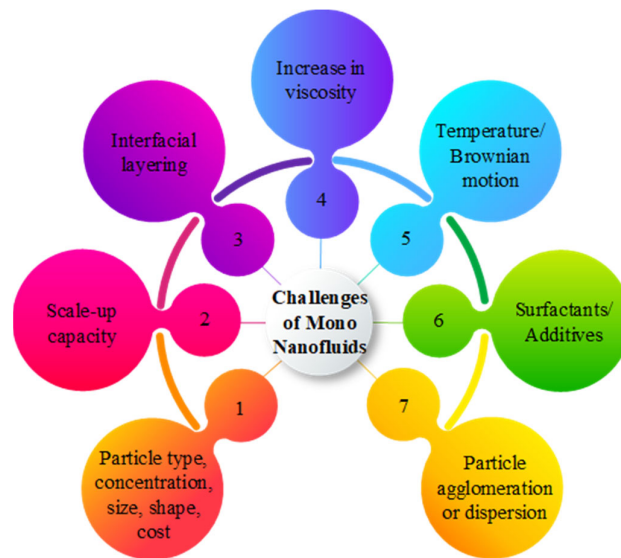


Figure 11. Challenges of mono nanofluids.

### 2.6.2. Hybrid Nanofluids

A new type of nanofluid, called a hybrid nanofluid, has recently been developed, attracting drawing attention because of its high stability, good chemical inertness, and enhanced thermophysical properties. Hybrid nanofluids have a combination of various desirable features of different nanoparticles combined in one single fluid, where two or more nanoparticles are dispersed into the base fluid to obtain better rheological and thermophysical properties. The shape, size, compatibility, purity, and dispersibility of nanoparticles significantly influence the performance of hybrid nanofluids. In addition, factors such as the volume concentration, surfactants, temperature, dispersion method, sonication method/time, shape and size, pH level, base fluid, and the type of nanoparticles notably affect the stability of hybrid nanofluids. As illustrated in Figure 12, hybrid nanofluids have been widely used in numerous heat transfer enhancement applications. Various examples of hybrid nanofluids used for heat transfer enhancement are presented in Table 10.

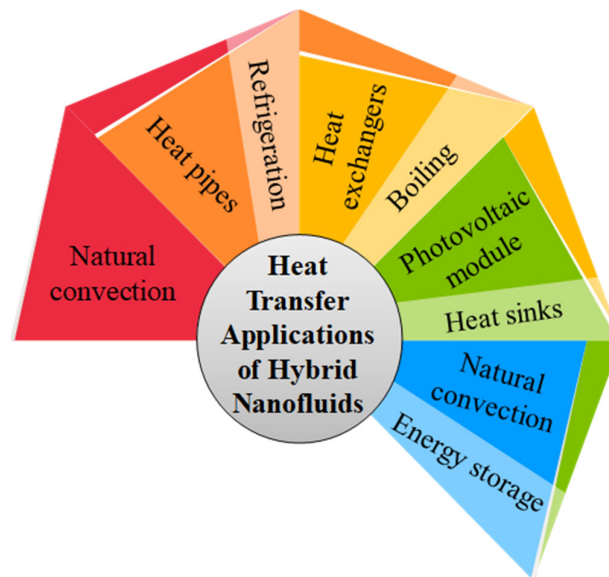
Table 10. Various examples of hybrid nanofluids used for heat transfer enhancement.

Author	Year	Type of Study	Base Fluid	Nanoparticle Concentration	Application	Remarks
Hussien et al. [280]	2017	Experimental	Water	Multi-wall carbon nano-tubes and Graphene nano-platelets 0.075, 0.125, 0.25 wt%	Mini circular tube with constant heat flux	- Thermal performance increases by 33.5%, with an increase of 11% in pressure drop compared to the base fluid.
Hamid et al. [281]	2018	Experimental	Water + Ethylene glycol	TiO <sub>2</sub> -SiO <sub>2</sub> 1 vol%	Circular tube with constant heat flux	- Thermal performance increases by 35.3%, while the friction factor also increases compared to the base fluid.

Nabil et al. [282]	2017	Experimental	Water + Ethylene glycol	TiO <sub>2</sub> -SiO <sub>2</sub>	0.5–3 vol%	Circular tube with constant heat flux	- Thermal performance increases by 80.9%, while the friction factor also increases compared to the base fluid.
Hussien et al. [283]	2019	Experimental	Water	Multi-wall carbon nanotubes and Graphene nanoplatelets	0–0.125 wt%	Circular micro tube with constant heat flux	- Thermal performance increases by 58.2%, with an increase of 12.4% in pressure drop compared to the base fluid.
Bahiraee et al. [284]	2018	Numerical	Water	Carbon nanotubes-Fe <sub>3</sub> O <sub>4</sub>	-	Double-pipe counterflow minichannel heat exchanger	- The maximum thermal performance improvement is 53.8% compared to the base fluid.
Singh et al. [285]	2018	Numerical	Water	Al <sub>2</sub> O <sub>3</sub> -Multi-wall carbon nanotubes; Al <sub>2</sub> O <sub>3</sub> -Ag; Al <sub>2</sub> O <sub>3</sub> -Cu; Al <sub>2</sub> O <sub>3</sub> -TiO <sub>2</sub>	0–1 vol%	Shell-and-tube condenser	- Al <sub>2</sub> O <sub>3</sub> -Ag/water could achieve the maximum thermal performance improvement of about 3.2% compared to the base fluid.
Anitha et al. [286]	2019	Numerical-Experimental	Water	Al <sub>2</sub> O <sub>3</sub> -Cu	0–0.2 vol%	Shell-and-tube heat exchanger	- Thermal performance increases by 139% compared to the base fluid.
Hung et al. [287]	2017	Experimental	Water	Hybrid carbon nanofluid	0.005–0.02 wt%	Air-cooled finned-tube heat exchanger	- Thermal performance increases by 11.7% compared to the base fluid.
Sahoo et al. [288]	2017	Numerical	Water	Al <sub>2</sub> O <sub>3</sub> -Ag; Al <sub>2</sub> O <sub>3</sub> -Cu; Al <sub>2</sub> O <sub>3</sub> -CuO; Al <sub>2</sub> O <sub>3</sub> -Fe <sub>2</sub> O <sub>3</sub> ; Al <sub>2</sub> O <sub>3</sub> -TiO <sub>2</sub>	-	Louver-finned flat-tube heat exchanger	- Al <sub>2</sub> O <sub>3</sub> -Ag/water could obtain the maximum thermal performance improvement of 3%, with an increase of 7.3% in pressure drop compared to the base fluid.
Sahoo et al. [289]	2017	Numerical	Ethylene glycol	Al <sub>2</sub> O <sub>3</sub> -Ag; Al <sub>2</sub> O <sub>3</sub> -Cu; Al <sub>2</sub> O <sub>3</sub> -SiC; Al <sub>2</sub> O <sub>3</sub> -CuO; Al <sub>2</sub> O <sub>3</sub> -TiO <sub>2</sub>	-	Louver-finned flat-tube heat exchanger	- Al <sub>2</sub> O <sub>3</sub> -Ag/Ethylene glycol could obtain the maximum thermal performance improvement of 5.4%, while the pressure drop increases compared to the base fluid.
Huminić et al. [290]	2018	Numerical	Water	Multi-wall carbon nanotubes-Fe <sub>3</sub> O <sub>4</sub> ; ND-Fe <sub>3</sub> O <sub>4</sub>	0–0.3 vol%	Flattened-tube automobile radiator	- Multi-wall carbon nanotubes and Fe <sub>3</sub> O <sub>4</sub> /water could achieve the maximum thermal performance improvement of about 21%, followed by ND-Fe <sub>3</sub> O <sub>4</sub> /water with 15%, compared to the base fluid.
Huminić et al. [291]	2019	Numerical	Ethylene glycol	MgO-Multi-wall carbon nanotubes	0–0.4 vol%	Flattened-tube automobile radiator	- Thermal performance increased by 16.3% compared to the base fluid.



Returi et al. [292]	2019	Numerical	Water	Al <sub>2</sub> O <sub>3</sub> -CuO; Al <sub>2</sub> O <sub>3</sub> -TiO <sub>2</sub>	2–4 vol%	Spiral plate heat exchanger	- Al <sub>2</sub> O <sub>3</sub> -CuO/water could obtain a thermal performance enhancement of about 10% better than Al <sub>2</sub> O <sub>3</sub> -TiO <sub>2</sub> /water.
Bhattad et al. [293]	2020	Experimental	Water	Al <sub>2</sub> O <sub>3</sub> -SiC; Al <sub>2</sub> O <sub>3</sub> -AlN; Al <sub>2</sub> O <sub>3</sub> -Mg; Al <sub>2</sub> O <sub>3</sub> -CuO; Al <sub>2</sub> O <sub>3</sub> -Multi-wall carbon nanotubes	0.1 vol%	Plate heat exchanger	- Al <sub>2</sub> O <sub>3</sub> -Multi-wall carbon nanotubes/water could obtain the maximum thermal performance improvement of 31.2% compared to the base fluid.
Bhattad et al. [294]	2019	Theoretical	Ethylene glycol-Water; Propylene glycol-Water	MgO-Ag; Al <sub>2</sub> O <sub>3</sub> -Ag	0–2 vol%	Plate heat exchanger	- Al <sub>2</sub> O <sub>3</sub> -Ag/Propylene glycol-water could obtain the maximum thermal performance improvement of 9.3% compared to the base fluid.
Uysal et al. [295]	2019	Numerical	Water	Diamond-Fe <sub>3</sub> O <sub>4</sub>	0.05–0.2 vol%	Rectangular minichannel	- Thermal performance increases by 30% compared to the base fluid.
Kumar et al. [296]	2018	Numerical	Water	Al <sub>2</sub> O <sub>3</sub> -Multi-wall carbon nanotubes	0.01 vol%	Minichannel heat sink	- Thermal performance increases by 15.6% compared to the base fluid.
Bahiraee et al. [297]	2019	Numerical	Water	Ag-Graphene	0–0.1 vol%	Microchannel heat sink	- Thermal performance increases by 17% compared to the base fluid.
Kumar et al. [298]	2019	Experimental	Water	Al <sub>2</sub> O <sub>3</sub> -Cu	0.1 vol%	Minichannel heat sink	- Thermal performance increases by 12.8% compared to the base fluid.
Javadi et al. [299]	2021	Numerical	Water	Ag-MgO; TiO <sub>2</sub> -Cu; Al <sub>2</sub> O <sub>3</sub> -CuO; Fe <sub>3</sub> O <sub>4</sub> -Multi-wall carbon nanotubes	5, 10, 15, 20 vol%	Borehole heat exchanger	- Ag-MgO/water could obtain the maximum thermal performance improvement of 37.02% while pressure drop increases, compared to the base fluid.
Zaboli et al. [135]	2021	Numerical	Water	Multi-wall carbon nanotubes-Fe <sub>3</sub> O <sub>4</sub> ; Ag-Graphene	1–4 vol%	Solar collector	- Multi-wall carbon nanotubes-Fe <sub>3</sub> O <sub>4</sub> /water could improve the thermal performance by 18.5% compared to the base fluid.
Mousavi Ajarostaghi et al. [300]	2021	Numerical	Water	Multi-wall carbon nanotubes-Fe <sub>3</sub> O <sub>4</sub> ; Ag-Graphene	1, 3, 5, 7 vol%	Pipe with vortex generator	- Multi-wall carbon nanotubes-Fe <sub>3</sub> O <sub>4</sub> /water could increase the thermal performance by 11.3% compared to the base fluid.
Hashemi Karouei et al. [301]	2021	Numerical	Water	Multi-wall carbon nanotubes-Fe <sub>3</sub> O <sub>4</sub> ; Ag-Graphene	-	Double-pipe heat exchanger	- Ag-Graphene/water could obtain higher thermal performance than the other nanofluids.



**Figure 12.** Heat transfer applications of hybrid nanofluids.

The equations related to the thermophysical properties of the hybrid nanofluids are given below [135,299–301]:

The density of a hybrid nanofluid:

$$\rho_{HNF} = \phi_{NP1}\rho_{NP1} + \phi_{NP2}\rho_{NP2} + (1 - \phi_{NP1} - \phi_{NP2})\rho_{BF} \quad (5)$$

The specific heat capacity of a hybrid nanofluid:

$$(C_p)_{HNF} = \frac{\phi_{NP1}(\rho C_p)_{NP1} + \phi_{NP2}(\rho C_p)_{NP2} + (1 - \phi_{NP1} - \phi_{NP2})(\rho C_p)_{BF}}{\rho_{HNF}} \quad (6)$$

The viscosity of a hybrid nanofluid:

$$\mu_{HNF} = \frac{\mu_{BF}}{(1 - \phi_{NP1} - \phi_{NP2})^{2.5}} \quad (7)$$

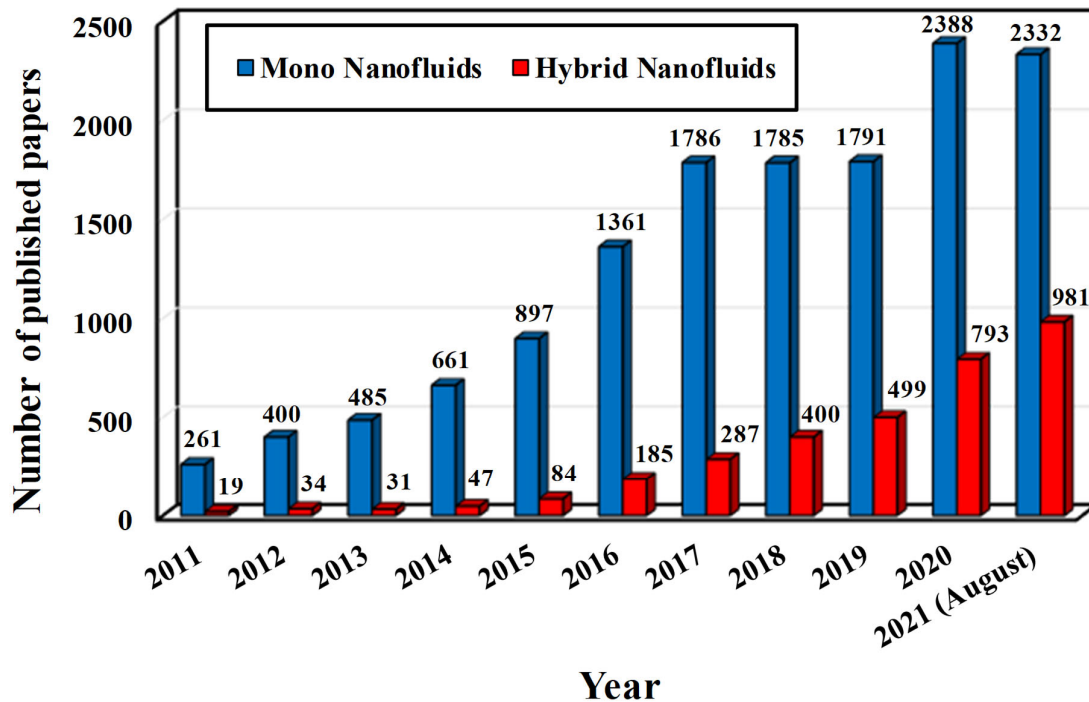
The thermal conductivity of a hybrid nanofluid:

$$k_{HNF} = \frac{2(\phi_{NP1}k_{NP1} + \phi_{NP2}k_{NP2}) - 2k_{BF}(\phi_{NP1} + \phi_{NP2}) + 2k_{BF} + \left[ \frac{\phi_{NP1}k_{NP1} + \phi_{NP2}k_{NP2}}{\phi_{NP1} + \phi_{NP2}} \right]}{-(\phi_{NP1}k_{NP1} + \phi_{NP2}k_{NP2}) - k_{BF}(\phi_{NP1} + \phi_{NP2}) + 2k_{BF} + \left[ \frac{\phi_{NP1}k_{NP1} + \phi_{NP2}k_{NP2}}{\phi_{NP1} + \phi_{NP2}} \right]} \quad (8)$$

The subscripts of *HNF*, *BF*, *NP1*, and *NP2* represent the hybrid nanofluid, the base fluid, nanoparticle 1, and nanoparticle 2, respectively.

The number breakdown of the published papers concerning mono nanofluids and hybrid nanofluids from 2011 to 2021 (according to ScienceDirect) is demonstrated in Figure 13. It can be seen that the number of published papers concerning mono nanofluids was 92% higher than those dealing with hybrid nanofluids in 2011. From 2012 to 2017, the difference in the number of published papers regarding mono nanofluids and hybrid nanofluids remained constant (almost 88% on average). Then, the number of published papers regarding hybrid nanofluids increased by 42% from 2017 to 2019, while the corresponding number regarding mono nanofluids was nearly fixed. After that, it can be seen that there was an increase of 25% in articles concerning mono nanofluids for the following

two years, whereas the number papers dealing with hybrid nanofluid experienced a growth of 50% during this period. Nevertheless, the difference between the corresponding numbers of published papers for these two types of working fluids is still considered high through 2021.



**Figure 13.** The number breakdown of the papers published concerning mono nanofluids and hybrid nanofluids in ScienceDirect from 2011 to 2021.

### 3. Conclusions

Given the several advantages of the heat transfer enhancement methods in various applications, many studies have examined their influence on the thermal performance of the energy conversion systems. Amongst the three types of heat transfer enhancement methods, this paper studied passive techniques thoroughly since they are reliable, cost-effective, and they do not require any extra power to promote the energy conversion systems' thermal efficiency when compared to the active and compound methods. The passive heat transfer enhancement methods considered were inserts (twisted tapes, conical strips, baffles, winglets), extended surfaces (fins), porous materials/surfaces, coil tubes, rough surfaces (corrugated/ribbed surfaces), and nanofluids (mono and hybrid nanofluids). The main conclusions derived are given as follows:

- The height, pitch, arrangement, and shape of rough surfaces are considered the geometrical parameters that considerably affect thermal performance. Among the various types of channel corrugation influencing the heat transfer and pressure drop of the systems, the sinusoidal corrugated channel is the most-studied type compared to the rectangular corrugated channel, trapezoidal-shaped corrugated channel, sharp corrugated channel, triangular-shaped corrugated channel, and the arc-shaped corrugated channel.
- Concerning the application of various types of foam for heat transfer augmentation, copper foams have been selected as an efficient method for electronic cooling applications and can be a great alternative to finned heat sinks. Moreover, the copper foam and the PCM composite remarkably increase the heat transfer rate and keep the

phase transition steady. The maximum reduction percentage in the charging time reported in the reviewed research works was approximately 89%.

- The reviewed literature on the enhancement technique of metal foam use exhibited that copper foam is the most-investigated thermal conductivity enhancer. Another type of foam is aluminum foam which showed superior potential in decreasing the melting rate when mixed with a PCM (up to 100%), thanks to its high conductivity. Furthermore, nickel foam is suitable for high-temperature uses because its thermal conductivity is relatively lower than copper and aluminum. Nevertheless, the effective thermal conductivity of a mixture of nickel foam and PCM increases, but the latent heat decreases. It should be noted that the balance should be considered, and it was shown here that the impact of metal foam on the thermal storage capacity has been less considered than its effect on the phase change process. Moreover, for high-temperature PCM applications, expanded graphite is known for its ability to considerably enhance the PCM composites' effective thermal conductivity (up to 183%) because of its durability and compatibility with high temperatures, without a notable decrease in thermal energy storage capacity.
- Nanofluids, including mono and hybrid nanofluids, have rheological and thermo-physical properties superior to those of the conventional heat transfer/working fluids, notably leading to an enhanced heat transfer rate. In contrast, the increase in pressure drop caused by hybrid nanofluids should be considered.

**Author Contributions:** Conceptualization, S.S.M.A., M.Z. and H.J.; methodology, S.S.M.A., M.Z. and H.J.; formal analysis, S.S.M.A., M.Z. and H.J.; investigation, S.S.M.A., M.Z. and H.J.; resources, S.S.M.A., M.Z. and H.J.; data curation, S.S.M.A., M.Z. and H.J.; writing—original draft preparation, S.S.M.A., M.Z. and H.J.; writing—review and editing, S.S.M.A., M.Z., H.J., J.F.U. and B.B.; supervision, J.F.U. and B.B. All authors have read and agreed to the published version of the manuscript.

**Funding:** This research received no external funding.

**Conflicts of Interest:** The authors declare no conflict of interest.

## References

1. Guo, Z. A review on heat transfer enhancement with nanofluids. *J. Enhanc. Heat Transf.* **2020**, *27*, 1–70.
2. Yilmazoglu, M.Z.; Gokalp, O.; Biyikoglu, A. Heat Removal Improvement in an Enclosure with Electronic Components for Air Conditioning Devices. *J. Enhanc. Heat Transf.* **2019**, *26*, 1–14.
3. Alva, G.; Lin, Y.; Fang, G. An overview of thermal energy storage systems. *Energy* **2018**, *144*, 341–378.
4. Wang, J.; Xie, H.; Guo, Z.; Cai, L.; Zhang, K. Using organic phase-change materials for enhanced energy storage in water heaters: An experimental study. *J. Enhanc. Heat Transf.* **2019**, *26*, 167–178.
5. Zhang, X.-D.; Gao, J.Y.; Zhang, P.-J.; Liu, J. Comparison on enhanced phase change heat transfer of low melting point metal melting using different heating methods. *J. Enhanc. Heat Transf.* **2019**, *26*, 179–194.
6. Dong, F.; Cao, T.; Hou, L.; Ni, J. Optimization study of artificial cavities on subcooled flow boiling performance of water in a horizontal simulated engine cooling passage. *J. Enhanc. Heat Transf.* **2019**, *26*, 37–57.
7. Kim, N.-H. Steam condensation enhancement and fouling in titanium corrugated tubes. *J. Enhanc. Heat Transf.* **2019**, *26*, 59–74.
8. Nasir, F.M.; Abdullah, M.Z.; Ismail, M.A. Experimental investigation on the heat transfer performance of heat pipes in cooling HEV Lithium-ion batteries. *Heat Transf. Res.* **2018**, *49*, 1745–1760.
9. Terekhov, V.I.; Khafaji, H.Q.; Gorbachev, M.V. Heat and mass transfer enhancement in laminar forced convection wet channel flows with uniform wall heat flux. *J. Enhanc. Heat Transf.* **2018**, *25*, 565–577.
10. Matysiak, L.; Platek, R. Analytical, numerical, and experimental study of a robot controller with a forced cooling system. *Heat Transf. Res.* **2019**, *50*, 195–216.
11. Ligrani, P.; McInturff, P.; Suzuki, M.; Nakamata, C. Winglet-pair target surface roughness influences on impingement jet array heat transfer. *J. Enhanc. Heat Transf.* **2019**, *26*, 15–35.
12. Abbood, S.A.; Wang, J.; Wu, Z.; Sundén, B. Analysis of natural convection of Cu and TiO<sub>2</sub> nanofluids inside nonconventional enclosures. *J. Enhanc. Heat Transf.* **2018**, *25*, 315–332.
13. Zhang, W.-H.; Lin, W.-K.; Yeh, C.-T.; Chiang, S.-B.; Jao, C.-S. A novel liquid-packaging technology for highly reliable UV-LED encapsulation. *Heat Transf. Res.* **2019**, *50*, 349–360.
14. Iasiello, M.; Cunsolo, S.; Bianco, N.; Chiu, W.K.S.; Naso, V. Fully developed convection heat transfer in open-cell foams. *J. Enhanc. Heat Transf.* **2018**, *25*, 333–346.

15. Huang, Kuo, and Xianhe Deng. Enhanced heat and mass transfer of falling liquid films in vertical tubes. *J. Enhanc. Heat Transf.* **2018**, *25*, 79–96.
16. Bergles, A.E.; Nirmalan, V.; Junkhan, G.H.; Webb, R.L. *Bibliography on Augmentation of Convective Heat and Mass Transfer-II*; Technical Report ISU-ERI-AMES-84221; Iowa State University of Science and Technology, Heat Transfer Laboratory: Ames, IA, USA, December 1983.
17. Bergles, A.E.; Jensen, M.K.; Somerscales, E.F.C.; Manglik, R.M. *Literature Review of Heat Transfer Enhancement Technology for Heat Exchanges in Gas-Fired Applications*; Technical Report ACRC TR-105; Gas Research Institute: Chicago, IL, USA, 1991.
18. Bergles, A.E. *Techniques to Enhance Heat Transfer. Handbook of Heat Transfer*; McGraw-Hill: New York, NY, USA, 1998.
19. Webb, R.L.; Kim, N.H. *Principles of Enhanced Heat Transfer*, 2nd ed.; Taylor & Francis: Boca Raton, FL, USA, 2005.
20. Léal, L.; Miscevic, M.; Lavieille, P.; Amokrane, M.; Pigache, F.; Topin, F.; Nogarède, B.; Tadríst, L. An overview of heat transfer enhancement methods and new perspectives: Focus on active methods using electroactive materials. *Int. J. Heat Mass Transf.* **2013**, *61*, 505–524.
21. Rashidi, S.; Eskandarian, M.; Mahian, O.; Poncet, S. Combination of nanofluid and inserts for heat transfer enhancement. *J. Therm. Anal. Calorim.* **2019**, *135*, 437–460.
22. Bovand, M.; Rashidi, S.; Esfahani, J.A. Heat transfer enhancement and pressure drop penalty in porous solar heaters: Numerical simulations. *Sol. Energy* **2016**, *123*, 145–159.
23. Rashidi, S.; Esfahani, J.A.; Rashidi, A. A review on the applications of porous materials in solar energy systems. *Renew. Sustain. Energy Rev.* **2017**, *73*, 1198–1210.
24. Rashidi, S.; Akbarzadeh, M.; Masoodi, R.; Languri, E.M. Thermal-hydraulic and entropy generation analysis for turbulent flow inside a corrugated channel. *Int. J. Heat Mass Transf.* **2017**, *109*, 812–823.
25. Zade, N.M.; Akar, S.; Rashidi, S.; Esfahani, J.A. Thermo-hydraulic analysis for a novel eccentric helical screw tape insert in a three dimensional tube. *Appl. Therm. Eng.* **2017**, *124*, 413–421.
26. Hasanpour, A.; Farhadi, M.; Sedighi, K. A review study on twisted tape inserts on turbulent flow heat exchangers: The overall enhancement ratio criteria. *Int. Commun. Heat Mass Transf.* **2014**, *55*, 53–62.
27. Keklikcioglu, O.; Ozceyhan, V. A review of heat transfer enhancement methods using coiled wire and twisted tape inserts. *Heat Transf. Models Methods Appl.* **2018**, 199–217. <http://doi.org/10.5772/intechopen.74516>.
28. He, J.; Deng, Q.; Feng, Z. Heat transfer enhancement of impingement cooling with corrugated target surface. *Int. J. Therm. Sci.* **2022**, *171*, 107251.
29. Rashidi, S.; Mahian, O.; Languri, E.M. Applications of nanofluids in condensing and evaporating systems. *J. Therm. Anal. Calorim.* **2018**, *131*, 2027–2039.
30. Amirahmadi, S.; Rashidi, S.; Esfahani, J.A. Minimization of exergy losses in a trapezoidal duct with turbulator, roughness and beveled corners. *Appl. Therm. Eng.* **2016**, *107*, 533–543.
31. Olabi, A.G.; Wilberforce, T.; Sayed, E.T.; Elsaid, K.; Rahman, S.M.A.; Abdelkareem, M.A. Geometrical effect coupled with nanofluid on heat transfer enhancement in heat exchangers. *Int. J. Thermo-fluids* **2021**, *10*, 100072.
32. Bergles, A.E. ExHFT for fourth generation heat transfer technology. *Exp. Therm. Fluid Sci.* **2002**, *26*, 335–344.
33. Bergles, A.E. Recent developments in enhanced heat transfer. *Heat Mass Transf.* **2011**, *47*, 1001–1008.
34. Gugulothu, R.; Reddy, K.V.K.; Somanchi, N.S.; Adithya, E.L. A review on enhancement of heat transfer techniques. *Mater. Today Proc.* **2017**, *4*, 1051–1056.
35. Maradiya, C.; Vadher, J.; Agarwal, R. The heat transfer enhancement techniques and their thermal performance factor. *Beni-Suef Univ. J. Basic Appl. Sci.* **2018**, *7*, 1–21.
36. Murugesan, P.; Mayilsamy, K.; Suresh, S. Turbulent heat transfer and pressure drop in tube fitted with square-cut twisted tape. *Chin. J. Chem. Eng.* **2010**, *18*, 609–617.
37. Shaji, K. Numerical analysis on a double pipe heat exchanger with twisted tape induced swirl flow on both sides. *Procedia Technol.* **2016**, *24*, 436–443.
38. Lin, Z.-M.; Wang, L.-B.; Lin, M.; Dang, W.; Zhang, Y.-H. Numerical study of the laminar flow and heat transfer characteristics in a tube inserting a twisted tape having parallelogram winglet vortex generators. *Appl. Therm. Eng.* **2017**, *115*, 644–658.
39. Eiamsa-Ard, S.; Thianpong, C.; Eiamsa-Ard, P.; Promvong, P. Convective heat transfer in a circular tube with short-length twisted tape insert. *Int. Commun. Heat Mass Transf.* **2010**, *36*, 365–371.
40. Suri, A.R.S.; Kumar, A.; Maithani, R. Experimental investigation of heat transfer and fluid flow behaviour in multiple square perforated twisted tape with square wing inserts heat exchanger tube. *Heat Mass Transf.* **2018**, *54*, 1813–1826.
41. Salam, B.; Biswas, S.; Saha, S.; Bhuiya, M.M.K. Heat transfer enhancement in a tube using rectangular-cut twisted tape insert. *Procedia Eng.* **2013**, *56*, 96–103.
42. Eiamsa-Ard, S.; Promthaisong, P.; Thianpong, C.; Pimsarn, M.; Chuwattanakul, V. Influence of three-start spirally twisted tube combined with triple-channel twisted tape insert on heat transfer enhancement. *Chem. Eng. Process. Process Intensif.* **2016**, *102*, 117–129.
43. Suri, A.R.S.; Kumar, A.; Maithani, R. Heat transfer enhancement of heat exchanger tube with multiple square perforated twisted tape inserts: Experimental investigation and correlation development. *Chem. Eng. Process. Process Intensif.* **2017**, *116*, 76–96.
44. Man, C.; Lv, X.; Hu, J.; Sun, P.; Tang, Y. Experimental study on effect of heat transfer enhancement for single-phase forced convective flow with twisted tape inserts. *Int. J. Heat Mass Transf.* **2017**, *106*, 877–883.

45. Zheng, L.; Xie, Y.; Zhang, D. Numerical investigation on heat transfer performance and flow characteristics in circular tubes with dimpled twisted tapes using  $\text{Al}_2\text{O}_3$ -water nanofluid. *Int. J. Heat Mass Transf.* **2017**, *111*, 962–981.
46. Hong, Y.; Du, J.; Wang, S.; Huang, S.-M.; Ye, W.-B. Effect of decaying swirl flow on tubular turbulent heat transfer enhancement by using short length helical tapes. *Chem. Eng. Res. Des.* **2018**, *138*, 1–12.
47. Li, Z.; Sheikholeslami, M.; Jafaryar, M.; Shafee, A.; Chamkha, A.J. Investigation of nanofluid entropy generation in a heat exchanger with helical twisted tapes. *J. Mol. Liq.* **2018**, *266*, 797–805.
48. Nakhchi, M.E.; Esfahani, J.A. Performance intensification of turbulent flow through heat exchanger tube using double V-cut twisted tape inserts. *Chem. Eng. Process. Process Intensif.* **2019**, *141*, 107533.
49. Murugan, M.; Vijayan, R.; Saravanan, A. Improving performance of a trapezoidal-trough thermosyphon solar collector using peripherally wing-cut swirl generator. *Int. J. Green Energy* **2019**, *16*, 1196–1209.
50. Bhattacharyya, S. The effects of short length and full length swirl generators on heat transfer and flow fields in a solar air heater tube. *J. Therm. Anal. Calorim.* **2020**, *140*, 1355–1369.
51. Gnanavel, C.; Saravanan, R.; Chandrasekaran, M. Heat transfer enhancement through nano-fluids and twisted tape insert with rectangular cut on its rib in a double pipe heat exchanger. *Mater. Today Proc.* **2020**, *21*, 865–869.
52. He, W.; Toghraie, D.; Lotfipour, A.; Pourfattah, F.; Karimipour, A.; Afrand, M. Effect of twisted-tape inserts and nanofluid on flow field and heat transfer characteristics in a tube. *Int. Commun. Heat Mass Transf.* **2020**, *110*, 104440.
53. Bahiraei, M.; Mazaheri, N.; Moayedi, H. Entropy generation and exergy destruction for flow of a biologically functionalized graphene nanoplatelets nanofluid within tube enhanced with a novel rotary coaxial cross double-twisted tape. *Int. Commun. Heat Mass Transf.* **2020**, *113*, 104546.
54. Murali, G.; Nagendra, B.; Jaya, J. CFD analysis on heat transfer and pressure drop characteristics of turbulent flow in a tube fitted with trapezoidal-cut twisted tape insert using  $\text{Fe}_3\text{O}_4$  nano fluid. *Mater. Today Proc.* **2020**, *21*, 313–319.
55. Paneliya, S.; Khanna, S.; Mankad, V.; Ray, A.; Prajapati, P.; Mukhopadhyay, I. Comparative study of heat transfer characteristics of a tube equipped with X-shaped and twisted tape insert. *Mater. Today Proc.* **2020**, *28*, 1175–1180.
56. Samruaisin, P.; Kunnarak, K.; Chuwattanakul, V.; Eiamsa-Ard, S. Effect of sparsely placed twisted tapes installed with multiple-transverse twisted-baffles on heat transfer enhancement. *J. Therm. Anal. Calorim.* **2020**, *140*, 1159–1175.
57. Noorbakhsh, M.; Zaboli, M.; Ajarostaghi, S.S.M. Numerical evaluation of the effect of using twisted tapes as turbulator with various geometries in both sides of a double-pipe heat exchanger. *J. Therm. Anal. Calorim.* **2020**, *140*, 1341–1353.
58. Farhan, A.A.; Al Jubury, I.M.A.; Ahmed, H.E. Energetic and exergetic efficiency analysis of a v-corrugated solar air heater integrated with twisted tape inserts. *Renew. Energy* **2021**, *169*, 1373–1385.
59. Kumar, R.; Nandan, G.; Dwivedi, G.; Shukla, A.K.; Shrivastava, R. Modeling of triangular perforated twisted tape with V-Cuts in double pipe heat exchanger. *Mater. Today Proc.* **2021**, *46*, 5389–5395.
60. Wijayanta, A.T.; Muhammad, A. Heat transfer augmentation of internal flow using twisted tape insert in turbulent flow. *Heat Transf. Eng.* **2020**, *41*, 1288–1300.
61. Yaningsih, I.; Wijayanta, A.T.; Miyazaki, T.; Koyama, S. V-cut twisted tape insert effect on heat transfer enhancement of single phase turbulent flow heat exchanger. *AIP Conf. Proc.* **2018**, *1931*, 030038.
62. Wijayanta, A.T.; Kristiawan, B.; Aziz, M. Internal flow in an enhanced tube having square-cut twisted tape insert. *Energies* **2019**, *12*, 306.
63. Yaningsih, I.; Wijayanta, A.T. Concentric tube heat exchanger installed by twisted tapes using various wings with alternate axes. *AIP Conf. Proc.* **2017**, *1788*, 030005.
64. Yaningsih, I.; Istanto, T.; Wijayanta, A.T. Experimental study of heat transfer enhancement in a concentric double pipe heat exchanger with different axial pitch ratio of perforated twisted tape inserts. *AIP Conf. Proc.* **2016**, *1717*, 030012.
65. Outokesh, M.; Ajarostaghi, S.S.M.; Bozorgzadeh, A.; Sedighi, K. Numerical evaluation of the effect of utilizing twisted tape with curved profile as a turbulator on heat transfer enhancement in a pipe. *J. Therm. Anal. Calorim.* **2020**, *140*, 1537–1553.
66. Afsharpanah, F.; Sheshpoli, A.Z.; Pakzad, K.; Ajarostaghi, S.S.M. Numerical investigation of non-uniform heat transfer enhancement in parabolic trough solar collectors using dual modified twisted-tape inserts. *J. Therm. Eng.* **2021**, *7*, 133–147.
67. Liu, P.; Zheng, N.; Shan, F.; Liu, Z.; Liu, W. An experimental and numerical study on the laminar heat transfer and flow characteristics of a circular tube fitted with multiple conical strips inserts. *Int. J. Heat Mass Transf.* **2018**, *117*, 691–709.
68. Liu, P.; Zheng, N.; Shan, F.; Liu, Z.; Liu, W. Heat transfer enhancement for laminar flow in a tube using bidirectional conical strip inserts. *Int. J. Heat Mass Transf.* **2018**, *127*, 1064–1076.
69. Ibrahim, M.M.; Essa, M.A.; Mostafa, N.H. A computational study of heat transfer analysis for a circular tube with conical ring turbulators. *Int. J. Therm. Sci.* **2019**, *137*, 138–160.
70. Liu, P.; Zheng, N.; Liu, Z.; Liu, W. Thermal-hydraulic performance and entropy generation analysis of a parabolic trough receiver with conical strip inserts. *Energy Convers. Manag.* **2019**, *179*, 30–45.
71. Bahiraei, M.; Gharagozloo, K. Experimental investigation of hydrothermal characteristics for flow within a circular tube equipped with twisted conical strip inserts under different alignments. *J. Taiwan Inst. Chem. Eng.* **2020**, *114*, 24–35.
72. Amani, K.; Ebrahimpour, M.; Akbarzadeh, S.; Valipour, M.S. The utilization of conical strip inserts in a parabolic trough collector. *J. Therm. Anal. Calorim.* **2020**, *140*, 1625–1631.
73. Mashayekhi, R.; Arasteh, H.; Toghraie, D.; Motaharpour, H.S.; Keshmiri, A.; Afrand, M. Heat transfer enhancement of Water- $\text{Al}_2\text{O}_3$  nanofluid in an oval channel equipped with two rows of twisted conical strip inserts in various directions: A two-phase approach. *Comput. Math. Appl.* **2020**, *79*, 2203–2215.

74. Bahiraei, M.; Rahimi, Z.; Nazari, F. A combined multi-criterion optimization to determine optimum geometrical parameters for flow of an ecofriendly graphene-based nanofluid inside tube enhanced with twisted conical strip inserts. *Powder Technol.* **2021**, *377*, 336–349.
75. Wijayanta, A.T.; Kristiawan, B.; Premono, A.; Aziz, M. Computational Fluid Dynamics Analysis of an Enhanced Tube with Backward Louvered Strip Insert. *Energies* **2019**, *12*, 3370.
76. Yaningsih, I.; Wijayanta, A.T.; Miyazaki, T.; Koyama, S. Thermal hydraulic characteristics of turbulent single-phase flow in an enhanced tube using louvered strip insert with various slant angles. *Int. J. Therm. Sci.* **2018**, *134*, 355–362.
77. Mellal, M.; Benzeguir, R.; Sahel, D.; Ameer, H. Hydro-thermal shell-side performance evaluation of a shell and tube heat exchanger under different baffle arrangement and orientation. *Int. J. Therm. Sci.* **2017**, *121*, 138–149.
78. Zhou, G.-Y.; Xiao, J.; Zhu, L.; Wang, J.; Tu, S.-T. A numerical study on the shell-side turbulent heat transfer enhancement of shell-and-tube heat exchanger with trefoil-hole baffles. *Energy Procedia* **2015**, *75*, 3174–3179.
79. Jedsadaratanachai, W.; Jayranaiwachira, N.; Promvong, P. 3D numerical study on flow structure and heat transfer in a circular tube with V-baffles. *Chin. J. Chem. Eng.* **2015**, *23*, 342–349.
80. Sriromreun, P.; Thianpong, C.; Promvong, P. Experimental and numerical study on heat transfer enhancement in a channel with Z-shaped baffles. *Int. Commun. Heat Mass Transf.* **2012**, *39*, 945–952.
81. Wang, S.; Wen, J.; Yang, H.; Xue, Y.; Tuo, H. Experimental investigation on heat transfer enhancement of a heat exchanger with helical baffles through blockage of triangle leakage zones. *Appl. Therm. Eng.* **2014**, *67*, 122–130.
82. El Maakoul, A.; Laknizi, A.; Saadeddine, S.; Abdellah, A.B.; Meziane, M.; El Metoui, M. Numerical design and investigation of heat transfer enhancement and performance for an annulus with continuous helical baffles in a double-pipe heat exchanger. *Energy Convers. Manag.* **2017**, *133*, 76–86.
83. Kumar, R.; Kumar, A.; Chauhan, R.; Sethi, M. Heat transfer enhancement in solar air channel with broken multiple V-type baffle. *Case Stud. Therm. Eng.* **2016**, *8*, 187–197.
84. Kumar, R.; Kumar, A.; Sharma, A.; Chauhan, R.; Sethi, M. Experimental study of heat transfer enhancement in a rectangular duct distributed by multi V-perforated baffle of different relative baffle width. *Heat Mass Transf.* **2017**, *53*, 1289–1304.
85. Andrzejczyk, R.; Muszynski, T.; Gosz, M. Experimental investigations on heat transfer enhancement in shell coil heat exchanger with variable baffles geometry. *Chem. Eng. Process. Process Intensif.* **2018**, *132*, 114–126.
86. Sahel, D.; Ameer, H.; Benzeguir, R.; Kamla, Y. Enhancement of heat transfer in a rectangular channel with perforated baffles. *Appl. Therm. Eng.* **2016**, *101*, 156–164.
87. Zhang, X.; Han, D.; He, W.; Yue, C.; Pu, W. Numerical simulation on a novel shell-and-tube heat exchanger with screw cinque-foil orifice baffles. *Adv. Mech. Eng.* **2017**, *9*, 1–12. <https://doi.org/10.1177/1687814017717665>.
88. Chen, J.; Lu, X.; Wang, Q.; Zeng, M. Experimental investigation on thermal-hydraulic performance of a novel shell-and-tube heat exchanger with unilateral ladder type helical baffles. *Appl. Therm. Eng.* **2019**, *161*, 114099.
89. Gu, X.; Luo, Y.; Xiong, X.; Wang, K.; Wang, Y. Numerical and experimental investigation of the heat exchanger with trapezoidal baffle. *Int. J. Heat Mass Transf.* **2018**, *127*, 598–606.
90. Xiao, J.; Wang, S.; Ye, S.; Wang, J.; Wen, J.; Tu, T. Experimental investigation on pre-heating technology of coal water slurry with different concentration in shell-and-tube heat exchangers with ladder-type fold baffles. *Int. J. Heat Mass Transf.* **2019**, *132*, 1116–1125.
91. Liu, Y.; Wen, J.; Wang, S.; Tu, J. Numerical investigation on the shell and tube heat exchanger with baffle leakage zones blocked. *Int. J. Therm. Sci.* **2021**, *165*, 106959.
92. Arani, A.A.A.; Moradi, R. Shell and tube heat exchanger optimization using new baffle and tube configuration. *Appl. Therm. Eng.* **2019**, *157*, 113736.
93. Abbasi, H.R.; Sedeh, E.S.; Pourrahmani, H.; Mohammadi, M.H. Shape optimization of segmental porous baffles for enhanced thermo-hydraulic performance of shell-and-tube heat exchanger. *Appl. Therm. Eng.* **2020**, *180*, 115835.
94. Biçer, N.; Engin, T.; Yaşar, H.; Büyükkaya, E.; Aydın, A.; Topuz, A. Design optimization of a shell-and-tube heat exchanger with novel three-zonal baffle by using CFD and taguchi method. *Int. J. Therm. Sci.* **2020**, *155*, 106417.
95. Chen, J.; Zhao, P.; Wang, Q.; Zeng, M. Experimental investigation of shell-side performance and optimal design of shell-and-tube heat exchanger with different flower baffles. *Heat Transf. Eng.* **2021**, *42*, 613–626.
96. Bahiraei, M.; Naseri, M.; Monavari, A. Irreversibility features of a shell-and-tube heat exchanger fitted with novel trapezoidal oblique baffles: Application of a nanofluid with different particle shapes. *Int. Commun. Heat Mass Transf.* **2021**, *126*, 105352.
97. Arani, A.A.A.; Uosofvand, H. Double-pass shell-and-tube heat exchanger performance enhancement with new combined baffle and elliptical tube bundle arrangement. *Int. J. Therm. Sci.* **2021**, *167*, 106999.
98. El-Said, E.M.S.; Elsheikh, A.H.; El-Tahan, H.R. Effect of curved segmental baffle on a shell and tube heat exchanger thermohydraulic performance: Numerical investigation. *Int. J. Therm. Sci.* **2021**, *165*, 106922.
99. Uosofvand, H.; Arani, A.A.A. Shell-and-tube heat exchangers performance improvement employing hybrid segmental–helical baffles and ribbed tubes combination. *J. Braz. Soc. Mech. Sci. Eng.* **2021**, *43*, 399.
100. Hu, J.; Liu, K.; Ma, L.; Sun, X. Parameter optimization of solar air collectors with holes on baffle and analysis of flow and heat transfer characteristics. *Sol. Energy* **2018**, *174*, 878–887.
101. Ansari, M.; Amani, E. Micro-combustor performance enhancement using a novel combined baffle-bluff configuration. *Chem. Eng. Sci.* **2018**, *175*, 243–256.

102. Saravanakumar, T.; Kumar, D.S. Performance analysis on heat transfer characteristics of heat SINK with baffles attachment. *Int. J. Therm. Sci.* **2019**, *142*, 14–19.
103. Karami, M.; Tashakor, S.; Afsari, A.; Hashemi-Tilehnoee, M. Effect of the baffle on the performance of a micro pin fin heat sink. *Therm. Sci. Eng. Prog.* **2019**, *14*, 100417.
104. Hu, J.; Liu, K.; Guo, M.; Zhang, G.; Chu, Z.; Wang, M. Performance improvement of baffle-type solar air collector based on first chamber narrowing. *Renew. Energy* **2019**, *135*, 701–710.
105. Khanlari, A.; Güler, H.Ö.; Tuncer, A.D.; Şirin, C.; Bilge, Y.C.; Yılmaz, Y.; Güngör, A. Experimental and numerical study of the effect of integrating plus-shaped perforated baffles to solar air collector in drying application. *Renew. Energy* **2020**, *145*, 1677–1692.
106. Olfian, H.; Sheshpoli, A.Z.; Ajarostaghi, S.S.M. Numerical evaluation of the thermal performance of a solar air heater equipped with two different types of baffles. *Heat Transf.* **2020**, *49*, 1149–1169.
107. Promvongse, P.; Eiamsa-Ard, S.; Wongcharee, K.; Chuwattanakul, V.; Samruaisin, P.; Chokphoemphun, S.; Nanan, K.; Eiamsa-Ard, P. Characterization of heat transfer and artificial neural networks prediction on overall performance index of a channel installed with arc-shaped baffle turbulators. *Case Stud. Therm. Eng.* **2021**, *26*, 101067.
108. Hewitt, G.F.; Afgan, N.; Taborek, J.; (Eds.) *Heat Exchangers: Theory and Practice*; Hemisphere Publishing Corporation: London, UK, 1983.
109. Salviano, L.O.; Dezan, D.J.; Yanagihara, J.I. Multi-Objective Optimization of Vortex Generators Positions and Angles in Fin-Tube Compact Heat Exchanger at Low Reynolds Number Using Neural Network and Genetic Algorithm. In Proceedings of the 15th International Heat Transfer Conference, Kyoto, Japan, 10–15 August 2014; Begel House Inc.: Danbury, CT, USA, 2014; pp. 5955–5972.
110. Huisseune, H.; T'Joene, C.; De Jaeger, P.; Ameel, B.; De Schampheleire, S.; De Paepe, M. Influence of the louver and delta winglet geometry on the thermal hydraulic performance of a compound heat exchanger. *Int. J. Heat Mass Transf.* **2013**, *57*, 58–72.
111. Khanjian, A.; Habchi, C.; Russeil, S.; Bougeard, D.; Lemenand, T. Effect of rectangular winglet pair roll angle on the heat transfer enhancement in laminar channel flow. *Int. J. Therm. Sci.* **2017**, *114*, 1–14.
112. Oneissi, M.; Habchi, C.; Russeil, S.; Lemenand, T.; Bougeard, D. Heat transfer enhancement of inclined projected winglet pair vortex generators with protrusions. *Int. J. Therm. Sci.* **2018**, *134*, 541–551.
113. Modi, A.J.; Rathod, M.K. Comparative study of heat transfer enhancement and pressure drop for fin-and-circular tube compact heat exchangers with sinusoidal wavy and elliptical curved rectangular winglet vortex generator. *Int. J. Heat Mass Transf.* **2019**, *141*, 310–326.
114. Chamoli, S.; Lu, R.; Xu, D.; Yu, P. Thermal performance improvement of a solar air heater fitted with winglet vortex generators. *Sol. Energy* **2018**, *159*, 966–983.
115. Samadifar, M.; Toghraie, D. Numerical simulation of heat transfer enhancement in a plate-fin heat exchanger using a new type of vortex generators. *Appl. Therm. Eng.* **2018**, *133*, 671–681.
116. Luo, C.; Wu, S.; Song, K.; Hua, L.; Wang, L. Thermo-hydraulic performance optimization of wavy fin heat exchanger by combining delta winglet vortex generators. *Appl. Therm. Eng.* **2019**, *163*, 114343.
117. Zhai, C.; Islam, M.D.; Simmons, R.; Barsoum, I. Heat transfer augmentation in a circular tube with delta winglet vortex generator pairs. *Int. J. Therm. Sci.* **2019**, *140*, 480–490.
118. Sun, Z.; Zhang, K.; Li, W.; Chen, Q.; Zheng, N. Investigations of the turbulent thermal-hydraulic performance in circular heat exchanger tubes with multiple rectangular winglet vortex generators. *Appl. Therm. Eng.* **2020**, *168*, 114838.
119. Kumar, A.; Layek, A. Nusselt number and friction characteristics of a solar air heater that has a winglet type vortex generator in the absorber surface. *Exp. Therm. Fluid Sci.* **2020**, *119*, 110204.
120. Modi, A.J.; Kalel, N.A.; Rathod, M.K. Thermal performance augmentation of fin-and-tube heat exchanger using rectangular winglet vortex generators having circular punched holes. *Int. J. Heat Mass Transf.* **2020**, *158*, 119724.
121. Promvongse, P.; Promthaisong, P.; Skullong, S. Numerical heat transfer in a solar air heater duct with punched delta-winglet vortex generators. *Case Stud. Therm. Eng.* **2021**, *26*, 101088.
122. Shi, W.; Liu, T.; Song, K.; Zhang, Q.; Hu, W.; Wang, L. The optimal longitudinal location of curved winglets for better thermal performance of a finned-tube heat exchanger. *Int. J. Therm. Sci.* **2021**, *167*, 107035.
123. Khan, M.Z.A.; Aziz, M.; Wijayanta, A.T. Prediction of heat transfer enhancement of delta-wing tape inserts using artificial neural network. *Case Stud. Therm. Eng.* **2021**, *27*, 101322.
124. Wijayanta, A.T.; Yaningsih, I.; Juwana, W.E.; Aziz, M.; Miyazaki, T. Effect of wing-pitch ratio of double-sided delta-wing tape insert on the improvement of convective heat transfer. *Int. J. Therm. Sci.* **2020**, *151*, 106261.
125. Wijayanta, A.T.; Yaningsih, I.; Aziz, M.; Miyazaki, T.; Koyama, S. Double-sided delta-wing tape inserts to enhance convective heat transfer and fluid flow characteristics of a double-pipe heat exchanger. *Appl. Therm. Eng.* **2018**, *145*, 27–37.
126. Wijayanta, A.T.; Aziz, M.; Kariya, K.; Miyara, A. Numerical study of heat transfer enhancement of internal flow using double-sided delta-winglet tape insert. *Energies* **2018**, *11*, 3170.
127. Yaningsih, I.; Wijayanta, A.T.; Miyazaki, T.; Koyama, S. Impact of blockage ratio on thermal performance of delta-winglet vortex generators. *Appl. Sci.* **2018**, *8*, 181.
128. Wijayanta, A.T.; Istanto, T.; Kariya, K.; Miyara, A. Heat transfer enhancement of internal flow by inserting punched delta winglet vortex generators with various attack angles. *Exp. Therm. Fluid Sci.* **2017**, *87*, 141–148.
129. Dastmalchi, M.; Sheikhzadeh, G.A.; Arefmanesh, A. Optimization of micro-finned tubes in double pipe heat exchangers using particle swarm algorithm. *Appl. Therm. Eng.* **2017**, *119*, 1–9.



130. Lotfi, B.; Sundén, B.; Wang, Q. An investigation of the thermo-hydraulic performance of the smooth wavy fin-and-elliptical tube HEXs utilizing new type vortex generators. *Appl. Energy* **2016**, *162*, 1282–1302.
131. Kim, G.W.; Lim, H.M.; Rhee, G.H. Numerical studies of heat transfer enhancement by cross-cut flow control in wavy fin heat exchangers. *Int. J. Heat Mass Transf.* **2016**, *96*, 110–117.
132. Singh, P.; Patil, A.K. Experimental investigation of heat transfer enhancement through embossed fin heat sink under natural convection. *Exp. Therm. Fluid Sci.* **2015**, *61*, 24–33.
133. Awasarmol, U.V.; Pise, A.T. An experimental investigation of natural convection heat transfer enhancement from perforated rectangular fins array at different inclinations. *Exp. Therm. Fluid Sci.* **2015**, *68*, 145–154.
134. Lotfi, B.; Zeng, M.; Sundén, B.; Wang, Q. 3D numerical investigation of flow and heat transfer characteristics in smooth wavy fin-and-elliptical tube heat exchangers using new type vortex generators. *Energy* **2014**, *73*, 233–257.
135. Zaboli, M.; Ajarostaghi, S.S.M.; Saedodin, S.; Kiani, B. Hybrid nanofluid flow and heat transfer in a parabolic trough solar collector with inner helical axial fins as turbulator. *Eur. Phys. J. Plus* **2021**, *136*, 841.
136. Zaboli, M.; Ajarostaghi, S.S.M.; Saedodin, S.; Pour, M.S. Thermal Performance Enhancement Using Absorber Tube with Inner Helical Axial Fins in a Parabolic Trough Solar Collector. *Appl. Sci.* **2021**, *11*, 7423.
137. Saeidi, R.; Noorollahi, Y.; Esfahanian, V. Numerical simulation of a novel spiral type ground heat exchanger for enhancing heat transfer performance of geothermal heat pump. *Energy Convers. Manag.* **2018**, *168*, 296–307.
138. Xue, Y.; Ge, Z.; Du, X.; Yang, L. On the heat transfer enhancement of plate fin heat exchanger. *Energies* **2018**, *11*, 1398.
139. Vyas, A.M.; Parikh, R.; Patdiwala, U. Analysis of IC Engine Fins for Effective Cooling Performance. *Int. J. Sci. Technol. Eng.* **2018**, *5*, 16–21.
140. Borhani, S.M.; Hosseini, M.J.; Ranjbar, A.A.; Bahrapoury, R. Investigation of phase change in a spiral-fin heat exchanger. *Appl. Math. Model.* **2019**, *67*, 297–314.
141. Zhang, J.-N.; Cheng, M.; Ding, Y.D.; Fu, Q.; Chen, Z.-Y. Influence of geometric parameters on the gas-side heat transfer and pressure drop characteristics of three-dimensional finned tube. *Int. J. Heat Mass Transf.* **2019**, *133*, 192–202.
142. Hussain, A.A.; Freegah, B.; Khalaf, B.S.; Towsyfyhan, H. Numerical investigation of heat transfer enhancement in plate-fin heat sinks: Effect of flow direction and fillet profile. *Case Stud. Therm. Eng.* **2019**, *13*, 100388.
143. Hajmohammadi, M.R.; Doustahadi, A.; Ahmadian-Elmi, M. Heat transfer enhancement by a circumferentially non-uniform array of longitudinal fins assembled inside a circular channel. *Int. J. Heat Mass Transf.* **2020**, *158*, 120020.
144. Freegah, B.; Hussain, A.A.; Falih, A.H.; Towsyfyhan, H. CFD analysis of heat transfer enhancement in plate-fin heat sinks with fillet profile: Investigation of new designs. *Therm. Sci. Eng. Prog.* **2020**, *17*, 100458.
145. Kim, T.; Choi, B.-I.; Han, Y.S.; Do, K.H. Experimental and analytical investigation of a wavy fin recuperator for a micro gas turbine. *Int. J. Heat Mass Transf.* **2020**, *148*, 118998.
146. Liu, L.; Cao, Z.; Shen, T.; Zhang, L.; Zhang, L. Experimental and numerical investigation on flow and heat transfer characteristics of a multi-waves internally spiral finned tube. *Int. J. Heat Mass Transf.* **2021**, *172*, 121104.
147. Gong, J.-H.; Wang, J.; Lund, P.D.; Zhao, D.-D.; Xu, J.-W.; Jin, Y.-H. Comparative study of heat transfer enhancement using different fins in semi-circular absorber tube for large-aperture trough solar concentrator. *Renew. Energy* **2021**, *169*, 1229–1241.
148. Saedodin, S.; Zaboli, M.; Ajarostaghi, S.S.M. Hydrothermal analysis of heat transfer and thermal performance characteristics in a parabolic trough solar collector with Turbulence-Inducing elements. *Sustain. Energy Technol. Assess.* **2021**, *46*, 101266.
149. Sahel, D.; Bellahcene, L.; Yousfi, A.; Subasi, A. Numerical investigation and optimization of a heat sink having hemispherical pin fins. *Int. Commun. Heat Mass Transf.* **2021**, *122*, 105133.
150. Zhang, K.; Li, M.-J.; Liu, H.; Xiong, J.-G.; He, Y.-L. Experimental and numerical study and comparison of performance for heringbone wavy fin and enhanced fin with convex-strips in fin-and-tube heat exchanger. *Int. J. Heat Mass Transf.* **2021**, *175*, 121390.
151. Sandhya, M.; Ramasamy, D.; Sudhakar, K.; Kadirgama, K.; Harun, W.S.W. Enhancement of the heat transfer in radiator with louvered fin by using Graphene-based hybrid nanofluids. *IOP Conf. Ser. Mater. Sci. Eng.* **2021**, *1062*, 012014.
152. Kumar, E.P.; Solanki, A.K.; Kumar, M.M.J. Numerical investigation of heat transfer and pressure drop characteristics in the micro-fin helically coiled tubes. *Appl. Therm. Eng.* **2021**, *182*, 116093.
153. Yan, Y.; Zhao, T.; He, Z.; Yang, Z.; Zhang, L. Numerical investigation on the characteristics of flow and heat transfer enhancement by micro pin-fin array heat sink with fin-shaped strips. *Chem. Eng. Process. Process Intensif.* **2021**, *160*, 108273.
154. Liang, C.; Rao, Y. Numerical study of turbulent flow and heat transfer in channels with detached pin fin arrays under stationary and rotating conditions. *Int. J. Therm. Sci.* **2021**, *160*, 106659.
155. Baragh, S.; Shokouhmand, H.; Ajarostaghi, S.S.M.; Nikian, M. An experimental investigation on forced convection heat transfer of single-phase flow in a channel with different arrangements of porous media. *Int. J. Therm. Sci.* **2018**, *134*, 370–379.
156. Baragh, S.; Shokouhmand, H.; Ajarostaghi, S.S.M. Experiments on mist flow and heat transfer in a tube fitted with porous media. *Int. J. Therm. Sci.* **2019**, *137*, 388–398.
157. Ajarostaghi, S.S.M.; Delavar, M.A.; Poncet, S. Thermal mixing, cooling and entropy generation in a micromixer with a porous zone by the lattice Boltzmann method. *J. Therm. Anal. Calorim.* **2020**, *140*, 1321–1339.
158. Xu, H.J.; Xing, Z.B.; Wang, F.Q.; Cheng, Z.M. Review on heat conduction, heat convection, thermal radiation and phase change heat transfer of nanofluids in porous media: Fundamentals and applications. *Chem. Eng. Sci.* **2019**, *195*, 462–483.
159. Hashemi-Valikboni, S.Z.; Ajarostaghi, S.S.M.; Delavar, M.A.; Sedighi, K. Numerical prediction of humidification process in planar porous membrane humidifier of a PEM fuel cell system to evaluate the effects of operating and geometrical parameters. *J. Therm. Anal. Calorim.* **2020**, *141*, 1687–1701.

160. Hamzah, J.A.; Nima, M.A. Experimental study of heat transfer enhancement in double-pipe heat exchanger integrated with metal foam fins. *Arab. J. Sci. Eng.* **2020**, *45*, 5153–5167.
161. Wang, J.; Kong, H.; Xu, Y.; Wu, J. Experimental investigation of heat transfer and flow characteristics in finned copper foam heat sinks subjected to jet impingement cooling. *Appl. Energy* **2019**, *241*, 433–443.
162. Mancin, S.; Zilio, C.; Diani, A.; Rossetto, L. Experimental air heat transfer and pressure drop through copper foams. *Exp. Therm. Fluid Sci.* **2012**, *36*, 224–232.
163. Nilpueng, K.; Asirvatham, L.G.; Dalkılıç, A.S.; Mahian, O.; Ahn, H.S.; Wongwises, S. Heat transfer and fluid flow characteristics in a plate heat exchanger filled with copper foam. *Heat Mass Transf.* **2020**, *56*, 3261–3271.
164. Teggari, M.; Ajarostaghi, S.S.M.; Yıldız, Ç.; Arıcı, M.; Ismail, K.A.R.; Niyas, H.; Lino, F.A.M.; Mert, M.S.; Khalid, M. Performance enhancement of latent heat storage systems by using extended surfaces and porous materials: A state-of-the-art review. *J. Energy Storage* **2021**, *44*, 103340.
165. Teggari, M.; Arıcı, M.; Mert, M.S.; Ajarostaghi, S.S.M.; Niyas, H.; Tunçbilek, E.; Ismail, K.A.R.; Younsi, Z.; Benhouia, A.T.; Mezaache, E.H. A comprehensive review of micro/nano enhanced phase change materials. *J. Therm. Anal. Calorim.* **2021**, 1–28. <https://doi.org/10.1007/s10973-021-10808-0>.
166. Cui, H.T. Experimental investigation on the heat charging process by paraffin filled with high porosity copper foam. *Appl. Therm. Eng.* **2012**, *39*, 26–28.
167. Mancin, S.; Diani, A.; Doretti, L.; Hooman, K.; Rossetto, L. Experimental analysis of phase change phenomenon of paraffin waxes embedded in copper foams. *Int. J. Therm. Sci.* **2015**, *90*, 79–89.
168. Wang, C.; Lin, T.; Li, N.; Zheng, H. Heat transfer enhancement of phase change composite material: Copper foam/paraffin. *Renew. Energy* **2016**, *96*, 960–965.
169. Li, T.X.; Wu, D.L.; He, F.; Wang, R.Z. Experimental investigation on copper foam/hydrated salt composite phase change material for thermal energy storage. *Int. J. Heat Mass Transf.* **2017**, *115*, 148–157.
170. Jin, H.-Q.; Fan, L.-W.; Liu, M.-J.; Zhu, Z.-Q.; Yu, Z.-T. A pore-scale visualized study of melting heat transfer of a paraffin wax saturated in a copper foam: Effects of the pore size. *Int. J. Heat Mass Transf.* **2017**, *112*, 39–44.
171. Zheng, H.; Wang, C.; Liu, Q.; Tian, Z.; Fan, X. Thermal performance of copper foam/paraffin composite phase change material. *Energy Convers. Manag.* **2018**, *157*, 372–381.
172. Yang, X.; Wei, P.; Cui, X.; Jin, L.; He, Y.-L. Thermal response of annuli filled with metal foam for thermal energy storage: An experimental study. *Appl. Energy* **2019**, *250*, 1457–1467.
173. Yang, X.; Yu, J.; Guo, Z.; Jin, L.; He, Y.-L. Role of porous metal foam on the heat transfer enhancement for a thermal energy storage tube. *Appl. Energy* **2019**, *239*, 142–156.
174. Hu, X.; Zhu, F.; Gong, X. Numerical investigation of the effects of heating and contact conditions on the thermal charging performance of composite phase change material. *J. Energy Storage* **2020**, *30*, 101444.
175. Duan, J. A novel heat sink for cooling concentrator photovoltaic system using PCM-porous system. *Appl. Therm. Eng.* **2021**, *186*, 116522.
176. Li, W.Q.; Guo, S.J.; Tan, L.; Liu, L.L.; Ao, W. Heat transfer enhancement of nano-encapsulated phase change material (NEPCM) using metal foam for thermal energy storage. *Int. J. Heat Mass Transf.* **2021**, *166*, 120737.
177. Meng, X.; Yan, L.; He, F. Filling copper foam partly on thermal behavior of phase-change material in a rectangular enclosure. *J. Energy Storage* **2020**, *32*, 101867.
178. Zadeh, S.M.H.; Mehryan, S.A.M.; Ghalambaz, M.; Ghodrati, M.; Young, J.; Chamkha, A. Hybrid thermal performance enhancement of a circular latent heat storage system by utilizing partially filled copper foam and Cu/GO nano-additives. *Energy* **2020**, *213*, 118761.
179. Chen, Z.; Gu, M.; Peng, D. Heat transfer performance analysis of a solar flat-plate collector with an integrated metal foam porous structure filled with paraffin. *Appl. Therm. Eng.* **2010**, *30*, 1967–1973.
180. Atal, A.; Wang, Y.; Harsha, M.; Sengupta, S. Effect of porosity of conducting matrix on a phase change energy storage device. *Int. J. Heat Mass Transf.* **2016**, *93*, 9–16.
181. Fleming, E.; Wen, S.; Shi, L.; da Silva, A.K. Experimental and theoretical analysis of an aluminum foam enhanced phase change thermal storage unit. *Int. J. Heat Mass Transf.* **2015**, *82*, 273–281.
182. Wang, H.; Qin, Q.-H. Numerical Analysis of Enhanced Heat Transfer in the Metal Foam System Filled with Phase Change Materials. *Int. J. Eng. Inf. Syst.* **2017**, *1*, 129–142.
183. Sundarram, S.S.; Li, W. The effect of pore size and porosity on thermal management performance of phase change material infiltrated microcellular metal foams. *Appl. Therm. Eng.* **2014**, *64*, 147–154.
184. Sardari, P.T.; Babaei-Mahani, R.; Giddings, D.; Yasserli, S.; Moghimi, M.A.; Bahai, H. Energy recovery from domestic radiators using a compact composite metal Foam/PCM latent heat storage. *J. Clean. Prod.* **2020**, *257*, 120504.
185. Zhu, F.; Hu, X.; Wang, X.; Zhang, C.; Gong, X. Experimental and numerical investigation of the melting process of aluminum foam/paraffin composite with low porosity. *Numer. Heat Transf. Part A Appl.* **2020**, *77*, 998–1013.
186. Oya, T.; Nomura, T.; Okinaka, N.; Akiyama, T. Phase change composite based on porous nickel and erythritol. *Appl. Therm. Eng.* **2012**, *40*, 373–377.
187. Xiao, X.; Zhang, P.; Li, M. Effective thermal conductivity of open-cell metal foams impregnated with pure paraffin for latent heat storage. *Int. J. Therm. Sci.* **2014**, *81*, 94–105.

188. Liang, W.; Zhang, G.; Sun, H.; Chen, P.; Zhu, Z.; Li, A. Graphene–nickel/n-carboxylic acids composites as form-stable phase change materials for thermal energy storage. *Sol. Energy Mater. Sol. Cells* **2015**, *132*, 425–430.
189. Huang, X.; Lin, Y.; Alva, G.; Fang, G. Thermal properties and thermal conductivity enhancement of composite phase change materials using myristyl alcohol/metal foam for solar thermal storage. *Sol. Energy Mater. Sol. Cells* **2017**, *170*, 68–76.
190. Zhong, Y.; Li, S.; Wei, X.; Liu, Z.; Guo, Q.; Shi, J.; Liu, L. Heat transfer enhancement of paraffin wax using compressed expanded natural graphite for thermal energy storage. *Carbon* **2010**, *48*, 300–304.
191. Pokhrel, R.; Gonzalez, J.E.; Hight, T.; Adalsteinsson, T. Analysis and design of a paraffin/graphite composite PCM integrated in a thermal storage unit. *J. Sol. Energy Eng.* **2010**, *132*, 041006.
192. Wang, T.; Wang, K.; Ye, F.; Ren, Y.; Xu, C. Characterization and thermal properties of a shape-stable Na<sub>2</sub>CO<sub>3</sub>-K<sub>2</sub>CO<sub>3</sub>/coal fly ash/expanded graphite composite phase change materials for high-temperature thermal energy storage. *J. Energy Storage* **2021**, *33*, 102123.
193. Jin, X.; Xiao, Q.; Xu, T.; Huang, G.; Wu, H.; Wang, D.; Liu, Y.; Zhang, H.; Lai, A.C.K. Thermal conductivity enhancement of a sodium acetate trihydrate–potassium chloride–urea/expanded graphite composite phase-change material for latent heat thermal energy storage. *Energy Build.* **2021**, *231*, 110615.
194. Opolot, M.; Zhao, C.; Liu, M.; Mancin, S.; Bruno, F.; Hooman, K. Influence of cascaded graphite foams on thermal performance of high temperature phase change material storage systems. *Appl. Therm. Eng.* **2020**, *180*, 115618.
195. Javadi, H.; Ajarostaghi, S.S.M.; Rosen, M.A.; Pourfallah, M. Performance of ground heat exchangers: A comprehensive review of recent advances. *Energy* **2019**, *178*, 207–233.
196. Javadi, H.; Ajarostaghi, S.S.M.; Rosen, M.A.; Pourfallah, M. A comprehensive review of backfill materials and their effects on ground heat exchanger performance. *Sustainability* **2018**, *10*, 4486.
197. Ajarostaghi, S.S.M.; Sedighi, K.; Delavar, M.A.; Poncet, S. Numerical study of a horizontal and vertical shell and tube ice storage systems considering three types of tube. *Appl. Sci.* **2020**, *10*, 1059.
198. Zaboli, M.; Nourbakhsh, M.; Ajarostaghi, S.S.M. Numerical evaluation of the heat transfer and fluid flow in a corrugated coil tube with lobe-shaped cross-section and two types of spiral twisted tape as swirl generator. *J. Therm. Anal. Calorim.* **2022**, *147*, 999–1015.
199. Andrzejczyk, R.; Muszynski, T. Thermodynamic and geometrical characteristics of mixed convection heat transfer in the shell and coil tube heat exchanger with baffles. *Appl. Therm. Eng.* **2017**, *121*, 115–125.
200. Gholamalizadeh, E.; Hosseini, E.; Jamnani, M.B.; Amiri, A.; Alimoradi, A. Study of intensification of the heat transfer in helically coiled tube heat exchangers via coiled wire inserts. *Int. J. Therm. Sci.* **2019**, *141*, 72–83.
201. Palanisamy, K.; Kumar, P.C.M. Experimental investigation on convective heat transfer and pressure drop of cone helically coiled tube heat exchanger using carbon nanotubes/water nanofluids. *Heliyon* **2019**, *5*, e01705.
202. Alimoradi, A.; Olfati, M.; Maghareh, M. Numerical investigation of heat transfer intensification in shell and helically coiled finned tube heat exchangers and design optimization. *Chem. Eng. Process. Process Intensif.* **2017**, *121*, 125–143.
203. Javadi, H.; Ajarostaghi, S.S.M.; Pourfallah, M.; Zaboli, M. Performance analysis of helical ground heat exchangers with different configurations. *Appl. Therm. Eng.* **2019**, *154*, 24–36.
204. Afsharpanah, F.; Ajarostaghi, S.S.M.; Sedighi, K. The influence of geometrical parameters on the ice formation enhancement in a shell and double coil ice storage system. *SN Appl. Sci.* **2019**, *1*, 1264.
205. Pakzad, K.; Ajarostaghi, S.S.M.; Sedighi, K. Numerical simulation of solidification process in an ice-on-coil ice storage system with serpentine tubes. *SN Appl. Sci.* **2019**, *1*, 1258.
206. Saydam, V.; Parsazadeh, M.; Radeef, M.; Duan, X. Design and experimental analysis of a helical coil phase change heat exchanger for thermal energy storage. *J. Energy Storage* **2019**, *21*, 9–17.
207. Ajarostaghi, S.S.M.; Poncet, S.; Sedighi, K.; Delavar, M.A. Numerical modeling of the melting process in a shell and coil tube ice storage system for air-conditioning application. *Appl. Sci.* **2019**, *9*, 2726.
208. Zheng, X.; Xie, N.; Chen, C.; Gao, X.; Huang, Z.; Zhang, Z. Numerical investigation on paraffin/expanded graphite composite phase change material based latent thermal energy storage system with double spiral coil tube. *Appl. Therm. Eng.* **2018**, *137*, 164–172.
209. Javadi, H.; Ajarostaghi, S.S.M.; Mousavi, S.S.; Pourfallah, M. Thermal analysis of a triple helix ground heat exchanger using numerical simulation and multiple linear regression. *Geothermics* **2019**, *81*, 53–73.
210. Olfian, H.; Ajarostaghi, S.S.M.; Farhadi, M.; Ramiar, A. Melting and solidification processes of phase change material in evacuated tube solar collector with U-shaped spirally corrugated tube. *Appl. Therm. Eng.* **2021**, *182*, 116149.
211. Moghadam, H.K.; Ajarostaghi, S.S.M.; Poncet, S. Extensive numerical analysis of the thermal performance of a corrugated tube with coiled wire. *J. Therm. Anal. Calorim.* **2020**, *140*, 1469–1481.
212. Mohammadi, S.; Ajarostaghi, S.S.M.; Pourfallah, M. The latent heat recovery from boiler exhaust flue gas using shell and corrugated tube heat exchanger: A numerical study. *Heat Transf.* **2020**, *49*, 3797–3815.
213. Moghadam, K.H.; Ajarostaghi, S.S.M.; Poncet, S. Numerical modeling of an innovative arc shape rib based solar air heater. *Proc. Inst. Mech. Eng. Part C J. Mech. Eng. Sci.* **2021**, *235*, 7992–8012.
214. Masoumpour-Samakoush, M.; Miansari, M.; Ajarostaghi, S.S.M.; Arici, M. Impact of innovative fin combination of triangular and rectangular fins on melting process of phase change material in a cavity. *J. Energy Storage* **2021**, *45*, 103545.
215. Elshafei, E.A.M.; Awad, M.M.; El-Negiry, E.; Ali, A.G. Heat transfer and pressure drop in corrugated channels. *Energy* **2010**, *35*, 101–110.

216. Yin, J.; Yang, G.; Li, Y. The effects of wavy plate phase shift on flow and heat transfer characteristics in corrugated channel. *Energy Procedia* **2012**, *14*, 1566–1573.
217. Sui, Y.; Teo, C.J.; Lee, P.S. Direct numerical simulation of fluid flow and heat transfer in periodic wavy channels with rectangular cross-sections. *Int. J. Heat Mass Transf.* **2012**, *55*, 73–88.
218. Forooghi, P.; Hooman, K. Effect of buoyancy on turbulent convection heat transfer in corrugated channels—A numerical study. *Int. J. Heat Mass Transf.* **2013**, *64*, 850–862.
219. Sui, Y.; Teo, C.J.; Lee, P.S.; Chew, Y.T.; Shu, C. Fluid flow and heat transfer in wavy microchannels. *Int. J. Heat Mass Transf.* **2010**, *53*, 2760–2772.
220. Sarkar, M.; Paramane, S.B.; Sharma, A. Periodically fully developed heat and fluid flow characteristics in a furrowed wavy channel. *Heat Transf. Eng.* **2017**, *38*, 278–288.
221. Jafari, M.; Farhadi, M.; Sedighi, K. Pulsating flow effects on convection heat transfer in a corrugated channel: A LBM approach. *Int. Commun. Heat Mass Transf.* **2013**, *45*, 146–154.
222. Tokgoz, N.; Tunay, T.; Sahin, B. Effect of corrugated channel phase shifts on flow structures and heat transfer rate. *Exp. Therm. Fluid Sci.* **2018**, *99*, 374–391.
223. Paisarn, N. Study on the heat-transfer characteristics and pressure drop in channels with arc-shaped wavy plates. *J. Eng. Phys. Thermophys.* **2010**, *83*, 1061–1069.
224. Akbarzadeh, M.; Rashidi, S.; Esfahani, J.A. Influences of corrugation profiles on entropy generation, heat transfer, pressure drop, and performance in a wavy channel. *Appl. Therm. Eng.* **2017**, *116*, 278–291.
225. Huang, P.; Pan, M. Secondary heat transfer enhancement design of variable cross-section microchannels based on entransy analysis. *Renew. Sustain. Energy Rev.* **2021**, *141*, 110834.
226. Soontarapiromsook, J.; Asirvatham, L.G.; Dalkılıç, A.S.; Mahian, O.; Wongwises, S.; Ahn, H.S. Experimental investigation on two-phase heat transfer of R-134a during vaporization in a plate heat exchanger with rough surface. *Int. J. Heat Mass Transf.* **2020**, *160*, 120221.
227. Akbarzadeh, S.; Valipour, M.S. Experimental study on the heat transfer enhancement in helically corrugated tubes under the non-uniform heat flux. *J. Therm. Anal. Calorim.* **2020**, *140*, 1611–1623.
228. Begag, A.; Saim, R.; Abboudi, S.; Öztop, H.F. Effect of internal and external corrugated surfaces on the characteristics of heat transfer and pressure drop in a concentric tube heat exchanger. *Int. J. Therm. Sci.* **2021**, *165*, 106930.
229. Al-Obaidi, A.R.; Alhamid, J. Investigation of flow pattern, thermohydraulic performance and heat transfer improvement in 3D corrugated circular pipe under varying structure configuration parameters with development different correlations. *Int. Commun. Heat Mass Transf.* **2021**, *126*, 105394.
230. Ashouri, M.; Rahmati, P.; Hakkaki-Fard, A. On the effect of corrugated conical frustum on pool boiling heat transfer. *Exp. Therm. Fluid Sci.* **2021**, *130*, 110494.
231. Mazhar, A.R.; Liu, S.; Shukla, A. Numerical investigation of the heat transfer enhancement using corrugated pipes in a PCM for grey water harnessing. *Therm. Sci. Eng. Prog.* **2021**, *23*, 100909.
232. Dong, Z.; Liu, P.; Xiao, H.; Liu, Z.; Liu, W. A study on heat transfer enhancement for solar air heaters with ripple surface. *Renew. Energy* **2021**, *172*, 477–487.
233. Cruz, G.G.; Mendes, M.M.A.; Pereira, J.M.C.; Santos, H.; Nikulin, A.; Moita, A.S. Experimental and numerical characterization of single-phase pressure drop and heat transfer enhancement in helical corrugated tubes. *Int. J. Heat Mass Transf.* **2021**, *179*, 121632.
234. Khoshvaght-Aliabadi, M.; Feizabadi, A. Compound heat transfer enhancement of helical channel with corrugated wall structure. *Int. J. Heat Mass Transf.* **2020**, *146*, 118858.
235. Zontul, H.; Hamzah, H.; Kurtulmuş, N.; Şahin, B. Investigation of convective heat transfer and flow hydrodynamics in rectangular grooved channels. *Int. Commun. Heat Mass Transf.* **2021**, *126*, 105366.
236. Qingchan, M.A.; Yanxia, Y.A.N.G.; Yuqing, Z.U.O. Thermal performance optimization of heat exchanger with mixed cross-corrugated sinusoidal plate channels. *Appl. Therm. Eng.* **2021**, *195*, 117138.
237. Shirzad, M.; Delavar, M.A.; Ajarostaghi, S.S.M.; Sedighi, K. Evaluation the effects of geometrical parameters on the performance of pillow plate heat exchanger. *Chem. Eng. Res. Des.* **2019**, *150*, 74–83.
238. Khoshvaght-Aliabadi, M.; Deldar, S.; Salimi, A.; Rashidi, M.M. Effects of cross-section geometry on performance of corrugated miniature heat sink: Uniform, convergent, divergent, and hybrid cases. *Int. Commun. Heat Mass Transf.* **2021**, *127*, 105269.
239. Hu, Q.; Yuan, K.; Peng, W.; Zhao, G.; Wang, J. A numerical study of heat transfer enhancement by helically corrugated tubes in the intermediate heat exchanger of a very-high-temperature gas-cooled reactor. *Nucl. Eng. Des.* **2021**, *380*, 11275.
240. Abd Rahim, A.T.; Hilo, A.K. Fluid flow and heat transfer over corrugated backward facing step channel. *Case Stud. Therm. Eng.* **2021**, *24*, 100862.
241. Al-Obaidi, A.R.; Alhamid, J. Numerical investigation of fluid flow, characteristics of thermal performance and enhancement of heat transfer of corrugated pipes with various configurations. *J. Phys. Conf. Ser.* **2021**, *1733*, 012004.
242. Yang, C.; Chen, M.-R.; Qian, J.-Y.; Wu, Z.; Jin, Z.-J.; Sunden, B. Heat transfer study of a hybrid smooth and spirally corrugated tube. *Heat Transf. Eng.* **2021**, *42*, 242–250.
243. Chaurasiya, P.K.; Singh, S.K.; Jain, P.K.; Rajak, U.; Verma, T.N.; Azad, A.K.; Choudhary, K.; Alosaimi, A.M.; Khan, A. Heat transfer and friction factor correlations for double pipe heat exchanger with inner and outer corrugation. *Energy Sources Part A Recovery Util. Environ. Eff.* **2021**, 1–28. <https://doi.org/10.1080/15567036.2021.1953635>.

244. Hamedani, F.A.; Ajarostaghi, S.S.M.; Hosseini, S.A. Numerical evaluation of the effect of geometrical and operational parameters on thermal performance of nanofluid flow in convergent–divergent tube. *J. Therm. Anal. Calorim.* **2020**, *140*, 1483–1505.
245. Chen, H.; Moria, H.; Ahmed, S.Y.; Nisar, K.S.; Mohamed, A.M.; Heidarshenas, B.; Arsalanloo, A.; Youshanlouei, M.M. Thermal/exergy and economic efficiency analysis of circumferentially corrugated helical tube with constant wall temperature. *Case Stud. Therm. Eng.* **2021**, *23*, 100803.
246. Olfian, H.; Ajarostaghi, S.S.M.; Ebrahimnataj, M. Development on evacuated tube solar collectors: A review of the last decade results of using nanofluids. *Sol. Energy* **2020**, *211*, 265–282.
247. Laouer, A.; Arıcı, M.; Tegger, M.; Bouabdallah, S.; Yıldız, Ç.; Ismail, K.A.R.; Ajarostaghi, S.S.M.; Mezaache, E.H. Effect of magnetic field and nanoparticle concentration on melting of cu-ice in a rectangular cavity under fluctuating temperatures. *J. Energy Storage* **2021**, *36*, 102421.
248. Muruganandam, M.; Kumar, P.C.M. Experimental analysis on internal combustion engine using MWCNT/water nanofluid as a coolant. *Mater. Today Proc.* **2020**, *21*, 248–252.
249. Rasheed, A.H.; Alias, H.B.; Salman, S.D. Experimental and numerical investigations of heat transfer enhancement in shell and helically microtube heat exchanger using nanofluids. *Int. J. Therm. Sci.* **2021**, *159*, 106547.
250. Tong, Y.; Lee, H.; Kang, W.; Cho, H. Energy and exergy comparison of a flat-plate solar collector using water, Al<sub>2</sub>O<sub>3</sub> nanofluid, and CuO nanofluid. *Appl. Therm. Eng.* **2019**, *159*, 113959.
251. Ahmed, F.; Abir, A.M.; Redwan, S.A.M.; Bhuiyan, A.A.; Mollah, A.S. The impact of D-shaped jaggedness on heat transfer enhancement technique using Al<sub>2</sub>O<sub>3</sub> based nanoparticles. *Int. J. Thermofluids* **2021**, *10*, 100069.
252. Lari, M.O.; Sahin, A.Z. Design, performance and economic analysis of a nanofluid-based photovoltaic/thermal system for residential applications. *Energy Convers. Manag.* **2017**, *149*, 467–484.
253. Nithiyantham, U.; González-Fernández, L.; Grosu, Y.; Zaki, A.; Igartua, J.M.; Faik, A. Shape effect of Al<sub>2</sub>O<sub>3</sub> nanoparticles on the thermophysical properties and viscosity of molten salt nanofluids for TES application at CSP plants. *Appl. Therm. Eng.* **2020**, *169*, 114942.
254. Chaudhari, S.S.; Chakule, R.R.; Talmale, P.S. Experimental study of heat transfer characteristics of Al<sub>2</sub>O<sub>3</sub> and CuO nanofluids for machining application. *Mater. Today Proc.* **2019**, *18*, 788–797.
255. Teruel, M.; Aguilar, T.; Martinez-Merino, P.; Carrillo-Berdugo, I.; Gallardo-Bernal, J.J.; Gomez-Villarejo, R.; Alcántara, R.; Fernandez-Lorenzo, C.; Navas, J. 2D MoSe<sub>2</sub>-based nanofluids prepared by liquid phase exfoliation for heat transfer applications in concentrating solar power. *Sol. Energy Mater. Sol. Cells* **2019**, *200*, 109972.
256. Esmaili-Faraj, S.H.; Esfahany, M.N.; Darvanjooghi, M.H.K. Application of water based nanofluids in bioscrubber for improvement of biogas sweetening in a pilot scale. *Chem. Eng. Process. Process Intensif.* **2019**, *143*, 107603.
257. Nazari, S.; Safarzadeh, H.; Bahiraei, M. Experimental and analytical investigations of productivity, energy and exergy efficiency of a single slope solar still enhanced with thermoelectric channel and nanofluid. *Renew. Energy* **2019**, *135*, 729–744.
258. Soltani, S.; Kasaeian, A.; Sarrafha, H.; Wen, D. An experimental investigation of a hybrid photovoltaic/thermoelectric system with nanofluid application. *Sol. Energy* **2017**, *155*, 1033–1043.
259. Ahammed, N.; Asirvatham, L.G.; Wongwises, S. Thermoelectric cooling of electronic devices with nanofluid in a multiport minichannel heat exchanger. *Exp. Therm. Fluid Sci.* **2016**, *74*, 81–90.
260. Mohammadian, S.K.; Zhang, Y. Analysis of nanofluid effects on thermoelectric cooling by micro-pin-fin heat exchangers. *Appl. Therm. Eng.* **2014**, *70*, 282–290.
261. Ahammed, N.; Asirvatham, L.G.; Wongwises, S. Entropy generation analysis of graphene–alumina hybrid nanofluid in multiport minichannel heat exchanger coupled with thermoelectric cooler. *Int. J. Heat Mass Transf.* **2016**, *103*, 1084–1097.
262. Karana, D.R.; Sahoo, R.R. Effect on TEG performance for waste heat recovery of automobiles using MgO and ZnO nanofluid coolants. *Case Stud. Therm. Eng.* **2018**, *12*, 358–364.
263. Duan, L.; Han, J.; Cao, L.; Huo, C. Experimental study on heat transfer characteristics of CNTs/Al<sub>2</sub>O<sub>3</sub> nanofluids in personal cooling system based on thermoelectric refrigeration. *Procedia Eng.* **2017**, *205*, 588–595.
264. Javadi, H.; Urchueguia, J.F.; Ajarostaghi, S.S.M.; Badenes, B. Numerical study on the thermal performance of a single U-tube borehole heat exchanger using nano-enhanced phase change materials. *Energies* **2020**, *13*, 5156.
265. Shirzad, M.; Ajarostaghi, S.S.M.; Delavar, M.A.; Sedighi, K. Improve the thermal performance of the pillow plate heat exchanger by using nanofluid: Numerical simulation. *Adv. Powder Technol.* **2019**, *30*, 1356–1365.
266. Zaboli, M.; Ajarostaghi, S.S.M.; Noorbakhsh, M.; Delavar, M.M.A. Effects of geometrical and operational parameters on heat transfer and fluid flow of three various water based nanofluids in a shell and coil tube heat exchanger. *SN Appl. Sci.* **2019**, *1*, 1387.
267. Ajarostaghi, S.S.M.; Shirzad, M.; Rashidi, S.; Li, L.K.B. Heat transfer performance of a nanofluid-filled tube with wall corrugations and center-cleared twisted-tape inserts. *Energy Sources Part A Recovery Util. Environ. Eff.* **2020**, 1–21. <https://doi.org/10.1080/15567036.2020.1841860>.
268. Noorbakhsh, M.; Ajarostaghi, S.S.M.; Zaboli, M.; Kiani, B. Thermal analysis of nanofluids flow in a double pipe heat exchanger with twisted tapes insert in both sides. *J. Therm. Anal. Calorim.* **2021**, 1–12. <https://doi.org/10.1007/s10973-021-10738-x>.
269. Zaboli, M.; Saedodin, S.; Ajarostaghi, S.S.M.; Noorbakhsh, M. Numerical evaluation of the heat transfer in a shell and corrugated coil tube heat exchanger with three various water-based nanofluids. *Heat Transf.* **2021**, *50*, 6043–6067.
270. Shahi, P.; Agarwal, S.; Saini, S.; Niazmand, A.; Bansode, P.; Agonafer, D. CFD analysis on liquid cooled cold plate using copper nanoparticles. In Proceedings of the International Electronic Packaging Technical Conference and Exhibition, Guangzhou, China, 12–15 August 2020.

271. Yang, D.; Sun, B.; Xu, T.; Liu, B.; Li, H. Experimental and numerical study on the flow and heat transfer characteristic of nanofluid in the recirculation zone of backward-facing step microchannels. *Appl. Therm. Eng.* **2021**, *199*, 117527.
272. Niazmand, A.; Sola, J.F.; Alinejad, F.; Dehghan, F.R. Investigation of mixed convection in a cylindrical lid driven cavity filled with water-Cu nanofluid. *Inventions* **2019**, *4*, 60.
273. Niazmand, A.; Murthy, P.; Saini, S.; Shahi, P.; Bansode, P.; Agonafer, D. Numerical Analysis of Oil Immersion Cooling of a Server Using Mineral Oil and Al<sub>2</sub>O<sub>3</sub> Nanofluid. In Proceedings of the International Electronic Packaging Technical Conference and Exhibition, Guangzhou, China, 12–15 August 2020.
274. Kristiawan, B.; Wijayanta, A.T.; Enoki, K.; Miyazaki, T.; Aziz, M. Heat transfer enhancement of TiO<sub>2</sub>/water nanofluids flowing inside a square minichannel with a microfin structure: A numerical investigation. *Energies* **2019**, *12*, 3041.
275. Kristiawan, B.; Santoso, B.; Wijayanta, A.T.; Aziz, M.; Miyazaki, T. Heat transfer enhancement of TiO<sub>2</sub>/water nanofluid at laminar and turbulent flows: A numerical approach for evaluating the effect of nanoparticle loadings. *Energies* **2018**, *11*, 1584.
276. Rifa'i, A.I.; Hasan, M.F.; Kristiawan, B.; Wijayanta, A.T.; Miyazaki, T.; Thu, K.; Enoki, K. Experimental study of heat transfer enhancement and pressure drop using TiO<sub>2</sub>/distilled water nanofluid inside counter flow double tube heat exchanger. *AIP Conf. Proc.* **2019**, *2097*, 030043.
277. Kristiawan, B.; Rifa'i, A.I.; Enoki, K.; Wijayanta, A.T.; Miyazaki, T. Enhancing the thermal performance of TiO<sub>2</sub>/water nanofluids flowing in a helical microfin tube. *Powder Technol.* **2020**, *376*, 254–262.
278. Ajarostaghi, S.S.M.; Aghanezhad, M.; Davudi, H.; Amiri, M.M. Numerical evaluation of the heat transfer enhancement in a tube with a curved conical turbulator insert. *Int. J. Ambient. Energy* **2021**, 1–23. <https://doi.org/10.1080/01430750.2021.1945490>.
279. Abbaspour, M.; Ajarostaghi, S.S.M.; Rad, S.S.A.H.; Nimafar, M. Heat transfer improvement in a tube by inserting perforated conical ring and wire coil as turbulators. *Heat Transf.* **2021**, *50*, 6164–6188.
280. Hussien, A.A.; Abdullah, M.Z.; Yusop, N.M.; Al-Nimr, M.A.; Atieh, M.A.; Mehrli, M. Experiment on forced convective heat transfer enhancement using MWCNTs/GNPs hybrid nanofluid and mini-tube. *Int. J. Heat Mass Transf.* **2017**, *115*, 1121–1131.
281. Hamid, K.A.; Azmi, W.H.; Nabil, M.F.; Mamat, R. Experimental investigation of nanoparticle mixture ratios on TiO<sub>2</sub>-SiO<sub>2</sub> nanofluids heat transfer performance under turbulent flow. *Int. J. Heat Mass Transf.* **2018**, *118*, 617–627.
282. Nabil, M.F.; Azmi, W.H.; Hamid, K.A.; Mamat, R. Heat transfer and friction factor of composite TiO<sub>2</sub>-SiO<sub>2</sub> nanofluids in water-ethylene glycol (60:40) mixture. *IOP Conf. Ser. Mater. Sci. Eng.* **2017**, *257*, 012066.
283. Hussien, A.A.; Abdullah, M.Z.; Yusop, N.M.; Al-Kouz, W.; Mahmoudi, E.; Mehrli, M. Heat transfer and entropy generation abilities of MWCNTs/GNPs hybrid nanofluids in microtubes. *Entropy* **2019**, *21*, 480.
284. Bahiraei, M.; Godini, A.; Shahsavari, A. Thermal and hydraulic characteristics of a minichannel heat exchanger operated with a non-Newtonian hybrid nanofluid. *J. Taiwan Inst. Chem. Eng.* **2018**, *84*, 149–161.
285. Singh, S.K.; Sarkar, J. Energy, exergy and economic assessments of shell and tube condenser using hybrid nanofluid as coolant. *Int. Commun. Heat Mass Transf.* **2018**, *98*, 41–48.
286. Anitha, S.; Thomas, T.; Parthiban, V.; Pichumani, M. What dominates heat transfer performance of hybrid nanofluid in single pass shell and tube heat exchanger. *Adv. Powder Technol.* **2019**, *30*, 3107–3117.
287. Hung, Y.-H.; Wang, W.-P.; Hsu, Y.-C.; Teng, T.-P. Performance evaluation of an air-cooled heat exchange system for hybrid nanofluids. *Exp. Therm. Fluid Sci.* **2017**, *81*, 43–55.
288. Sahoo, R.R.; Ghosh, P.; Sarkar, J. Performance analysis of a louvered fin automotive radiator using hybrid nanofluid as coolant. *Heat Transf. — Asian Res.* **2017**, *46*, 978–995.
289. Sahoo, R.R.; Sarkar, J. Heat transfer performance characteristics of hybrid nanofluids as coolant in louvered fin automotive radiator. *Heat Mass Transf.* **2017**, *53*, 1923–1931.
290. Humnic, G.; Humnic, A. The heat transfer performances and entropy generation analysis of hybrid nanofluids in a flattened tube. *Int. J. Heat Mass Transf.* **2018**, *119*, 813–827.
291. Humnic, G.; Humnic, A. The influence of hybrid nanofluids on the performances of elliptical tube: Recent research and numerical study. *Int. J. Heat Mass Transf.* **2019**, *129*, 132–143.
292. Returi, M.C.; Konijeti, R.; Dasore, A. Heat transfer enhancement using hybrid nanofluids in spiral plate heat exchangers. *Heat Transf. — Asian Res.* **2019**, *48*, 3128–3143.
293. Bhattad, A.; Sarkar, J.; Ghosh, P. Hydrothermal performance of different alumina hybrid nanofluid types in plate heat exchanger. *J. Therm. Anal. Calorim.* **2020**, *139*, 3777–3787.
294. Bhattad, A.; Sarkar, J.; Ghosh, P. Energetic and exergetic performances of plate heat exchanger using brine-based hybrid nanofluid for milk chilling application. *Heat Transf. Eng.* **2019**, 1–14. <https://doi.org/10.1080/01457632.2018.1546770>.
295. Uysal, C.; Gedik, E.; Chamkha, A.J. A numerical analysis of laminar forced convection and entropy generation of a diamond-Fe<sub>3</sub>O<sub>4</sub>/water hybrid nanofluid in a rectangular minichannel. *J. Appl. Fluid Mech.* **2019**, *12*, 391–402.
296. Kumar, V.; Sarkar, J. Two-phase numerical simulation of hybrid nanofluid heat transfer in minichannel heat sink and experimental validation. *Int. Commun. Heat Mass Transf.* **2018**, *91*, 239–247.
297. Bahiraei, M.; Jamshidmofid, M.; Goodarzi, M. Efficacy of a hybrid nanofluid in a new microchannel heat sink equipped with both secondary channels and ribs. *J. Mol. Liq.* **2019**, *273*, 88–98.
298. Kumar, V.; Sarkar, J. Numerical and experimental investigations on heat transfer and pressure drop characteristics of Al<sub>2</sub>O<sub>3</sub>-TiO<sub>2</sub> hybrid nanofluid in minichannel heat sink with different mixture ratio. *Powder Technol.* **2019**, *345*, 717–727.
299. Javadi, H.; Urchueguia, J.F.; Ajarostaghi, S.S.M.; Badenes, B. Impact of Employing Hybrid Nanofluids as Heat Carrier Fluid on the Thermal Performance of a Borehole Heat Exchanger. *Energies* **2021**, *14*, 2892.

300. Mousavi, A.; Soheil, S.; Zaboli, M.; Nourbakhsh, M. Numerical evaluation of turbulence heat transfer and fluid flow of hybrid nanofluids in a pipe with innovative vortex generator. *J. Therm. Anal. Calorim.* **2021**, *143*, 1583–1597.
301. Karouei, S.H.H.; Ajarostaghi, S.S.M.; Gorji-Bandpy, M.; Fard, S.R.H. Laminar heat transfer and fluid flow of two various hybrid nanofluids in a helical double-pipe heat exchanger equipped with an innovative curved conical turbulator. *J. Therm. Anal. Calorim.* **2021**, *143*, 1455–1466.